Recognising surface versus sub-surface deformation of soft-sediments: Consequences and considerations for palaeoseismic studies

G.I. Alsop[1], S. Marco[2], T. Levi[3]

1) Department of Geology and Geophysics, School of Geosciences, University of Aberdeen, Aberdeen, UK. (e-mail: ian.alsop@abdn.ac.uk)
2) Department of Geophysics, Tel Aviv University, Israel.
3) Geological survey of Israel, Jerusalem, Israel.

Abstract

Soft-sediment deformation structures associated with slumps and mass transport deposits (MTDs) are generally considered to form at the surface when unlithified sediment moves downslope under the influence of gravity. Where stratigraphic sequences contain several deformed horizons, the question arises as to whether repeated slope failure at the sediment surface has systematically built-up multiple MTDs in the stratigraphic record in a 'sequential failure model'. Alternatively, a single failure event may concurrently create surficial and sub-surface deformed 'intrastratal' horizons at different stratigraphic levels in a 'synchronous failure model'. The implications of these differing models are important as sub-surface deformation can be significantly younger than the depositional age of beds it affects thereby weakening age-depth correlations used to estimate the timing of palaeo-earthquakes. In order to investigate the potential for sub-surface deformation, we examine the late Pleistocene Lisan Formation exposed around the Dead Sea Basin that contains numerous MTDs and gravity-driven fold and thrust systems. Surficial deformation is recognised by identifying irregular erosive surfaces above MTDs that are overlain by sedimentary caps deposited out of suspension following the failure event. Such surficial deformation is also characterised by thickened sedimentary successions that create 'growth' sequences. Conversely, sub-surface intrastratal deformation is typified by detachment-bound folds and thrusts that are marked by repetitions of stratigraphy across the upper detachment surface, fluidised sediment that intrudes upwards into the overlying sequence, together with abrupt truncations of older faults developed in overburden above the detachment. MTDs created at the surface form relatively competent horizons when subsequently buried as they are internally disrupted and lack 'layer-cake' geometries, while repeated seismicity can lead to dewatering and compaction resulting in 'seismic strengthening'. Later sub-surface deformation may therefore be focussed adjacent to earlier MTDs that influence the mechanical stratigraphy, leading to secondary failures and complications when attempting to 'balance' extension and contraction that may be of different ages. Sub-surface deformation is localised along discrete detachments that carry the overlying sequence downslope as relatively intact slides, affecting what appear to be 'undeformed' beds between individual MTDs. As sub-surface deformation does not directly correlate with sedimentary caps, the rates of movement on deeper detachments remain unconstrained and may be significantly slower than surficial deformation resulting in downslope creep of the sediment pile.

Key Words: mass transport deposit; fold and thrust system; soft-sediment deformation; Dead Sea

1. Introduction

The downslope movement of subaqueous sediments to create mass transport deposits (MTDs) is increasingly documented across a range of m-km scales in both outcrop-based studies (e.g. Gibert et al., 2005; Garcia-Tortosa et al., 2011; Sharman et al., 2015; Korneva et al., 2016; Sobiesiak et al., 2017; Cardona et al., 2020) and seismic analysis from offshore areas (e.g. Reis et al., 2016; Scarselli et al., 2016; Jolly et al., 2016; Kumar et al., 2021). MTDs have been recognised from subaqueous settings varying from lacustrine (e.g. Van Daele et al., 2015; Sammartini et al., 2020; Liang et al., 2021) to deep marine (e.g. Huhn et al., 2020), resulting in a number of recent collections of papers (e.g. Van Loon, 2014; Krastel et al., 2014; Lamarche et al., 2016; Ogata et al., 2020; Georgiopoulou et al., 2020).

MTDs incorporate several processes including creep, (which is defined as "the slow, more or less continuous downslope movement of mineral, rock, and soil particles under gravitational stresses"; Bates and

Jackson, 1980, p.146), slides (where stratigraphy remains intact and downslope movement occurs in coherent sheets), slumps (where the translated mass is internally deformed) and relatively fast debris flows (Posamentier and Martinsen, 2011, p.8; Moscardelli and Wood, 2008; Armandita et al., 2015). Where several MTDs are developed in a sequence then the term mass transport complex (MTC) is commonly applied (e.g. Bull et al., 2009; Ogata et al., 2012; 2014). Such repeated deposits are generally considered to represent recurrent slope failure and are typically separated from one another by intervening undeformed beds deposited during periods of stability (e.g. Kumar et al., 2021). Downslope movement of sediments may be achieved through gravity-driven fold and thrust systems (FATS) that form in the poorly lithified sediments (Alsop et al., 2017a, b; Morley et al., 2017). In such FATS, thrusting can breach the sediment surface and become emergent, or be buried under the sediment pile where intrastratal deformation is bound by upper and lower detachments that create sub-surface duplexes (e.g. Auchter et al., 2016; Alsop et al., 2021a). Auchter et al., (2016, p.13) define intrastratal deformation as "stratigraphically isolated zones of deformation bounded above and below by concordant and undeformed strata".

Deformation within both surficial MTDs and sub-surface intrastratal FATS is considered to affect unlithified or only poorly-lithified sediments such that soft-sediment deformation (SSD) structures are produced (see Maltman 1984, 1994a, b for definitions of SSD; Shanmugam, 2017). SSD folds created during gravity-driven slumping share a close morphological similarity with folds and structures formed during tectonic deformation, potentially complicating their distinction especially in the rock record (e.g. Maltman, 1994a, Festa et al., 2016; Alsop et al., 2019). SSD can be triggered by either external deformation (allogenic/exogenic triggers), such as tectonics and earthquakes, or by processes that develop in the depositional environment (autogenic/endogenic triggers), including rapid sedimentation and floods (e.g., Chakraborty et al., 2019). These different triggers have been discussed by Moretti and Sabato (2007); Moretti and Van Loon (2014) and Van Loon (2014).

While it has previously been recognised from outcrop and seismic data that MTDs can 'ride' on lower or 'basal' detachments (e.g. Alves, 2015; Cardona et al., 2020; Kumar et al., 2021), it is generally assumed that their upper bounding surface was emergent and formed an irregular bathymetry on the seabed (Frey-Martinez et al., 2005, 2006; Ireland, 2011; Sobiesiak et al., 2020, p.99). This uneven surface, if buried by subsequent sedimentation, will be preserved as an unconformity in the stratigraphic record. The lower detachment may also ramp up to the sediment surface where it forms a basal shear zone as it over-rides the downslope sediments in frontally-emergent MTDs (Frey-Martinez et al., 2005, 2006; Sobiesiak et al., 2018). The implication of this model is two-fold: namely a) that all deformation in MTDs is surficial, and b) that all deformation is the same age or only slightly younger than the unlithified stratigraphy it affects. This close association between the age of sediment deposition and the timing of surficial deformation allows the dating of sediments to 'bracket' the age of deformation, and hence the date of earthquakes in seismogenic MTDs.

If deformation and associated structures are shown to be much younger and form in the sub-surface after sediments are buried, as in the case of some intrastratal FATS, then no clear or simple relationship can be drawn between the age of sediments and timing of deformation. In this case, Törő and Pratt, (2016, p.197) have noted that such intrastratal deformation hinders analysis of seismic recurrence intervals as it "increases the degree of uncertainty in the timing" and the value of SSDs in palaeoseismic studies is thereby diminished and could even be counterproductive. Furthermore, O'Leary and Laine (1996, p.305) highlight the difficulty in distinguishing surface versus sub-surface structures and state that "Intrastratal deformation is easily confused with buried slump or slide deposits formed initially at the sea ftoor". Given the significant implications of misidentifying surface and sub-surface deformation, we therefore aim to provide and catalogue some diagnostic outcrop-based criteria that help discriminate between structures formed in the two settings.

Distinguishing erosive truncations that cut surficial MTD structures from cut-offs linked to detachments and bed-parallel slip is crucial. The importance of erosive surfaces in distinguishing SSDs formed at the surface, versus those that potentially formed at depth, has been recognised by a range of authors. Törő

and Pratt (2016, p.180) note that intrastratal deformation is marked by an absence of overlying truncations created by erosive processes on the lake floor, combined with a transition into overlying and underlying beds that remain undeformed. Van Loon et al. (2016) and Belzyt et al. (2021) examined sediments deformed during post-glacial rebound and consider that deformed horizons at different stratigraphic levels are largely created by different seismic events. Conversely, Gibert et al. (2011) suggest that multiple deformed horizons may form at different stratigraphic levels during the same seismic event, while Törő and Pratt (2016, p.197) note that "it is possible a single earthquake could deform two or more closely spaced intervals separated by intact beds". In order to link deformation to the sediment surface, it is of critical importance to identify erosive surfaces that cut underlying structures and this concept is applied to the analysis of MTDs.

While it has been suggested that some MTDs might conceal more than one seismic event, (Alsop and Marco, 2011; Alsop et al., 2016, 2020a; Jablonska et al., 2016, 2018), the role of younger deformation affecting buried sequences that contain older MTDs has so far not received the same attention. The aim of this work is therefore to provide clear descriptions and examples of structures that form at the sediment surface versus those that form in the sub-surface. The main research questions addressed are:

a) Which surface and sub-surface deformation models are applicable to MTDs?

b) What are the key diagnostic criteria to identify surface and sub-surface deformation?

c) What controls where and when sub-surface deformation localises?

d) What are the consequences of sub-surface deformation in MTDs?

Finely laminated sediments that are deposited in lacustrine settings act as an ideal template to record SSD. Such sequences are therefore increasingly used to constrain earthquake recurrence in palaeoseismic studies based on outcrops and in successions investigated via drill cores (e.g. Törő and Pratt, 2016; Hou et al., 2020; Gao et al., 2020; Lu et al., 2021a, b). We focus our attention on MTDs and horizons of SSD that are generally <1 m thick as these thinner deformed intervals can more precisely define earthquake events and have therefore been used for accurate and detailed palaeoseismic analysis in the stratigraphic record (e.g. Agnon et al., 2006; Dechen and Aiping, 2012; Hou et al., 2020; Tang et al., 2020; Belzyt et al., 2021).

2. Models of surficial versus sub-surface deformation of sediments

Deformation of poorly consolidated or only partially lithified sediments at the surface or sub-surface is known as soft-sediment deformation (SSD) (e.g. Maltman, 1984). This process has been described in terms of independent particulate flow that analyses the relationship between pore fluid pressure and cohesive strength due to grain weight (Knipe, 1986). Hydroplastic deformation develops where fluid pressure is less than grain weight and results in primary bedding being modified into structures such as folds similar to those observed in metamorphic rocks (see Alsop et al., 2020b). Conversely, liquefaction forms where fluid pressure is equal to grain weight leading to laminar flow of sediment and consequent destruction of bedding (e.g. Obermeier, 2009). Liquefaction occurs when "when grain weight is temporarily transferred to the pore fluid, through either the collapse of a loose grain packing or an increase in pore-fluid pressure" resulting in short-lived failure (Owen and Moretti, 2011, p.141). Finally, if fluid pressure exceeds grain weight then fluidisation develops in which grains are entrained and carried in turbulent flow that destroys bedding. Fluidisation is defined by Owen and Moretti (2011, p.141) as occurring "when the upward-directed shear of fluid flowing through a porous medium counteracts the grain weight, reducing the material strength". Fluidisation can lead to the injection of sediments into overlying sequences, indicating that the fluidised layer was buried at the time of deformation, which in some cases may be km's below the surface (e.g. Palladino et al., 2016, 2018, 2021). Horizons of SSDs created by variable components of hydroplastic deformation, liquefaction and fluidisation can form in a range of environments including accretionary complexes (e.g. Ogawa and Mori, 2021), although we here focus on surficial MTDs or sub-surface intrastratal FATS developed in gravity-driven systems. There are effectively two end member models when interpreting multiple horizons of SSD at different stratigraphic levels within a sedimentary sequence.

142
143 **2.1. Sequential failure model**
144 In the first model, that we term the '*sequential failure model*', it is considered that each successive horizon of
145 SSDs represents a new surficial event and that deformation therefore occurred sequentially up through the
146 sediment pile as new beds were deposited (e.g. see Sammartini et al., 2020 p.217; Kumar et al., 2021) (Fig.
147 1a). In our schematic summary, failure occurred in surficial sediments and created MTD 1 in time 2, while an
148 overlying sedimentary cap was deposited out of suspension immediately afterwards in time 3 (Fig. 1a). The
149 sedimentary cap is formed of fine-grained sediment that was thrown into suspension during slope failure and
150 subsequently settled through the water column to create a depositional cap that drapes the underlying MTD
151 (e.g. Alsop et al., 2021a). Overlying sediments accumulated prior to a further failure event 2 that affected
152 surficial sediments at time 6 (Fig. 1a). Repeated surficial failures therefore sequentially created multiple MTD
153 horizons through the succession. As deformation was contemporaneous with deposition, the number of
154 deformed MTD horizons and associated sedimentary caps therefore represents the number of failure events.
155
156 **2.2. Synchronous failure model**

157 In the second model, that we term the '*synchronous failure model*', it is considered that multiple SSDs form at
158 different stratigraphic levels at the same time (Fig. 1b). In this scenario, some deformed horizons develop at,
159 or close to, the contemporary surface, whereas others form deeper in the sediment pile during intrastratal
160 deformation. Intrastratal deformation has long been recognised in sedimentary sequences with large-scale
161 gravity-driven 'intraformational sliding' beneath overlying sediments being reported by Baldry (1938) and
162 Brown (1938) (see Miller, 1922; Williams, 1960 and Maltman, 1994, p.18 for historical perspectives). Rich
163 (1950, p.729) suggested that unconsolidated and fluid rich layers "served as a zone of gliding along which the
164 entire mass of overlying sediment crept down a slope and, in the process, crumpled the bedding within the
165 siltstone". More recently, Törő and Pratt (2015b, p.382) show several stacked intrastratal deformation horizons
166 displaying duplex structures and separated by undeformed beds on the m scale. They also recognised MTDs in
167 the same sequence that are marked by erosive bases that formed at the sediment surface.

168 In our schematic summary of the synchronous failure model, the first failure event (1) did not occur
169 until time 6 after a significant thickness of sediment had already been deposited (Fig. 1b). This failure event
170 occurred in surficial sediments and created MTD 1 in time 6, and also developed concurrently in the sub-
171 surface where a detachment-bound intrastratal FATS formed in the buried sediments (Fig. 1b). This sub-
172 surface failure in time 6 deformed sediments that were originally deposited in time 1 and are therefore
173 significantly older (Fig. 1b). It therefore represents an instance of younger structures forming at depth in an
174 older sequence, with a single failure event creating synchronous surficial (MTD) and sub-surface intrastratal
175 deformation in the sequence (Fig. 1b). As deformation was contemporaneous with a single event, but not
176 necessarily with deposition of the deformed beds that it affects, then multiple deformed horizons can form
177 synchronously that significantly post-date the age of sediment (Fig. 1b). Importantly, the number of deformed
178 MTD and intrastratal FATS horizons does not therefore represent the number of failure events.
179
180 **2.3. Secondary failure model**
181 It is entirely possible that variations of the synchronous model develop and early MTDs, that later become
182 buried in the sequence, control where secondary deformation and reworking forms in the sub-surface (Fig. 1c).
183 This was recognised from high resolution seismics by O'Leary and Laine (1996, p.308) who state that "both
184 mass movement and intrastratal deformation may figure in the origin of a single layer". In our schematic
185 summary, failure initially occurred at the surface to create MTD 1 in time 2, and this was later covered by
186 overburden (Fig. 1c). During a second failure event during time 6, a new surficial MTD 2 was formed at the
187 same time as secondary deformation was focussed along the boundaries of the earlier MTD 1 in the sub-
188 surface (Fig. 1c). Reworking results in detachments and reflects the control exerted by the earlier MTD 1 on

the mechanical stratigraphy. Bed-parallel detachments that developed along earlier MTDs result in slides where relatively intact stratigraphy moves downslope over a period of time. Clearly reworking of earlier MTDs by later secondary deformation could result in overprinting of surficial structures and a potential for miscounting the number of deformational events.

In our schematic summary we only show two failure events in each model (Fig. 1a, c), but the process of several horizons being deformed at the same time may be repeated up through the sequence during deposition of successive layers and repeated major events. This ultimately builds a stratigraphy containing numerous deformed horizons separated by apparently undeformed beds, as frequently observed in successions incorporating SSDs and MTDs. In order to distinguish the different end-member models, we need to carefully explore the relationships between deformation and the sediment surface as the '*sequential failure model*' largely restricts deformation to the sediment-water interface marked by syn-depositional structures, whereas the '*synchronous failure model*' and '*secondary failure model*' permits sub-surface intrastratal deformation deeper in the sediment pile. We use the late Pleistocene lacustrine sediments of the Dead Sea Basin to test these different models and examine the effects of deformation in sedimentary sequences.

3. Geological setting

3.1. Regional geology

The Dead Sea Basin is a continental depression bound by the left-lateral eastern border fault and the western border fault zone which is characterised by a series of oblique-normal step faults (Fig. 2a, b) (e.g. Marco et al., 1996, 2003; Ken-Tor et al., 2001; Migowski et al., 2004; Begin et al., 2005). The Dead Sea Fault (DSF) system is believed to have been active from the early Miocene to Recent, (Nuriel et al., 2017) including during deposition of the late Pleistocene Lisan Formation at 70-14 Ka (e.g. Haase-Schramm et al., 2004). The present study focusses on the Lisan Formation that comprises detrital-rich layers washed into Lake Lisan during flood events, while mm-scale aragonite laminae were precipitated from the hypersaline waters during the summer (Begin et al., 1974; Ben-Dor et al., 2019) (Fig. 3a). Isotopic dating, when linked with counting of the aragonite-detrital varves implies average depositional rates of ~1 mm per year for the Lisan Formation (Prasad et al., 2009). Thicker (>10 cm) detrital-rich beds were deposited more rapidly following major floods and comprise very fine (60 – 70 μm) sands, while thin detrital laminae display grain sizes of ~8-10 μm (silt) (Haliva-Cohen et al., 2012). Compositionally, the detrital units consist of quartz and calcite grains with minor feldspar and clays (illite-smectite) (Haliva-Cohen et al., 2012). The Lisan Formation is considered to have been fluid saturated at the time of deformation and still contains ~25% fluid content (Arkin and Michaelli, 1986; Frydman et al., 2008).

3.2. Regional patterns of slope failure

The Lisan Formation extends for ~100 km along strike and is marked by very low <1° depositional dips that are directed towards the depocentre of the Dead Sea Basin. A range of gravity-driven structures associated with seismically-induced slope failure are created, including bed-parallel detachments (Alsop et al., 2020c), FATS (e.g. Alsop et al., 2021a, b), and MTDs (Alsop et al., 2020d). These structures collectively move sediment downslope towards the centre of the basin resulting in an overall radial pattern of slumping (Alsop et al., 2020a) (Fig. 2a, b). The Lisan Formation on the eastern shores of the Dead Sea in Jordan records westerly-directed movement (El-Isa and Mustafa, 1986), while the southern portion of the basin at Peratzim displays NE-directed slumping, the central portion is marked by E-directed MTDs, and the northern parts of the basin are dominated by SE-directed movements (Fig. 2b). The direction of slumping is supported by anisotropy of magnetic susceptibility (AMS) fabrics (Weinberger et al., 2017). This collective movement of sediment from the basin margins towards the centre results in the Lisan Formation being three times thicker in the depocentre where drill cores penetrate numerous MTDs (Lu et al., 2017, 2021a, b, c; Kagan et al., 2018).

3.3. Rationale for study area

Deformed horizons, breccias, slumps and MTDs within the Lisan Formation are correlated with repeated seismicity generated along the DSF (Marco et al., 1996; Agnon et al., 2006; Levi et al., 2018). In addition, gypsum horizons up to 1 m thick precipitate by overturn and mixing of the water column possibly following major earthquakes (Ichinose and Begin, 2004; Begin et al., 2005). The varve-like laminae of the Lisan Formation preserve detailed structures, making the Dead Sea Basin an ideal place to study sediment failure. The bilaminate sediments, that consist of varying proportions of aragonite and detrital input, simplify the mechanics of the resulting fold and thrust geometries (Alsop et al., 2020a, b; 2021a, b). In addition, the overall control on the kinematics of sediment movement exerted by the regional slope are well constrained, and provides a consistent framework for both surficial and sub-surface deformation. The best sections for structural analysis are preserved in the finely laminated upper 'White Cliff' part of the Lisan Formation dated at 31-15 ka (Torfstein et al., 2007). Previous work has shown this part of the Lisan Formation to contain:

a) MTDs that are overlain by erosive surfaces and sedimentary caps associated with surficial deformation (Alsop et al., 2018, 2020a),

b) shallowly-buried FATS <1 m below the sediment surface that are bound by upper detachments but may locally influence overlying sedimentation (Alsop et al., 2021a),

c) intrastratal detachments marked by bed-parallel slip that create slide surfaces at depths of up to 20 m in the sub-surface which represents the thickness of the upper 'White Cliff' Lisan sequence which hosts these structures (Bartov et al., 2002; Alsop et al., 2020c, p.16).

The Lisan Formation therefore contains a spectrum of deformation styles that were created at a range of depths below the sediment surface thereby providing an opportunity to examine the major influences on slope failure. The various types of gravity-driven structure are subsequently cut by clastic dykes which contain sediment that provides optically stimulated luminescence (OSL) dates of between 15 and 7 Ka (Porat et al., 2007). These dates therefore bracket the age of sub-surface deformation, which is younger than 30 Ka (depositional age of the 'White Cliff' section of the Lisan Formation) and older than 7 Ka (the age of the youngest cross-cutting clastic dykes).

The present study focuses on structures preserved in the Lisan Formation exposed along the western margins of the Dead Sea Basin at Miflat [N31°:21.42'' E35°:22.49''], Masada [N31°:20.02'' E35°:21.24''], Peratzim [N31°:04.56'' E35°:21.02''], Wadi Zin [N30°:53.41'' E35°:17.26''] (Fig. 2b). All of these sites are located ~1-2 km east of Cenomanian-Senonian carbonates that outcrop in the footwall of the Dead Sea western border fault zone (Fig. 2b). These marginal areas of Lake Lisan had the potential to periodically dry out, with maximum water depths of 100 m for the period between 70 and 28 Ka, and up to 200 m water depth for a short interval between 26-24 Ka (Bartov et al., 2002; 2003). Modern erosion associated with flash floods creates incised wadis that cut through the Lisan Formation and enable examination of vertical sections that form parallel to the movement direction of the earlier slope failures.

4. Criteria used to recognise surficial deformation

4.1. Erosive surfaces

Erosive surfaces that cut pre-existing structures are perhaps the single most important criteria to demonstrate that deformation took place at the surface (e.g. Törő and Pratt, 2016; Van Loon et al., 2016; Belzyt et al., 2021) and we therefore now document examples of these surfaces truncating different underlying structures. For consistency, East (or NE) which represents the downslope direction is towards the right on all figures, while scales on photographs are provided by a 15 mm diameter coin, 10 cm long chequered rule, 20 cm long yellow notebook and 23 cm long hammer.

278 *4.1.1. Erosive surfaces cutting neptunian dykes*

279 Neptunian dykes that are created by sediment infilling open fissures from above are formed at the sediment
280 surface. Within the Lisan Formation, our investigated neptunian dykes are up to 1 m in height, typically widen
281 upwards, and cross-cut the aragonite and detrital laminae that display no offset across the dyke (Fig. 3a, b).
282 The infill to the dyke comprises mixed aragonite and detrital sediment that displays crude sub-horizontal
283 stratification (Fig. 3c). Some dykes are infilled by rounded pebbles and cobbles that have been transported
284 greater distances (Fig. 3c). The lack of associated fracturing and vertical fabrics within the infills indicate that
285 these features are not part of the suite of late clastic dykes injected after deposition of the Lisan Formation
286 (e.g. Levi et al., 2006a, b,). We interpret them as 'neptunian dykes' associated with syn-depositional infilling
287 of fissures or desiccation cracks as Lake Lisan periodically shrunk and partially dried up. The neptunian dykes
288 are overlain by an unconformity marked by conglomerates that were deposited during a re-flooding event (Fig.
289 3a, b). Unconformity surfaces are irregular and typically erode more deeply into the underlying dykes (Fig. 3d-
290 g). Neptunian dykes that are truncated by unconformities are themselves subsequently offset by later normal
291 faults (Fig. 3d-g). Normal faults are then cut by bed-parallel detachments that represent a subsequent stage of
292 deformation (Fig. 3d-g). Irregular erosive surfaces potentially overlain by conglomerates and cutting
293 underlying neptunian dykes are a key indicator of surficial processes.

294 *4.1.2. Erosive surfaces cutting soft-sediment folds*

295 Instances of erosive surfaces cutting across slump folds in the Lisan Formation have been previously reported
296 (e.g. Alsop et al., 2021a) and we here provide some further cases (Fig. 3h, i). Soft-sediment slump folds form
297 within MTDs during downslope movement and develop with a range of attitudes from upright to reclined and
298 recumbent (Alsop et al., 2020b). Irregular erosive surfaces cut directly across the limbs and hinges of both
299 upright and recumbent folds (Fig. 3h, i). Erosion results in the potential removal of tens of cm's of folded
300 stratigraphy, although the exact amounts are difficult to estimate (e.g. Fig. 3h). The observation that the
301 erosive surface is irregular and locally cuts up and down the underlying earlier structures is consistent with
302 erosion along the sediment-water interface associated with high-energy flow (Alsop et al., 2021a).
303

304 ***4.2. Syn-depositional fold style***

305 Within the Lisan Formation, the initiation of folding is often associated with underlying aragonite-rich beds
306 overlain by detrital-rich beds that form upright 'billow' folds (Alsop and Marco, 2011) (Fig. 4a, b). The
307 aragonite beds form narrow antiforms separated by broad synforms composed of the detrital-rich units, with
308 the wavelength of the folds being systematically spaced (Fig. 4a, b). Aragonite-cored antiforms broaden out at
309 the crest, while the detrital-cored synforms broaden towards their troughs (Fig. 4a, b). This ultimately results
310 in a characteristic 'fanning' arrangement of folds and associated axial panes indicating that the sediments were
311 weak and potentially fluid-rich at the time of deformation (Alsop et al., 2021a) (Fig. 4c-e). Folds are truncated
312 by the overlying erosive surfaces and a sedimentary cap indicating that they formed at the sediment-water
313 interface (Fig. 4c-e). Upright billows are subsequently modified during downslope translation and carried on
314 later thrust ramps (Fig. 4f, g). Creation of new thrusts results in the upright billow folds being 'back-rotated'
315 away from the vertical, although new secondary vertical folds may grow off the older billows following
316 rotation (Fig. 4h, i). While billow folds can be modified by continued MTD movement, the initial geometries
317 associated with thickened crests and troughs is characteristic of deformation in weak surficial sediments.
318

319 ***4.3. Sedimentary caps***

320 Erosive surfaces are generally overlain by a 'mixed' bed comprising mud, silt, sand and mm-scale fragments
321 of aragonite and detrital laminae termed a 'sedimentary cap' (e.g. Alsop et al., 2016, 2019). Such caps are
322 extremely variable in thickness but are generally < 10 cm, although locally can exceed 30 cm and infill
323 underlying irregularities along the erosive surfaces (e.g. Fig. 3h, i). The top of the cap is horizontal and is

succeeded by aragonite-rich and detrital-rich couplets representing typical background sedimentation in the Lisan Formation (Figs. 3h, i, 5a). Sedimentary caps may be graded and also contain 2-3 cm long aragonite fragments that are concentrated towards the base of the bed and interpreted to be clasts 'ripped-up' from the underlying sequence (Fig. 5a, b). The mixed and graded nature of the sedimentary cap, coupled with the infilling of underlying topography, suggests that it was deposited out of suspension from the water column following the catastrophic downslope movement of surficial sediments in an MTD (Alsop et al., 2016, 2019). As such it represents syn-slumping deposition confirming that the immediately underlying folding and deformation also formed at the surface.

4.4. Syn-depositional faulting - growth sequences across normal faults

The hangingwall of syn-sedimentary normal faults are down-faulted leading to local topography being infilled by the deposition of a greater thickness of sediment to create 'growth faults' (see Fossen, 2016, p.183). In the present case study, MTDs and adjacent beds display a thickening in the hangingwall of normal faults (Fig. 5c-h). Stratigraphy underlying the MTD is thickened on the downthrown side indicating that the normal fault was already active prior to deposition of the MTD (Fig. 5c-e). Sequences overlying the MTD are also thickened on the downthrown side, while they are thinned and 'draped' over the culmination and footwall of the fault, indicating that in this case the active faulting had ceased by the time of their deposition (Fig. 5f-h). In both examples of growth faulting, the syn-sedimentary normal faults are later cut by bed-parallel detachments which generate 'sawtooth' profiles (Alsop et al., 2020c) (Fig. 5f-h). The direct influence on sedimentation of 'growth faults' is clear evidence for MTD deformation at the sediment surface.

4.5. Syn-depositional folding – growth sequences across culminations

4.5.1. Folding at the sediment surface

Deformation at the time of deposition of the sedimentary cap results in laminated aragonite-rich beds being interfolded with the overlying detrital-rich beds and sedimentary cap (Fig. 6a), or with the cap being 'draped' over syn-slumping folds (Fig. 6b). Although the top of the cap remains horizontal and undeformed, the detrital-rich beds that grade into the overlying sedimentary cap display dramatic changes in thickness from the crests of culminations to the troughs of synforms (Fig. 6a, b). This reflects the syn-depositional growth of the folds at the sediment surface. In other cases, culminations comprise folds and thrusts that not only cause a thinning of the sedimentary cap over the crest of the culmination, but also continue to influence deposition of sediments directly above the cap (Fig. 6c-e). The overlying detrital-rich beds onlap directly onto the structural high created by the underlying fold and thrust culmination Fig. 6c-e). The arching of the sedimentary cap and onlap of younger beds suggests that structures continued to form for some time after deposition of the cap and thereby provides clear evidence for more protracted syn-sedimentary deformation (Fig. 6c-e).

4.5.2. Folding immediately below the sediment surface

The timing of deformation relative to sedimentation is ascertained by examining the thickening or thinning of sediments that overlie culminations created by thrusting and folding. The stratigraphic position of this sedimentary thickening brackets the age of deformation (e.g. Fossen, 2016, p.184).

Thrusts and associated folds are bound by lower and upper detachments to create a duplex in laminated aragonite-rich sediments (Fig. 6f-j). Duplexing creates structural thickening that arches the upper detachment together with 3-4 cm thick panels of overlying sediment that maintain their thicknesses across the culminations, indicating that they were deposited prior to deformation (Fig. 6f-j). The uppermost layers within the arched roof panels are dark-grey detrital-rich beds that display constant 1-2 cm thickness across the underlying duplex and may have influenced mechanical stratigraphy (Fig. 6g, j). The immediately overlying detrital beds exhibit marked thickening off the crest of the culminations suggesting that they were deposited

during or slightly after the duplexing that created the underlying structural high and infilled topography on the lakebed (Fig. 6f-i). These observations, coupled with the lack of a sedimentary cap, suggest that deformation associated with duplexing formed in the shallow sub-surface at depths (<10 cm) that directly influenced deposition of the overlying sequence.

In another case of deformation immediately below the sediment surface, folds and thrusts form above a planar lower detachment and result in duplication and thickening in the fold and thrust package (Fig. 7a-c). This 'lens-shaped' pod is immediately overlain by a 7 cm thick sequence of aragonite and detrital laminae that are arched over the culmination and display little or no variation in thickness. However, a stratigraphically higher 4 cm thick detrital unit erodes into the underlying aragonite laminae and thins to just 1 cm over the crest of the culmination (Fig. 7a-c). The lack of thickness variation in the 7 cm thick arched roof sequence indicates that these sediments were deposited prior to deformation of the underlying sequence, while erosion of this arch, coupled with thinning of the detrital bed, indicates that the culmination formed immediately prior to deposition at this level. The deformation is therefore younger than the sediment it affects and cannot be viewed as synchronous with its deposition, although it is broadly coeval with the thinned detrital bed.

In a further example, fold and thrust beds form an overall lens-shaped pod that is bound by lower and upper detachments. The fold pod depresses the underlying detachment leading to footwall cut-offs of lower beds, while the upper detachment is arched upwards (Fig. 7d-h). The stratigraphic sequence overlying the fold pod maintains its thickness across the culmination and is simply arched upwards. However, beds 0.5 m above the fold pod show thinning over the crest of the culmination while the flanks are thicker. indicating that the underlying fold pod formed in the shallow (<1 m) sub-surface and influenced later sedimentation. This sedimentary signature 0.5 m stratigraphically above the deformed horizon brackets the age of deformation, which is notably younger than the age of the beds it affects.

4.5.3. Stacked erosive surfaces

Evidence for deformation in the shallow sub-surface is provided by multiple unconformity surfaces that are themselves deformed by the growth of an underlying culmination. Upright folding developed along a basal detachment was cut and displaced by a shallowly-dipping thrust (Fig. 7i, j). The overlying sequence is gently folded into a culmination that is truncated by an irregular erosive surface forming a local unconformity (1). Beds overlying this unconformity are also gently warped before being cut by a second unconformity (2) (Fig. 7i, j). The crests of culminations below each unconformity are vertically stacked above one another indicating that there has been no lateral movement across the surfaces. The progressive deformation and arching of older unconformities reflects continued growth of the underlying culmination and indicates that deformation occurred in the shallow sub-surface over a period of time i.e. deformation in the shallow sub-surface occurred at the time of deposition of the overlying 'signature' beds.

5. Criteria used to recognise deeper sub-surface deformation

5.1. Details of detachment surfaces

Bed-parallel detachments are best observed where they truncate earlier cross-cutting features such as steep faults, and can therefore be precisely located within the laminated sediments (e.g. Alsop et al., 2020c) (Fig. 8a-j). In a representative case study from Masada, early conjugate normal faults are cut by bed-parallel lower and upper detachments which form several individual strands that locally anastomose (Fig. 8a-j). The deformed section is positioned between overlying and underlying gypsum horizons that form prominent benches in the Lisan Formation (Fig. 8a-inset). Within the detachment zone, conjugate normal faults defining horsts and grabens are sharply truncated by the upper detachment, although upslope (west) dipping normal faults may rotate into parallelism with the detachment (Fig. 8e-j). Normal faults developed in the overlying sequence are also truncated by the upper detachment demonstrating that it developed after deposition and faulting of this

overburden (Fig. 8c, d) (see section 5.3.). The detachments are sharp planar surfaces that are associated with a buff-coloured mixed detrital and aragonite gouge that has been described from faults in the Lisan Formation (Weinberger et al., 2017; Alsop et al., 2018, 2020d) (Fig. 8d, g, j). Layers of gouge are typically <5 mm thick, although can reach thicknesses of 10 mm where normal faults are truncated (Fig. 8d, g, j). While generally fine grained, gouge occasionally preserves larger (<10 mm) aragonite and detrital fragments. Gouge and associated detachments gently cut across laminae in the overlying sequence, demonstrating that the detachment formed in the sub-surface following deposition of the overburden (Fig. 8f, g).

5.2. Repetition of stratigraphy across the upper detachment surface

Interplay between early steep faults and later bed-parallel detachments can result in stratigraphic repetition (see Alsop et al., 2020c). As stratigraphic repetition is critical evidence for sub-surface deformation associated with detachments rather than erosive truncation, three separate cases of this process are provided to establish the relative timing of cross-cutting events ranked from older (1) to younger (3).

In our first example, early normal faults are cut by later detachments resulting in a repetition of stratigraphy across the detachment surface (Fig. 9a-c). An early detachment (labelled 1 in Fig. 9b) associated with thrusts and folds is subsequently downfaulted into a graben (labelled 2 in Fig. 9b). Continued movement on the detachment (3) then duplicates stratigraphy (Fig. 9c-e). The downfaulted early detachment (1) is at the same stratigraphic level below the 'purple' marker bed as the later detachment (3). Detachments that cut earlier faults may therefore result in a duplication of stratigraphy that is clear evidence of sub-surface repetition and cannot be created through erosion of a normal fault at the surface (Fig. 9e).

In our second case, an early bed-parallel detachment (labelled 1 in Fig. 9f-h) is downfaulted by normal faults that form conjugates (labelled 2 in Fig. 9f-h). Continued movement on non-downfaulted segments of detachments then results in duplication of stratigraphy across the upper detachment (labelled 3 in Fig. 9f-h). The downfaulted early detachment (1) is at the same stratigraphic level below the 'purple' marker bed as the later detachment (3). However, the stratigraphic sequence overlying the detachment is thinned compared to the same stratigraphy in the downfaulted segments, potentially reflecting attenuation of the hangingwall block as it slides downslope.

In our third example, we examine conjugate normal faults that form multiple horsts and grabens that are bound by lower and upper detachments (Fig. 10a-c). The normal faults downthrow portions of well-defined stratigraphy together with early bed-parallel detachments (labelled 1 in Fig. 10d-i,). The non-downfaulted portions of the detachment continue to move, leading to a repetition of stratigraphy across the grabens, while the crests of horsts are marked by portions of stratigraphy that are 'missing' across the detachment surface. The downfaulted early detachment (1) is at the same stratigraphic level as the later detachment (labelled 3 in Fig. 10d-i,). This suggests that the position of detachments is at least partially controlled by mechanical stratigraphy with horizons prone to slip being re-used during different phases of downslope movement. The stratigraphic sequence overlying the detachment is thinned compared to the same stratigraphy in the downfaulted segments, and possibly reflects attenuation during downslope movement. While the normal faults defining horsts and grabens are sharply truncated by the upper detachment, they rotate towards and flatten into the lower detachment to define listric geometries and pockets of gouge where faults meet (Fig. 10a-c, k, l). There is no evidence of stratigraphic repetition across the lower detachment with normal faults rooting downwards onto this basal detachment, rather than cutting it as occurs along the upper detachment. Both the detachments, together with normal faults, are subsequently transected by regional clastic dykes that inject across the previously deformed sequence (Fig. 10 j).

5.3. Detachments cutting faults in the overlying sequence

Normal faults are developed in the Lisan Formation must clearly be younger than the stratigraphy they offset. Such normal faults are subsequently cut by underlying bed-parallel detachments, which are therefore younger than the normal faults and the age of sediment offset by that normal fault (e.g. Alsop et al., 2020c). Where normal faults extend for several metres above the detachment they provide an estimate of the minimum depth at which the intrastratal detachment operated in the sub-surface (e.g. Pratt and Rule, 2021, p.21).

In the first case we describe a normal fault that is cut by a lower detachment zone and which is traced upwards for 1.5 m before being cut by an upper detachment that develops directly beneath a gypsum horizon (Fig. 11a-c). We use a displacement-distance (D-D) plot to compare the amount of displacement of marker beds across the normal fault with the hangingwall distance of that marker from a fixed reference point ('R') (Fig. 11a, d) (e.g. Muraoka and Kamata, 1983; Hughes and Shaw, 2014). As displacement across faults is usually considered to be time dependent then the older parts of faults accumulate the largest offsets, with the point(s) of maximum displacement on D-D plots corresponding to the site(s) of fault nucleation (e.g. Ellis and Dunlap, 1988; Ferrill et al., 2016). Here, the greatest displacement is recorded across the orange and pink detrital beds, suggesting that the normal fault nucleated in these competent marker beds immediately above where the detachment zone subsequently formed (Fig. 11a-d). The normal fault forms a high angle cut-off (>70°) with the lower detachment zone that abruptly truncates it (Fig. 11c, e, f). Where the normal fault is cut by several strands of the detachment zone, it forms a series of segments each displaced by < 30 cm downslope to create a 'staircase' geometry (see Alsop et al., 2020c) (Fig. 11c, e, f). The detachment zone is up to 30 cm thick and is bound by sharp curvi-planar upper and lower detachment surfaces that are linked by downslope-verging thrust faults and associated FATS, which form where the detachment zone ramps upwards through stratigraphy (Fig. 11e, f). Stratigraphy within the intrastratal detachment zone is laterally traceable for several metres and is correlated with the adjacent sequence developed above and below the detachment.

In our second example, conjugate normal faults are traced for 1.5 m above a lower detachment that markedly cross-cuts and truncates them (Fig. 12a, b). The normal faults displace thin MTD horizons before being cut by the underlying intrastratal detachment zone (Fig. 12a, b). This zone, which is bound by upper and lower detachments approximately 15 cm apart, contains beds that correlate with the overlying sequence, indicating stratigraphic repetition across the upper detachment (Fig. 12c, d). Within the detachment zone extensional faults form upslope of downslope verging folds (FATS) that are created where the detachment zone locally ramps downwards into the underlying sequence (Fig. 12c, d). The location of the detachment zone directly beneath a pre-existing MTD horizon suggests that the buried MTD could have influenced mechanical stratigraphy and the position of subsequent intrastratal deformation (see section 5.5.).

In our third case, conjugate normal faults are bound between upper and lower detachments that are themselves overlain by a gypsum horizon (Fig. 12e-g). The lower detachment is associated with multiple strands that are marked by downslope-verging folds and thrusts that are best developed directly below the normal faults (Fig. 12g-i). Antithetic normal faults that dip towards the west and up the regional slope are also associated with downslope-verging folds in the underlying detachment zone. This suggests that the footwalls to these normal faults have moved downslope thereby allowing the hangingwalls to drop down, resulting in excision of stratigraphy along the underlying detachment (Fig. 12g-i).

Finally, we examine normal faults that are truncated by detachments that develop directly beneath a gypsum horizon, but also root downwards onto detachments that form part of a deeper intrastratal detachment zone or system that develops up to 4 m below the gypsum (Fig. 13a-c). Normal faults become listric and sole into the underlying detachment zone (Fig. 13d, e), or alternatively are cut by the lower detachments indicating a coeval development (Fig. 13f, g). The lower detachment zone bounds folds and thrusts that develop downslope of where major listric normal faults sole into the detachment system, while the same unit upslope remains relatively unfolded (Fig. 13a-c). The observation that normal faults may offset folds and thrusts within the detachment zone, but are themselves truncated by the upper and lower detachments bounding this zone,

505 demonstrates that the detachments continued to operate after both the thrusting and normal faulting and could
506 have had a protracted history of downslope movement (Fig. 13f, g). These observations indicate that extension
507 and downslope movement along listric normal faults was transferred to the deeper detachment zone and
508 created local folds and thrusts bound by the detachments (Fig. 13f, g).

509

510 ***5.4. Faults affecting overlying gypsum horizons***

511 Gypsum horizons form prominent benches within the Lisan Formation (Fig. 13a, b). Faults and detachment
512 folds which cut the gypsum, and by inference the detachments that offset these faults, must therefore post-date
513 the creation of gypsum and are therefore potentially much younger than the sediments they affect.

514 *5.4.1. Thrust faults* - Deeply-rooted thrust faults may ramp upwards and deform overlying gypsum horizons
515 (Fig. 14a, b). Thrusts develop early (labelled 1 in Fig. 14b) and are then cut by detachments (labelled 2 in Fig.
516 14b) that displace the thrust ramps downslope towards the east. Detailed analysis reveals several strands of
517 anastomosing detachments that are concentrated beneath the competent gypsum horizon, suggesting that the
518 presence of gypsum has influenced the position of later intrastratal detachments (Fig. 14a, b).

519 *5.4.2. Normal faults* - Normal faults cut stratigraphy as well as overlying gypsum horizons where they create
520 local folds (Fig. 14c, d). Normal faults are later displaced by bed-parallel detachments with the upper block
521 moving downslope towards the east Fig. 14c, d). Several anastomosing detachment strands form ~1 m below
522 the gypsum horizon suggesting that their position is influenced by this horizon.

523 *5.4.3. Detachment folds* - Detachment folds generally form classic buckle fold geometries and are created
524 where a sequence has moved directly above an underlying detachment (e.g. Butler et al., 2020). Detachment
525 folds can be cut by subsequent thrust ramps (break-thrust folds) or simply be carried on the underlying
526 detachment. In our example, detrital-rich beds form class 1B (parallel) folds while the aragonite-rich beds
527 form Class 1C or Class 2 (similar) folds with thickened hinges indicating that the detrital-rich beds are more
528 competent at the time of folding (Alsop et al., 2020b, 2021a, b) (Fig. 14e). The buckle folds lack the 'billow'
529 shape noted for surficial folds and are commonly asymmetric with vergence directed downslope towards the
530 east. Detachment folds deform overlying gypsum beds that form competent horizons, and such deformation
531 must have operated after the gypsum horizon had precipitated (Fig. 14e) (Alsop et al., 2020c, p.6). In
532 summary, the deformation of gypsum horizons by underlying structures indicates that deformation not only
533 post-dates the gypsum and is therefore sub-surface, but that intrastratal detachments are concentrated beneath
534 the competent gypsum reflecting its role in the mechanical stratigraphy.

535

536 ***5.5. MTDs displaced by later faults***

537 Where MTDs and adjacent stratigraphy are cut by later faults that extend for several metres through the
538 overlying sequence, the later faulting significantly post-dates the MTD after it has become buried in the sub-
539 surface. In our example, MTDs form thin (<1 m) horizons that develop at the sediment surface and are
540 subsequently blanketed by a sedimentary cap that is deposited out of suspension (see section 3.3.). Following
541 further deposition and burial by overlying sediments, the whole sequence is subsequently cut by later normal
542 faults that transect several metres of stratigraphy above the MTD (e.g. Fig. 12a-d). This indicates that the
543 normal faults are unrelated to the original MTD as they offset both it and its associated sedimentary cap, with
544 the MTD itself having been sub-surface at the time of faulting.

545 In a further instance, multiple thin MTDs are offset by normal faults that are traced for 2 m above
546 detachments that form below the MTDs (Fig. 14f-h). The MTDs contain downslope verging folds and are
547 overlain by sedimentary caps which are displaced by the normal faults (Fig. 14f-h). This indicates that normal
548 faults entirely post-date the MTDs and their sedimentary caps, and that the lower detachment was developed at

least 2 m below the surface. These relationships collectively indicate that MTDs formed at the sediment surface while later normal faults and detachments developed in the sub-surface after the sequence was buried.

6. Sediment injections into overlying sequences

Where sediment becomes over-pressured and fluidised, it can mobilise and intrude into adjacent sequences to create sediment injections (e.g. Baldry, 1938, p352; Brown, 1938, p.396; Smith, 2000: Törő and Pratt, 2016, p.191) (Fig. 14i-k). Sediment injections may taper upwards indicating intrastratal injection up into overlying beds and intrusions are therefore younger than the stratigraphy they cross-cut (e.g. Törő et al., 2016, p.222; Törő and Pratt 2016, p.191) (Fig. 14i-k). In some cases, sediment injections are rooted directly into and develop off underlying detachments (e.g. Baldry, 1938, p.352; Brown, 1938, p.396; O'Leary and Laine, 1996, p.309), indicating that these detachments that generate the injections are also younger than the overlying sequence and therefore formed in the sub-surface (Fig. 14i-k). Sediment injections cut directly across the upper detachment suggesting that they formed shortly after movement on the FATS had ceased (Fig. 14i-k).

6.1. Injections above a thrust duplex

Gravity-driven FATS that are bound above and below by intrastratal detachments in the otherwise largely undeformed sequence may be associated with sedimentary injections (Fig. 15a-e). The sediment injections are formed of a fine-grained mixed aragonite and detrital matrix that contains larger (<10 mm) clasts of aragonite and detrital fragments, presumably sourced from the adjacent Lisan Formation (Fig. 15a-e). The injections take the form of rounded 'blobs' with no discernible deformation or offset of adjacent laminae in the host sediment. The gravity-driven FATS comprises folds and imbricate thrust ramps which join into the upper and lower detachments to create a duplex with a minimum of 0.5 m of overburden (Fig. 15a-c) (see Alsop et al., 2021a). The lower detachment locally cuts down section in the direction of transport and may also repeat stratigraphy from the footwall sequence (Fig. 15a-d). The upper detachment comprises an anastomosing system of braided strands that truncate and repeat stratigraphy, as well as truncating underlying folded layering (Fig. 15d, e). The injections form directly along the upper detachment, with traces of injected sediment preserved along the detachment surface, indicating that the injections were sourced from sediment that was mobilised along the detachment (Fig. 15a-e).

In a second example, sedimentary injections that form minor (cm-wide) dykes are displaced by thrust imbricates within FATS and also by bed-parallel detachments (Fig. 16a-c). Sedimentary dykes do not offset adjacent laminae, which they sharply cross-cut, although local down-warping of laminae and the underlying detachment suggests that the dykes were relatively competent at the time of deformation (Fig. 16d, e). Note that these sedimentary dykes appear to be sourced from adjacent to lower detachments in the FATS and should not be confused with the larger and extensive regional set of clastic dykes that cut across MTDs and FATS in the Lisan Formation (Levi et al., 2006a, b). The dykes act as displacement markers and suggest offsets of up to 40 cm across detachments, although an inability to correlate dykes across some detachments suggests displacement could be larger (Fig. 16b, c). Sedimentary dykes that develop above upper detachments and cut overlying stratigraphy are significant as they demonstrate that the overlying sequence was already deposited at the time of the FATS deformation that created injections (i.e. the deformation must be sub-surface).

6.2. Injections along upper detachments

In this example the gravity-driven FATS is bound above and below by bed-parallel detachments that are subsequently cut and displaced by a normal fault that extends into the underlying and overlying sequence for >0.5 m (Fig. 16f-h). No sedimentary cap is developed above the folds and thrusts within the FATS, and the upper contact is marked by a detachment that forms a sharp planar boundary above which the sedimentary injections develop (Fig. 16h-j). The upper detachment is marked by sediment injections that 'pond' upslope in

the hangingwall of the normal fault (Fig. 16h, j). The normal fault locally cuts the injection, suggesting that injections formed during movement along the upper detachment and shortly before the later normal fault that cross cuts both the detachment and injection. The injection does not offset the laminae in the host sediment, although it is notable that some detrital layers are thicker on the upslope flank of the injection (Fig. 16i). This suggests that there may have been a component of later layer-parallel compaction and thickening on the upslope margin of the injection that acted as a local buttress and barrier to continued downslope movement.

In summary, sedimentary injections that develop from upper detachments and cut overlying stratigraphy are significant as they demonstrate that the overlying sequence already formed an overburden at the time of the deformation that created the injections (e.g. Törő et al., 2015, p.222). As such, they provide critical evidence that the FATS and associated deformation must be sub-surface.

7. Reactivation of surficial MTD horizons by later MTDs

7.1. Folding of earlier MTD horizons

Where MTDs and their associated caps are folded or thrusted then it is clear that at least two episodes of surficial deformation, and potential seismicity, are recorded by the MTDs. In this example, both an older MTD (1) and younger MTD (2) are folded and repeated around a later recumbent fold that is oblique to the section (Fig. 17a-d). MTD 1 contains a 5 cm thick panel of undeformed aragonite-rich laminae that locally divides this MTD into two sub-units (Fig. 17 a-d). MTD 2 is marked by a sedimentary cap with a pronounced erosive base that is repeated around the later fold closure, while the top of the sedimentary cap remains unfolded (Fig. 17a-d). This indicates that the folding formed and continued during deposition of the sedimentary cap and is therefore a later stage feature of MTD 2 (Fig. 17a-d). This highlights the complications that can develop where locally undeformed beds divide MTDs into two sub-units (MTD 1a and b), or where sedimentary caps are repeated around fold closures (MTD 2). In both cases the duplication of MTDs and caps is a consequence of processes operating during MTD development and should not be viewed as a later process (Fig. 17a-d).

7.2. Thrusting of earlier MTD horizons

In this example, an older MTD 1 and its overlying sedimentary cap are cut across by younger thrusts associated with MTD 2 (Fig. 17e-h). The thrusts displace the sedimentary cap of MTD 1 and tip out into asymmetric folds in MTD 2 that are overlain by an undeformed sedimentary cap (2) (Fig. 17e-h). This deformed sequence that conceals two separate MTDs is itself overlain by a detachment system that contains a FATS duplex (3) (Fig. 17g-j). The roof to the duplex is arched over the culmination where the 50 cm thick overburden is locally truncated by an erosive surface, indicating that the duplex formed in the shallow sub-surface. The modification of MTD 1 by the overlying MTD 2 demonstrates that MTDs may conceal more than one episode of deformation that in many cases can only be distinguished by examination of the sedimentary cap that overlies the older MTD.

8. Reworking of surficial MTD horizons by secondary sub-surface deformation

MTD horizons represent major heterogeneities within a sedimentary sequence due to the mixed and irregular shape of the unit, internal faulting, folding and thrusting that disrupts original layers, and expulsion of fluids from within deforming sediments (e.g. Alsop et al., 2021a). Such mechanical heterogeneities caused by MTDs are particularly pronounced in otherwise well-bedded or laminated lacustrine sediments such as developed in the Lisan Formation. The mechanical heterogeneity introduced into an otherwise relatively uniform sequence by MTDs during surficial deformation may be utilised by later sub-surface deformation that focuses secondary intrastratal detachments and associated structures next to MTDs (Fig. 1c). Faults that cut the overburden above MTDs and extend downwards into detachments next to the MTD demonstrate that the detachments formed in the sub-surface after the MTD had become buried.

8.1. Secondary detachments above earlier MTDs

As noted above, secondary deformation becoming localised along the tops of pre-existing MTDs can result in duplexes being created that arch the overlying roof panel (Fig. 17h-j). In a further case that involves reworking and reactivation of earlier normal faults, upper and lower detachments bound a FATS that creates duplexes developed directly above detrital-rich MTDs (Fig. 18a, b). Stratigraphy is repeated both above the lower detachment and beneath the upper detachment, indicating that these truncating structures are detachments rather than erosive surfaces (Fig. 18a, b). Early normal faults that offset the MTD are locally reactivated by thrusting, while later normal faults cut across the entire detachment zone (Fig. 18a, b).

Normal faults can also form conjugate systems between detachments that develop above pre-existing MTDs (Fig. 18c-f). In some instances, upper and lower intrastratal detachments appear to be 'sandwiched' between underlying MTDs and thick overlying detrital-rich beds (Fig. 18c-f). The MTD contains billow folds with 'fanning' axial planes that are truncated by an irregular erosive surface at the base of the overlying sedimentary cap (Fig. 18f). The lower detachment forms a sharp contact a few cm above the sedimentary cap of the underlying MTD, while the upper detachment is developed within aragonite-rich beds and abruptly truncate normal faults that form a conjugate system between the two detachments (Fig. 18c-f). It is important to note that the upper detachment is within aragonite-rich units and is not therefore an erosive surface at the base of the overlying detrital-rich beds, while the lower detachment is also unrelated and separated from erosive processes along the sedimentary cap (Fig. 18f). In summary, the upper and lower detachments bound a zone of conjugate normal faulting that developed after deposition of the MTD, and also the overlying detrital beds that formed an overburden to the sub-surface intrastratal deformation.

8.2. Secondary detachments below earlier MTDs

Detailed examination is required to distinguish truncation of pre-existing structures by erosive surfaces that form along the base of MTDs, from intrastratal detachments that may subsequently localise along the base of MTDs and also cut across earlier faults. In our first example, a detachment forms beneath a MTD that contains large (>20 cm) clasts of aragonite, and which is itself overlain by a thick sequence of detrital beds (Fig. 19a-c). Normal faults are abruptly cut by the detachment that forms an extremely sharp truncation (Fig. 19a-c). The detachment is a planar bed-parallel surface that is associated with a thin (<1 cm) mixed gouge unit that is especially well developed where the detachment intersects detrital-rich beds in the footwall of normal faults (Fig. 19d, e). A critical observation is that a thin (2 cm) panel of aragonite-rich laminae is preserved above the detachment and below the base of the MTD (Fig. 19d, e). This panel of undeformed laminae proves that the truncation of the underlying normal faults has been created by the intrastratal detachment, rather than erosion along the base of the MTD which does not actually intersect the faults (Fig. 19d, e).

In the second case, a series of thin MTDs are developed that are offset by a listric normal fault and later detachment surface (Fig. 19f-h). The listric normal fault offsets MTD 1 and MTD 2 and is cut by an overlying bed-parallel detachment (Fig. 19f-h). A thin (3 cm) panel of aragonite-rich laminae is preserved above the detachment and below the base of the overlying thicker (25 cm) MTD 3 (Fig. 19i, j). In detail, thin mm-scale aragonite laminae that overlie the detachment are locally cut out, indicating that it is a later tectonic excision rather than an erosive unconformity (Fig. 19i, j). The thin panel of undeformed sediment that separate the detachment surface from the base of MTD 3 prove that the MTD has not created the truncation of faults. In summary, MTDs represent heterogeneity below which later sub-surface detachments may nucleate. It is critical to recognise thin panels of undeformed strata that demonstrate it is the intrastratal detachment that cuts the earlier faults rather than the erosive base of an MTD.

9. Discussion

The criteria described above to distinguish surface versus sub-surface deformation in gravity-driven MTDs and FATS developed around the Dead Sea are largely based on classical stratigraphic principles (cross-cutting relationships etc.) as well as fundamental observations linked to structural geology. As such, they may be equally applicable to deformation of sediments in other basinal settings, including accretionary complexes where the distinction between tectonic features and gravity-driven structures formed within soft-sediments may become more problematic (see Ogawa and Mori, 2021 for details).

9.1. Which surface and sub-surface deformation models are applicable to MTDs?

Sequential failure models have been typically applied to MTDs, whereby each MTD represents a separate failure event at the contemporary sediment surface that sequentially build up with deposition of new overlying sediment (Figs. 1a, 20a, b). Each deformed horizon therefore represents a new failure event that broadly corresponds to the age of the affected sediment (e.g. Basilone et al., 2014; Van Loon et al., 2016). Where pre-existing buried MTDs act as competent horizons in the sedimentary sequence, they can localise later intrastratal detachments and focus secondary failure along the margins of the MTD (Figs. 1c, 20a, c). Conversely synchronous failure models, where single failure events concurrently generate multiple deformed horizons at the surface and sub-surface, have so far largely been applied to sequences that lack downslope movement (e.g. Gibert et al., 2011) (Figs. 1b, 20a, d). Several deformed horizons may be generated during a single failure event and affect sediments that are significantly older than the age of the event (Figs. 1b, 20a, d).

9.1.1. Evidence for surficial deformation and the sequential failure model

The surficial failure model summarised in Fig. 1a is usually applied to both gravity-driven downslope deformation of unlithified sediments to create slumps and MTDs, and also where there is a lack of downslope movement and deformation is driven by contrasts in density of adjacent beds (e.g. Owen, 2003 for a review; Van Loon et al., 2016). Deformation is considered to be contemporaneous with deposition of each layer at the surface (e.g. Rossetti and Goes, 2000; Basilone et al., 2016, p.320; Kumar et al., 2021), with erosion above slump folds indicating that folding took place at the surface prior to deposition, and ‘blanketing’ by overlying beds (Ortner and Kilian, 2016, p.357). Surficial deformation and remobilisation of sediment occurred at depths of up to 20 cm from the sediment surface in Chilean lakes, with this depth increasing with greater slope angles and larger magnitude earthquakes (Molenaar et al., 2021). The stratigraphic record preserved by seismo-turbidites in basinal sediments is crucial to recognise earthquake-induced surficial deformation of sediments in slope settings (Molenaar et al., 2021).

The significance of turbidites that directly overlie units of SSDs in the sedimentary record from the Dead Sea has been recognised and analysed by Lu et al. (2021b, c). The link between deformation and the sedimentary record demonstrates that SSDs in these cases formed at the sediment surface in the depocentre of Lake Lisan. Within the case study area, six individual MTDs up to 2 m thick were analysed by Alsop et al. (2016). Each of these MTDs is separated from the others by undeformed beds, and each is overlain by a sedimentary cap with a locally erosive base that was deposited out of suspension after the failure event. These observations are summarised in Fig. 20a, b and collectively indicate that each individual MTD sequentially formed at the sediment surface during recurrent failure of the gentle slope.

9.1.2. Surficial deformation horizons that laterally bifurcate

In some instances, a single deformed horizon may bifurcate laterally into two or more deformed units at different stratigraphic levels and separated by intervening undeformed beds (e.g. Gibert et al., 2011, Morsilli et al., 2020). The upper deformed sub-unit may remain at the sediment surface, while the lower bifurcated unit will develop in the shallow sub-surface. This has been interpreted as a result of liquefaction at different levels in a multi-layered system during a single earthquake (Gibert et al., 2011). Morsilli et al. (2020) further suggest that the intervening undeformed sediments affected porosity and acted as a barrier to fluid flow and thereby facilitated liquefaction in adjacent sediments. Both of these cases focus on SSDs and seismites in sections

which are marked by fluidisation and liquefaction structures associated with density-driven deformation. They appear to lack significant preferred orientation and development of asymmetrical folds and faults that characterise downslope mass transport of sediments (Morsilli et al., 2020, p.12).

Within the Lisan Formation, examples of bifurcating deformed horizons are developed on the metre-scale where 5 cm thick panels of undeformed aragonite laminae locally separate MTDs into upper and lower sub-units (Figs. 17a-d, 19k, 20a, b). Only a single sedimentary cap is developed (above the upper unit) and this provides a reference for the position of the surface at the time of deformation. Despite the extensive exposures around the Dead Sea Basin, we find no evidence for larger scale bifurcating of MTD systems where individual slumps and MTDs are traced downslope for 500 m and consistently maintain distinct stratigraphic levels with each deformed horizon overlain by an individual sedimentary cap (Alsop et al., 2016). This may reflect the largely 'layer-cake' stratigraphy within the varved lake sediments, together with the simple bilaminate nature of sediments that comprises only aragonite- and detrital-rich beds. Clearly, even if deformed horizons were to bifurcate laterally into several individual horizons at different stratigraphic levels, there is still only one interface between sediment and the water column, and hence only a single sedimentary cap will form.

9.1.3. Evidence for sub-surface intrastratal deformation of buried MTDs and the secondary failure model

Pre-existing MTDs that formed at the surface can subsequently affect the mechanical stratigraphy of a sedimentary sequence and control where later secondary intrastratal deformation is focussed in the sub-surface (Figs. 1c, 20a, c). In a highly perceptive paper, Brown (1938) noted that sediment that had previously undergone folding nearer the surface could, after further burial, be overprinted by discrete, downslope-directed slide surfaces. Brown (1938, p.36) declared that "These large-scale slides will be superimposed on beds which have already suffered from sealing-wax flow (folding) and rupture on a small scale, mostly along bedding-planes". More recently, Sammartini et al. (2021) have shown from silt-dominated lacustrine sediments that when surficial MTDs are buried to depths >1.5 m, they have greater shear strengths than undeformed sediment of equivalent depth. It is considered that increasing deformation and lateral compaction in the central part of MTDs may have resulted in reduction in porosity and expulsion of water leading to increased absolute shear strength in the MTDs (Sammartini et al., 2021, p14). Similar relationships are recorded by Daxer et al. (2020, p.251) who note that slope failures in lacustrine sediments generally occur at <1 m depth below the sediment-water interface, with the top of older MTDs controlling where the basal slip surface of younger failure events develops. Sub-seismic scale MTDs may clearly play a role in acting as baffles and barriers to hydraulic flow across a range of scales in the sub-surface (e.g. Steventon et al., 2021).

Within the Lisan Formation, shallow sub-surface FATS can create duplexes where water is considered to be expelled from folds and thrusts and migrates upwards to weaken the overlying sequence and thereby help drive the upper detachment to the system (Alsop et al., 2021a). The consequence of this is that such deformed horizons become over-compacted and then act as baffles to later fluid flow. Overlying MTDs may themselves also act as barriers to fluid flow and influence where younger sub-surface intrastratal deformation focuses. MTDs and sub-surface FATS exert significant controls on subsequent fluid flow, and hence the localisation of secondary deformation, which is focussed adjacent to older deformed levels (Figs. 17-19).

9.1.4. Evidence for sub-surface intrastratal deformation and the synchronous failure model

The synchronous failure model involves deformation in both the surface and sub-surface during a single event (Fig. 1b) and therefore necessitates the identification of deeper-seated structures (Fig. 20a, d). Evidence for the sub-surface deformation of unlithified sediments has been provided in a number of previous studies including Budillon et al. (2014) who describe relatively deep gravity-driven slope failures which are associated with recurrent sediment failures along the seabed, and which also create internal slip planes within the MTD. Evidence for sub-surface deformation has also been presented by Moretti and Van Loon (2014, p.167) who suggest that deformation in marginal lake areas can take place at depths of up to 9 m in some environments. In

this setting, deeper water-saturated sediments are prone to liquefaction and deformation, especially where overlain by less permeable sediments (e.g. Moretti and Van Loon, 2014, p.167). Sub-surface deformation of unlithified sediments has also been reported from Lake Superior where high resolution seismic and sonar data from fine grained glacio-lacustrine sediments has revealed polygonal systems of normal faults that penetrate unlithified sediments (Wattrus et al., 2003). The faults terminate at a lower bed-parallel intrastratal surface where sediment has mobilised and flowed laterally at depths of 10 m below the sediment-water interface, presumably in response to movement on the overlying faults (Wattrus et al., 2003).

In a further example of the synchronous failure model, Auchter et al. (2016) suggest that the rapid emplacement of a thick MTD creates intrastratal deformation and thrust duplexing in the underlying sequence. Three intrastratal deformation zones are considered to have developed synchronously during this single event, with positions partially controlled by the morphology of depositional sand lobes within the sequence. Stratigraphic thicknesses suggest that these sub-surface intrastratal failures formed concurrently at depths of ~60-70 m, ~30-40 m, and ~10 m below the contemporary sediment surface (Auchter et al., 2016, p.20).

Seismicity linked to post-glacial rebound in late Pleistocene lacustrine deposits results in liquefaction occurring at depths of up to 0.6 m (Belzyt et al., 2021, p.12). Deformation that creates ball and pillow structures, load casts, and broken laminae, is considered to develop within decimetres of the sediment surface, with each SSD horizon generally forming during separate events. However, Belzyt et al. (2021, p.20) note that sediment injections intrude from underlying SSDs into the overlying sequence and cross-cut the younger SSD horizons, leading them to suggest that some deformed horizons that lack overlying erosional truncations could have developed concurrently during a single failure event. The lack of erosive surfaces truncating underlying structures meant that Belzyt et al. (2021) were unable to determine the maximum number of seismic triggering events for SSDs, although the number of erosive surfaces provides a minimum estimate.

Although many MTDs recorded in the Lisan Formation preserve sedimentary caps with erosive bases that formed at the sediment surface, there are also cases of deformed horizons where no cap or erosive surface is present (e.g. Figs. 8-13, 20a, d). In these cases the deformed horizon is bound by upper and lower bed-parallel detachments that form during sub-surface intrastratal deformation and the age relationship with surficial sediments is therefore lost.

9.2. What are the key diagnostic criteria to identify surface and sub-surface deformation?

Distinguishing gravity-driven surficial deformation and gravity-driven sub-surface structures might not be straightforward as both are governed by the same slope that creates similar kinematics and comparable orientations of downslope-verging structures. For instance, folds created above sub-surface detachments share the same orientation as folds formed in earlier MTDs (Alsop et al., 2020c). These movement directions have also been corroborated by magnetic fabrics in AMS studies of MTDs (Weinberger et al., 2017) confirming that movement is directed downslope around the basin. The orientation of folds and thrusts in MTDs or FATS is therefore of little value in distinguishing their mode of origin and further criteria need to be established.

9.2.1. Recognising erosive truncation versus bed-parallel detachments

It is crucial to distinguish surficial processes that create erosive surfaces from deeper-seated structures, such as intrastratal detachments that also cut across pre-existing structures but could be much younger than the overlying stratigraphy (Figs. 1b, 20a, b, d). Törő et al. (2015) record seismically generated intrastratal deformation in lacustrine deposits that lack erosive truncations, leading to an interpretation of intrastratal deformation rather than processes operating directly on the lake floor. Van Loon et al. (2016) and Belzyt et al. (2021) have also recognised the importance of identifying erosive surfaces in establishing surficial SSD in liquified horizons. If a detachment surface is established, then the associated deformation could have formed at depth in the sediment pile and the link to the surface (and precise age of deformation) is then

broken. While some erosive surfaces are planar, others display significant relief on the scale of metres, and are also irregular on the cm-scale (e.g. Fig. 3h, i). Such rugosity severely hinders displacement along a detachment surface and is therefore a characteristic feature that supports an erosive surficial origin.

Issues around establishing the true nature of a bed-parallel surface are more likely to arise when dealing with planiform erosive surfaces that display similar geometries to detachments. In some cases, bed-parallel slip is associated with stratabound horizons of microfractures that help identify intrastratal deformation that formed at depth below the sediment surface (e.g. Grimm and Orange, 1997). The difficulty in recognising bed-parallel slip that creates glide planes at the base of sediment packages has also been highlighted by Ortner (2007, p.112). Ortner (2007) recognised local ramps that enable identification of bed-parallel glide planes that operated at depths of 6-7 m below the sediment surface during tilting associated with regional tectonics. Basilone et al. (2014, p.320) described translational slides in deepwater carbonates where sediment moved downslope above a detachment with the slide block maintaining its coherency. The detachment zones contain units of relatively undeformed strata that are bound by lower and upper detachments (e.g. Basilone et al. (2014, p.313, their fig. 3). Regional uplift and overall tilting of the sea floor is, in this case, considered to drive the downslope movement along relatively discrete detachments (Basilone, 2017).

Within the Lisan Formation, no regional tilting has developed and the bed-parallel detachments translate overlying sediments down gentle (<1°) slopes towards the depocentre of the basin (Alsop et al., 2020c). Detachments are generally planar but are recognised by their offset of older faults (Fig. 20a, d). They are considered to operate within the upper 20 m of the Lisan Formation, with direct measurement of 10 m thick overburden above a detachment being deformed (e.g. Alsop et al., 2021a, p.3. their fig. 1c, d)

9.2.2. Recognising sedimentary caps versus fluidisation that creates erosion in the sub-surface

It has been suggested from experimental work that unconformable surfaces that truncate underlying structures may potentially develop within buried sedimentary sequences (Moretti et al., 1999, p.376). In this scenario, silty sand is considered to undergo selective fluidisation and be transported upwards through overlying medium-coarse grained sand to create an upper layer of fine-grained sediment. This fine-grained horizon will be discordant and can truncate structures in the underlying coarser sand layer, while the top of the layer is horizontal and parallel to the overlying beds (Moretti et al., 1999, p.376). These experimental observations suggest that unconformable and erosive relationships could potentially develop in the sub-surface and are therefore not necessarily diagnostic of surficial processes. The creation of unconformable surfaces in the sub-surface by diffuse fluidisation and elutriation of fine sediment does not leave clear evidence of focussed upward movement of fluids and could therefore be problematic to recognise in the sedimentary sequence.

Within the Lisan Formation, the sedimentary caps that overlie erosive surfaces contain larger cm-scale fragments of folded aragonite laminae, graded aragonite grains, evidence of currents resulting in cross laminations, and overall scouring resulting in irregular wave-like erosive surfaces along the base of the cap (e.g. Alsop and Marco, 2011; Alsop et al., 2016, 2021a). In addition, laminae, although folded and faulted, are generally preserved in the underlying deformed horizon, while caps thicken in the hangingwall of sedimentary faults to create ‘growth’ sequences (Figs 3h, i, 6a-e). These observations collectively indicate that sedimentary caps and underlying erosive surfaces in the Lisan Formation were created at the surface prior to deposition of the overlying sedimentary sequence that subsequently buried the unconformities.

9.2.3. Recognising sedimentary caps versus gouge along detachments

Given the importance of sedimentary caps in recognising surficial deformation, it is critical that they are clearly distinguished from gouge or breccia that forms during slip events (e.g. Weinberger et al., 2017; Alsop et al., 2020c) Examination of horizons of carbonate breccia led Van Loon et al. (2013) to suggest that breccia layers with vertical clasts may have formed in the sub-surface after deposition of overlying beds that acted as a seal. They propose that although original brecciation developed on the sediment surface, the subsequent

867 rotation of clasts to vertical attitudes reflects high pore fluid pressures leading to rapid fluid escape (Van Loon
868 et al., 2013). Vertical clasts are atypical of sedimentary deposition and developed in the shallow sub-surface
869 after the deformed horizon was buried by overlying sediments.

870 Within the Lisan Formation, gouge that is developed along steep-moderate dipping normal faults or
871 thrusts is readily identified due to the cross-cutting nature of the fault plane (e.g. Alsop et al., 2018). However,
872 gouge that forms along discrete bed-parallel detachments can be more problematic as it remains largely
873 parallel to the adjacent sedimentary layers (Fig. 8a-j). Gouge along detachments typically has a buff colour
874 that reflects the mixing of aragonite and detrital layers, and is especially well developed where the detachment
875 transects adjacent laminae. In addition, sediment injections may develop from the gouge layers and intrude
876 overlying beds (Figs. 15, 16), demonstrating that the gouge is created during high fluid pressures that develops
877 along the detachment and is inconsistent with deposition of a sedimentary cap at the surface.

878 *9.2.4. Recognising depositional infilling versus hydroplastic thickening of beds*

879 Over the past century it has been increasingly recognised that depositional infilling of underlying structures is
880 a key piece of evidence in support of surficial deformation with Miller (1922, p.602) noting that surficial
881 deformation is marked by "the distinct evidence of the filling of the depressions on the upper surface of the
882 corrugated zone before the general layers of overlying materials were laid down". Although it is commonly
883 observed that sediments will locally thicken and thin as they 'drape' over and fill irregular bathymetry at the
884 sediment-water interface (e.g. Basilone, 2017), beds may also display changes in thickness where they
885 undergo folding and thrusting associated with hydroplastic deformation in the sub-surface. In the Lisan
886 Formation, sedimentary caps frequently infill underlying erosive scours resulting in pronounced changes in
887 thickness to the cap (Fig. 3h, i). MTDs can also display growth and thickening in the hangingwall of normal
888 faults, indicating that the faults were active at the time of deposition (Fig. 5c-h). In other cases, the
889 sedimentary packages immediately above FATS maintain thickness across underlying culminations, and it is
890 detrital units higher in the stratigraphy that record changes in depositional thicknesses. The age of the
891 sediment package that displays changes in syn-tectonic thickness provides a bracket on the timing of the
892 deformation. It is normally detrital beds that record thickness changes as these units are deposited more rapidly
893 during flood events and in general form thicker units. Continued deformation may fold these growth
894 geometries (Fig. 7), that locally display onlapping relationships onto culminations indicating the surficial
895 nature of the deformation (Fig. 6c-e). Alternatively, aragonite layers can display marked thickness variations
896 around folds that were created in the sub-surface. In this case, the attenuation and thinning of units is achieved
897 though hydroplastic deformation that operates in the sub-surface (Figs 13f, g, 16f-h). In summary, depositional
898 infilling is normally accommodated by detrital-rich beds that are rapidly deposited from flood events, whereas
899 hydroplastic folding leads to thickening and attenuation concentrated in aragonite beds (Alsop et al., 2020b).

900 *9.2.5. Recognising surficial MTD folding versus sub-surface detachment folds*

901 Although there has been considerable effort to distinguish folds formed during SSD from those created during
902 hard rock tectonism in lithified sequences (e.g. Elliot and Williams, 1988; Waldron and Gagnon, 2011; Alsop
903 et al., 2019, 2020), there has been rather less work on discriminating between soft-sediment folds formed
904 directly at the sediment surface versus those created during intrastratal deformation in the sub-surface. While
905 much of the folding associated with SSD is frequently assumed to develop at the sediment surface, folding in
906 the sub-surface is also described with Ortner and Kilian (2016, p.350) noting that "Subsurface sediment
907 mobilization may also create soft-sediment folds that reflect either the downslope direction or fluid movement
908 after break of the seal (Ortner, 2007)." Distinguishing surficial and sub-surface intrastratal folding can be
909 relatively straight forward where folds are truncated by overlying erosive surfaces and sedimentary caps that
910 form at the surface (Fig. 20a, b), but is perhaps more problematic where such features do not exist and fold
911 styles and geometries become more important.

912 The upright billow folds that form in surficial MTDs of the Lisan Formation (Fig. 4a-g) are interpreted
913 to be a consequence of horizontal shortening associated with coaxial dominated deformation at the initial stage
914 of slumping (Alsop and Marco, 2011, p.449). The upright folding could also reflect density-driven fold
915 initiation where variations in density of aragonite-rich and detrital-rich beds lead to vertical movement driven
916 by Rayleigh-Taylor (inverse density gradient) or Kelvin Helmholz (normal-density gradient) instabilities (e.g.
917 Hefeitz et al., 2005; Wetzler et al., 2010; Lu et al., 2017, p.15; Lu et al., 2021, p.6.). The observation that
918 underlying aragonite-rich beds penetrate upwards as narrow antiformal 'fingers' into the overlying detrital-rich
919 beds suggests that the aragonite beds are less dense than the detrital-rich beds. We speculate that this partially
920 reflects the 'stellate' form of needle-like aragonite crystals that may trap significant volumes of interstitial
921 water, thereby reducing the overall density of aragonite-rich beds (see also section 9.3.3.). In other cases, the
922 detrital-rich beds display buckle folds (Class 1B parallel folds, Ramsay, 1967) suggesting that the detrital-rich
923 beds were more competent and formed via horizontal compression above a basal detachment in the sub-
924 surface (Figs. 7a-h, 12c-d) (see Alsop et al., 2020b). The initiation of folding in MTDs will therefore take a
925 variety of forms depending on the arrangement of beds of differing densities, and the amount of dewatering
926 that may already have occurred in beds prior to downslope movement.

927 *9.2.6. Recognising truncation of overlying structures*

928 Structures such as faults or folds may be truncated by either overlying erosive surfaces or by overlying
929 detachments, and as such, truncation from above is non-diagnostic. However, where faults are cut across by
930 underlying structures then this becomes a key observation as erosive surfaces clearly cannot truncate features
931 in the overlying sequence that was not deposited at the time of erosion (e.g. O'Leary and Laine, 1996, p.311).
932 Rotational slumps studied by Basilone et al (2016) comprise folded and faulted beds that are draped by
933 overlying undeformed beds indicating surficial deformation during creation of MTDs. Conversely, Basilone et
934 al. (2016, p.319 their table 1) also recognise a second type of 'gravity-slide' packages comprising relatively
935 undeformed beds that are shown to have an upper surface that truncates folds in the overlying sequence. This
936 relationship suggests that the overlying sediments were already deposited at the time of deformation, which
937 was therefore sub-surface. In addition, Pratt and Rule (2021, p.22) have used the length of faults developed in
938 overburden to suggest that intrastratal sliding occurred under 'tens of centimetres' of burial.

939 Within the Lisan Formation, normal faults that offset stratigraphy are themselves truncated by
940 underlying detachments (Figs. 11a-f, 12a-d, 14f-h, 20a, d). Similarly, aragonite-detrital laminae can also be
941 transected by underlying detachments, although the low-angle nature of the cut-offs makes such relationships
942 more difficult to identify (e.g. Fig. 8g). Normal faults therefore act as steep markers that allow underlying bed-
943 parallel intrastratal detachments to be identified (Alsop et al., 2020c). Where normal faults extend for several
944 metres above detachments then the detachment must be younger than the sediments affected by the normal
945 fault. This provides a minimum estimate for the depth at which the detachment operated. In the case of the
946 Lisan Formation this depth is typically 5 m before exposure is lost (Alsop et al., 2020c), although deformation
947 may potentially be up to 20 m below the surface (Alsop et al., 2020c). One of the important keys to identifying
948 and understanding bed-parallel detachments that operate in the sub-surface is the truncation of *overlying* faults
949 that extend upwards through stratigraphy towards the surface (Fig. 20a, d).
950

951 **9.3. What controls where and when sub-surface deformation localises?**

952 *9.3.1. Control on sub-surface deformation by de-watering and 'seismic strengthening'*

953 The focussing of sub-surface deformation into particular horizons reflects the overall strength of the sequence,
954 which is highly dependent on dewatering and build-up of fluid-pressures in the sedimentary pile (e.g. Owen,
955 2003; Locat et al., 2014). Ortner and Kilian (2016, p.350) note that "Incomplete dewatering near the sediment
956 surface can lead to sub-surface sediment mobilization at a later stage, after some burial". This subsequent
957 deeper mobilisation may result in sediment injections but can also weaken the entire sequence as

overpressured layers act as 'easy slip' horizons along which later deformation localises. Such weak horizons may include volcano-clastic beds that contain large amounts of fluid and influence the position of subsequent failure surfaces (e.g. Kuhlman et al., 2016).

Molenaar et al. (2021) also recognised that, although much of the deformation observed in sediment cores from lakes in Chile is linked to surficial deformation associated with megathrust earthquakes, other SSDs are created deeper in the sediment pile by seismic-induced dewatering of intercalated volcanic deposits, which would consequently weaken overlying sediment and facilitate sub-surface deformation (Moernaut et al., 2019). Tephra layers dewater during seismic shaking leading to an increase in density of these layers and a weakening of the overlying lake sediment, which then fails and translates downslope (Moernaut et al., 2019, p.100). Such tephra layers are typically 0.3-0.5 m below the sediment-water interface at the time of seismic shaking, while deeper buried tephra layers suffer repeated seismicity resulting in denser grain packing and 'seismic strengthening' over time (Moernaut et al., 2019). This seismic strengthening process involves the creation of excess pore-pressure during earthquakes, and subsequent dissipation and gentle escape of fluids during interseismic intervals, thereby leading to over-consolidated sequences (Moernaut et al., 2019; Lenz and Sawyer, 2021). However, it is possible for more deeply buried tephra layers to fail if the overburden reaches a critical thickness of >6 m sporadically resulting in larger scale translational sliding of the sequence (Moernaut et al., 2019, p.101). Molenaar et al. (2019, p.6021) examined sediments in the NE Japan trench and report increases in shear strength in sediments buried to 9 cm depth below the sediment-water interface, which they attribute to a reduction in voids associated with seismic strengthening. Sediments at 9-15 cm depth have shear strengths that are comparable to 3-7 m depth of burial in normally consolidated sequences, suggesting that repeated seismicity has increased the shear strength of shallowly-buried sediment.

Numerous earthquakes are reported along the DSF that cause repeated slope failures and creation of MTDs within the Lisan Formation. As noted above, recurrent seismicity may also lead to sediment repacking, dewatering and seismic strengthening that results in buried MTDs forming relatively competent horizons that focus later deformation in the stratigraphic sequence (see section 9.1.3.). Concentration of sub-surface detachments adjacent to MTDs in the secondary failure model creates the potential for overprinting of surficial structures created during original MTD emplacement by later intrastratal detachments formed during continued downslope movement in the sub-surface (Fig. 20a, c).

9.3.2. Control on sub-surface deformation by detrital-rich beds

The control exerted by original sedimentary layering on subsequent sub-surface deformation is an important factor with Brown (1938, p.360) originally noting that "sliding in more finely stratified beds is like that of a pack of cards". However, where significant variations in the depositional architecture is formed, such as thicker sandstone lobes, then these sedimentary geometries may control where later intrastratal deformation develops in the sub-surface (Auchter et al., 2016).

Within the Lisan Formation, it has been recognised that detrital beds focus detachments when they are deformed close (< 1 m) to the surface (Alsop et al., 2016, their fig 8c, d) suggesting they are relatively weak fluid-rich horizons. However, detailed analysis of thrust-related folding at potentially deeper levels in the sediment pile shows that detrital layers form more competent horizons, resulting in parallel (Class 1B) fold styles compared to similar (Class 2) folds in aragonite-rich beds (Alsop et al., 2020b, 2021a). We speculate that the differing relative competence of detrital and aragonite beds that varies with depth could reflect greater dewatering of detrital beds as they become buried. This is possibly related to more rounded detrital grains undergoing greater re-sorting and denser packing after repeated seismic events compared to the acicular aragonite crystals that form interlocked clusters that trap fluids. Competent detrital beds act as baffles or seals that trap fluids beneath them causing potential increases in pore fluid pressure and localising later sub-surface detachments (Alsop et al., 2018). The build-up in fluid pressure may ultimately cause fluidised sediment from along detachments to rupture and break through the overlying competent bed (Alsop et al., 2018).

9.3.3. Control on sub-surface deformation by early precipitation of cements

Mechanically distinctive horizons formed by early precipitation of cements may create heterogeneity within a sequence and control where subsequent sub-surface deformation develops. Intrastratal deformation in the shallow sub-surface can be created during downslope sliding of poorly-lithified carbonates which have undergone incipient cementation (Ettensohn et al., 2011; Pratt and Rule, 2021, p.21). In mixed clastic and carbonate sequences, clastic sediments undergo surficial deformation cut by erosive surfaces, while carbonate sediments experience early cementation and are marked by intrastratal deformation below the sediment surface (Chen and Lee, 2013). Some carbonates display folding in the upper part of the bed while the lower part remains undeformed, suggesting that the upper bed is weaker reflecting a vertical variation in cementation (Dechen and Aiping, 2012, p.81). The timing of precipitation of cements in carbonates can therefore play an important role in localising sub-surface deformation, with a number of recent studies highlighting intrastratal deformation in mixed silicalstic-carbonate sequences (e.g. Hou et al., 2020; Walker et al., 2021).

Within the Lisan Formation, gypsum horizons are considered to precipitate when the usually stratified water column of Lake Lisan was mixed and overturned, possibly following major earthquakes (Ichinose and Begin, 2004; Begin et al., 2005). The competent gypsum horizons subsequently act as baffles that hinder the upward migration of trapped fluids through the sedimentary pile. This can result in potential increases in fluid pressure and concomitant reductions in shear strength of sediments directly beneath the gypsum (e.g. Alsop et al., 2020c). The focussing of sub-surface deformation and detachments beneath gypsum could therefore be a consequence of increased fluid pressures at these particular levels. The control exerted by MTDs, overlying detrital beds, or gypsum horizons on later secondary deformation demonstrates that deformation developed after the overlying barrier to flow had already formed, thereby indicating sub-surface intrastratal deformation.

9.4. What are the consequences of sub-surface deformation in MTDs?

The critical importance of recognising intrastratal deformation has been highlighted by O'Leary and Laine (1996, p.305) who state "An accurate understanding of basin development and marine mass movement requires correct discrimination of intrastratal deformation from buried surficial slide deposits, as the origins and geological implications of these two kinds of stratiform features are significantly different". The realisation that sub-surface deformation, as well as surficial MTDs, develop during gravity-driven downslope movement of sediments has a number of important consequences.

9.4.1. Consequences for balancing of deformation – It is widely considered that extension developed in the upslope 'head' of gravity-driven MTDs should broadly balance and be equivalent to the amount of shortening preserved in the downslope 'toe' region (e.g. Farrell, 1984). However, several authors including Butler and Paton (2010), de Vera et al. (2010), Morley and Naghadeh (2018) and Steventon et al. (2019) have noted that extension and contraction do not balance in MTDs. A failure to recognise younger sub-surface deformation developed adjacent to older MTDs that are buried in the stratigraphic sequence has important implications for the balancing of shortening and extension in such systems. For instance, extensional conjugates associated with sub-surface deformation are developed adjacent to older contractional folds in MTDs (Fig. 18c-f). A confusion between structures formed during older surficial MTD movement and younger sub-surface intrastratal deformation will result in such systems failing to 'balance' as deformation is of two different ages.

9.4.2. Consequences for rates of deformation - Deformation associated with surficial MTDs is considered to be rapid as structures form before creation of the overlying erosive surface and sedimentary cap that is deposited out of suspension. Estimates of time required to deposit sediments out of suspension in lacustrine environments following an earthquake suggest settling of 1 μm particles from a 1 m thick suspension cloud would take ~2 weeks, while slightly coarser 4 μm particles could be deposited in a matter of hours or days (Wils et al., 2021) This is similar to previous estimates in the Lisan Formation where sedimentary caps are thought to be deposited out of suspension "in a matter of just hours or days" (Alsop et al., 2016, p.80). These

short-lived timescales linked to deposition therefore provide rigorous constraints on the rates of deformation within the surficial MTDs. However, once the direct 'link' to sediment deposition is broken during sub-surface deformation, then there are fewer controls and deformation could potentially be slower and relate to downslope creep of the sedimentary pile. Indeed, Ortner and Kilian (2016, p.361) have suggested that some slumps form by continuous creep down submarine slopes prior to complete lithification of the (carbonate) sediments. Similarly, Basilone (2017) also suggests that intact and coherent stratigraphic packages moved downslope on bed-parallel detachments via a process of sediment creep in deepwater carbonates.

Field evidence for slumping associated with creep processes within Holocene sediments around the Dead Sea Basin has been provided by Alsop and Weinberger (2020, p.13). Several observations collectively support downslope creep of sediments including: i) growth of evaporite concretions affecting developing fold geometries within slumps, ii) topography created above slumps infilled by sediment with several overlying beds thickening and 'ponding' in synformal depressions suggesting ongoing fold development, iii) continued and protracted thrusting affecting unconformities that form above slumps, and, iv) the lack of overlying sedimentary caps suggesting slumping was not rapid enough to throw sediment into suspension in the water column. Although these Holocene slumps are considered to be slow moving on slopes of 4-6°, they are still thought to develop at the sediment surface due to the presence of unconformites and erosive surfaces.

In the present study focussing on structures created in the sub-surface of the Lisan Formation, rates of movement are difficult to determine as the direct link to sedimentation is broken. However, the observation that the sedimentary cap itself is arched over underlying culminations (e.g. Fig. 6c-e), or that a number of overlying detrital beds are thinned over structural highs created by FATS (e.g. Fig. 7a-h), suggests that intrastratal deformation was more protracted than observed at the surface. Sequences of stacked unconformities that are deformed above growing culminations (e.g. Fig. 7i-j) also supports more prolonged deformation related to downslope creep of sediments immediately below the surface. In some cases, normal faults that develop in the overburden cut folds and thrusts in the detachment zone but are themselves truncated by the upper and lower detachments (Fig. 13f, g). This indicates that detachments continued to operate after FATS had formed in the sub-surface and suggests protracted downslope creep of the sediment pile can lead to reworking of structures that typifies deformation in the sub-surface.

9.4.3. Consequences for age of deformation – The potential role of seismicity during intrastratal deformation has been recognised over the past century with Miller (1922, p.600) noting intrastratal deformation in Quaternary sands and clays where "under the action of gravity or gravity aided by earthquake shocks, overlying beds have moved differentially over lower-level beds in the general direction of the dip". O'Leary and Laine (1996, p.305) studied high-resolution seismics from the continental slope and stated that "Intrastratal deformation that occurs within a few hundred metres below the sea floor may indicate rapid, non-disintegrative failure due to seismic shock", amongst other things. It has therefore been increasingly appreciated that the simple counting of the number of deformed horizons in the sedimentary record cannot be used to accurately determine the number and age of seismic events. Törő and Pratt (2016, p.196) summarise this dilemma by noting that "In the simplest sense, each deformed interval records a single earthquake, although it is clear that some [structures] do record a second or even a third event".

There are a range of factors that will affect the accuracy of using deformed horizons in palaeoseismic studies. In some cases, deformed horizons are created by processes entirely unrelated to seismicity, such as unequal loading or wave and tidal action (see Owen and Moretti, 2011; Owen et al, 2011, for a summary). In deformed horizons that are created by seismicity, multiple earthquakes can affect the same deformed horizon (e.g. Wils et al., 2021). In such cases, structures with different deformation styles can be superimposed on one another indicating that the deformed horizon was affected by more than one event (e.g. Berra and Felletti, 2011; Törő and Pratt, 2016). These overprinting relationships suggest that the sediments were at different stages of consolidation at the time of each deformation episode (Berra

and Felletti, 2011), and that the change from plastic to brittle structures records increasing sediment 'stiffness' with time (Törő and Pratt, 2016). In other cases, sediments may undergo liquefaction at the contemporary surface marked by erosional features, followed by later re-liquifaction of the same horizon after being buried in the sub-surface during repeated seismicity (Woźniak et al., 2021). Individual horizons can therefore conceal more than one earthquake event, while in other cases there may be a lack of suitable fluid-rich sediments that can easily deform and therefore they do not record any earthquake event (e.g. see Morsilli et al., 2020). Multiple generations of sedimentary dykes that overprint one another in deformed intrastratal horizons indicate several closely spaced injection events occurred in the sub-surface (e.g. Törő and Pratt, 2015b), potentially reflecting multiple seismic events affecting the same horizon.

The recognition in this and other studies that deformed horizons can bifurcate laterally into two or more separate horizons also has clear implications for the counting and use of such layers to estimate the recurrence times of palaeoseismic events (e.g. Gibert et al., 2011; Morsilli et al., 2020). Belzyt et al. (2021) were unable identify sedimentary caps above each of their deformed horizons leading them to suggest that some horizons could have deformed concurrently at the surface and sub-surface during a single seismic event.

Within this case study both surficial and sub-surface intrastratal deformation has been recognised and is schematically summarised in Fig. 20a-d. Following previous workers who studied SSD intervals that lack downslope movement (e.g. Van Loon et al., 2016, Belzyt et al., 2021), we have stressed the importance of recognising erosive surfaces and sedimentary caps that link MTDs with the surface. Sub-surface deformation of the sedimentary sequence clearly leads to issues with simple age-depth correlations where the timing of seismic events is estimated from the level (depth) of sediment that they affect and bracketed by dated horizons (see Moernaut, 2020 and Kempf and Moernaut, 2021 for reviews). The consequences of sub-surface intrastratal deformation is that the link with the age of the sediment is removed and it therefore cannot be assumed that deformation affecting stratigraphically lower beds is older and triggered by older earthquakes. The identification of sub-surface intrastratal deformation, coupled with the synchronous failure model, therefore raise fundamental issues for the use of SSD in palaeoseismic studies necessitating careful observations and application of the detailed criteria outlined in this study.

10. Conclusions

In this study we have used the Lisan Formation deposited around the Dead Sea to document features and stratigraphic relationships that form at the sediment surface during creation of MTDs and compared these with intrastratal structures that are created in the sub-surface during downslope movement of gravity-driven FATS. In such studies, the orientation and vergence of structures may be of little value in distinguishing surface versus sub-surface deformation as both are controlled by the same downslope movement and will therefore have similar trends. Key points arising from this study are highlighted below.

1) Gravity-driven deformation of sediments associated with slope failure is divided into two end-member models: i) sequential failure model where repeated slope failures at the sediment surface systematically build-up multiple MTDs in the stratigraphic record, and ii) synchronous failure model where a single event creates concurrent surficial and sub-surface intrastratal deformed horizons at different stratigraphic levels.

2) An intermediate secondary failure model, where buried MTDs subsequently focus later sub-surface deformation, is also developed. This reflects the fact that MTDs frequently form significant heterogeneities within the otherwise layer-cake stratigraphy of the lacustrine sediments due to earlier dewatering and seismic strengthening. Other markers, such as thick detrital beds and precipitated gypsum horizons, also localise later sub-surface intrastratal deformation beneath them.

3) Irregular erosive surfaces and overlying sedimentary caps deposited out of suspension are key features in recognising surficial deformations of MTDs. Sub-surface deformation associated with FATS are marked by upper detachments that display thin horizons of gouge, repetitions of stratigraphy across the detachment, and

truncation of faults in the overlying sequence. Additionally, injection of fluidised sediment that forms along detachment surfaces can intrude into the overlying sequence that buried the detachment.

4) Sub-surface deformation cuts through entire stratigraphic sequences containing several separate MTDs and therefore affects and locally repeats what are considered to be the 'undeformed' beds between individual MTDs. Sub-surface deformation tends to be focussed along discrete intrastratal detachments with the overlying sequence carried downslope as relatively intact 'slides'.

5) The recognition of both surficial MTDs and sub-surface intrastratal deformation within a sequence means that care must be taken to clearly differentiate structures of different ages and depths of deformation, as misidentification may lead to contractional-extensional systems failing to balance.

6) As sub-surface deformation is not directly correlated with the rapid deposition of sedimentary caps above MTDs, the rates of gravity-driven movement along deeper detachments are unconstrained and could be associated with slower downslope creep of the sediment pile.

7) As sub-surface intrastratal deformation is not directly correlated with the depositional age of the beds it affects, it cannot be assumed that deformation is older in stratigraphically lower beds. This weakens the age-depth correlations frequently used to estimate the timing of earthquake recurrence in palaeoseismic studies.

Acknowledgements

SM acknowledges the Israel Science Foundation (ISG Grant No. 1645/19) and the Ministry of National Infrastructures, Energy and Water Resources (grant #214-17-027). TL acknowledges the Israeli government GSI DS project 40706. We thank Fabrizio Agosta for efficient editorial handling and two reviewers for constructive comments that helped improve the manuscript.

References

Agnon, A., Migowski, C., Marco, S., 2006. Intraclast breccia layers in laminated sequences: recorders of paleo-earthquakes, in Enzel, Y., Agnon, A., and Stein, M., eds., New Frontiers in Dead Sea Paleoenvironmental Research, Geological Society of America Special Publication, p.195-214.

Alsop, G.I., Marco, S. 2011. Soft-sediment deformation within seismogenic slumps of the Dead Sea Basin. *Journal of Structural Geology* 33, 433-457.

Alsop, G.I., Marco, S., Weinberger, R., Levi, T. 2016. Sedimentary and structural controls on seismogenic slumping within Mass Transport Deposits from the Dead Sea Basin. Sedimentary Geology 344, 71-90.

Alsop, G.I., Marco, S., Levi, T., Weinberger, R. 2017a. Fold and thrust systems in Mass Transport Deposits. Journal of Structural Geology 94, 98-115.

Alsop, G.I., Marco, S., Weinberger, R., Levi, T. 2017b. Upslope-verging back thrusts developed during downslope-directed slumping of mass transport deposits. Journal of Structural Geology 100, 45-61.

Alsop, G.I., Weinberger, R., Marco, S. 2018. Distinguishing thrust sequences in gravity-driven fold and thrust belts. Journal of Structural Geology 109, 99-119.

Alsop, G.I., Weinberger, R., Marco, S., Levi, T. 2019. Identifying soft-sediment deformation in rocks. *Journal of Structural Geology 125, 248-255. doi*.org/10.1016/j.jsg.2017.09.001

Alsop, G.I., Weinberger, R., 2020. Are slump folds reliable indicators of downslope flow in recent mass transport deposits? *Journal of Structural Geology 135, 104037.* https://doi.org/10.1016/j.jsg.2020.104037

Alsop, G.I., Weinberger, R., Marco, S., Levi, T. 2020a. Fold and thrust systems in mass transport deposits around the Dead Sea Basin. In: Ogata, K., Festa, A., Pini, G.A. (Editors). Submarine landslides: subaqueous mass transport deposits from outcrops to seismic profiles. American Geophysical Union Monograph Series. 246, p.139-154. John Wiley & Sons Inc. 384pp. ISBN: 978-1-119-50058-2.

1185 Alsop, G.I., Weinberger, R., Marco, S., Levi, T. 2020b. Folding during soft-sediment deformation.
1186 Geological Society Special Publication, Bond, C.E. and Lebit, H.D. (Editors) Folding and fracturing of
1187 rocks: 50 years since the seminal text book of J.G. Ramsay. 487, 81-104. doi.org/10.1144/SP487.1

1188 Alsop, G.I., Weinberger, R., Marco, S., Levi, T. 2020c. Bed-parallel slip: Identifying missing displacement in
1189 mass transport deposits. *Journal of Structural Geology 131, 103952.*

1190 Alsop, G.I., Weinberger, R., Marco, S., Levi, T. 2020d. Distinguishing coeval patterns of contraction and
1191 collapse around flow lobes in mass transport deposits. Journal of Structural Geology 134, 104013

1192 Alsop, G.I., Weinberger, R., Marco, S., Levi, T. 2021a. Detachment fold duplexes within gravity-driven fold
1193 and thrust systems. *Journal of Structural Geology, 142, 104207. https://doi.org/10.1016/j.jsg.2020.104207*

1194 Alsop, G.I., Weinberger, R., Marco, S., Levi, T. 2021b. Criteria to discriminate between different models of
1195 thrust ramping in gravity-driven fold and thrust systems. *Journal of Structural Geology, 150, 104396.*
1196 https://doi.org/10.1016/j.jsg.2021.104396

1197 Alves, T.M. 2015. Submarine slide blocks and associated soft-sediment deformation in deep-water basins: A
1198 review. Marine and Petroleum Geology 67, 262-285.

1199 Arkin, Y., Michaeli, L. 1986. The significance of shear strength in the deformation of laminated sediments in
1200 the Dead Sea area. Israel Journal of Earth Sciences 35, 61-72.

1201 Armandita, C., Morley, C.K., Rowell, P. 2015. Origin, structural geometry, and the development of a giant
1202 slide: The South Makassar Strait mass transport complex. Geosphere, 11, 376-403.

1203 Auchter, N.C., Romans, B.W., Hubbard, S.M. 2016. Influence of deposit architecture on intrastratal
1204 deformation, slope deposits of the Tres Pasos Formation, Chile. Sedimentary Geology 341, 13-26.

1205 Baldry, R.A. 1938. Slip-planes and breccia zones in the Tertiary rocks of Peru. Quarterly Journal of the
1206 Geological Society, 94, p.347-358.

1207 Bartov, Y., Stein, M., Enzel, Y., Agnon, A., Reches, Z., 2002. Lake levels and sequence stratigraphy of
1208 Lake Lisan, the late Pleistocene precursor of the Dead Sea. Quaternary Research 57, 9-21.

1209 Bartov, Y., Goldstein, S.L., Stein, M., Enzel, Y. 2003. Catastrophic arid episodes in the Eastern
1210 Mediterranean linked with the North Atlantic Heinrich events. Geology 31, 439-442.

1211 Basilone, L., Lena, G., Gasparo-Morticelli, M., 2014. Synsedimentary tectonic, soft sediment deformation and
1212 volcanism in the rifted Tethyan margin from the Upper Triassic-Middle Jurassic deep-water carbonates in
1213 Central Sicily. Sedimentary Geology 308:63–79. http://dx.doi.org/10.1016/j.sedgeo.2014.05.002.

1214 Basilone, L., Sulli, A., Gasparo Morticelli, M. 2016. The relationships between soft-sediment deformation
1215 structures and synsedimentary extensional tectonics in Upper Triassic deep-water carbonate succession
1216 (Southern Tethyan rifted continental margin — Central Sicily) Sedimentary Geology 344, 310-322.

1217 Basilone, L. 2017. Seismogenic rotational slumps and translational glides in pelagic deep-water carbonates.
1218 Upper Tithonian-Berriasian of Southern Tethyan margin (W Sicily, Italy). Sedimentary Geology 356, 1-14.

1219 Bates, R.L., Jackson, J.A., 1980. Glossary of Geology, second edition. American Geological Institute, Falls
1220 Church, Virginia, USA, p. 751.

1221 Begin, Z.B., Ehrlich, A., Nathan, Y., 1974, Lake Lisan, the Pleistocene precursor of the Dead Sea:
1222 Geological Survey of Israel Bulletin, 63, p.30.

1223 Begin, B.Z., Steinberg, D.M., Ichinose, G.A., Marco, S., 2005. A 40,000 years unchanging of the seismic
1224 regime in the Dead Sea rift. Geology 33, 257–260

1225 Belzyt, S., Pisarska-Jamrozy, M., Bitinas, A., Woronko, B., Phillips, E.R., Piotrowski, J.A., Jusiene, A. 2021.
1226 Repetitive Late Pleistocene soft-sediment deformation by seismicity-induced liquefaction in north-western
1227 Lithuania. Sedimentology https://doi.org/10.1111/sed.12883

1228 Berra, F., Felletti, F. 2011. Syndepositional tectonics recorded by soft-sediment deformation and liquefaction
1229 structures (continental Lower Permian sediments, Southern Alps, Northern Italy): Stratigraphic significance.
1230 Sedimentary Geology 235, 249-263.

1231 Brown, C.B. 1938. On a theory of gravitational sliding applied to the Tertiary of Ancon, Ecuador. Quarterly
1232 Journal of the Geological Society 94, p.359-368

1233 Budillon, F., Cesarano, M., Conforti, A., Pappone, G., Di Martino, G., Pelosi, N. 2014. Recurrent superficial
1234 sediment failure and deep gravitational deformation in a Pleistocene slope marine succession: The Poseidonia
1235 Slide (Salerno Bay, Tyrrhenian Sea). In: Krastel, S., Behrmann, J-H., V¨olker, D., Stipp, M., Berndt, C.,
1236 Urgeles, R., Chaytor, J., Huhn, K., Strasser, M., Harbitz, C.B. (eds.), Submarine Mass Movements and Their
1237 Consequences, Advances in Natural and Technological Hazards Research 37, 273-284. DOI 10.1007/978-3-
1238 319-00972-8 24, © Springer International Publishing Switzerland 2014.

1239 Bull, S., Cartwright, J., Huuse, M. 2009. A review of kinematic indicators from mass-transport complexes
1240 using 3D seismic data. Marine and Petroleum Geology 26, 1132-1151.

1241 Butler, R.W.H., Paton, D.A. 2010. Evaluating lateral compaction in deepwater fold and thrust belts: How
1242 much are we missing from "nature's sandbox"? GSA Today 20, 4-10.

1243 Butler, R.W.H., Bond, C.E., Cooper, M.A., Watkins, H. 2020. Fold-thrust structures – where have all the
1244 buckles gone? Geological Society Special Publication, Bond, C.E. and Lebit, H.D. (Editors) Folding and
1245 fracturing of rocks: 50 years since the seminal text book of J.G. Ramsay. 487, 21-44.

1246 Cardona, S., Wood, L.J., Dugan, B., Jobe, Z., Strachan, L.J. 2020. Characterization of the Rapanui mass-
1247 transport deposit and the basal shear zone: Mount Messenger Formation, Taranaki Basin, New Zealand.
1248 Sedimentology 67, 2111-2148. doi: 10.1111/sed.12697

1249 Chakraborty, P.P., Sharma, R., Kumar, P. 2019. Earthquake-induced soft sediment deformation (SSD)
1250 structures from the Bilara limestone formation, Marwar basin, India. Journal of Earth System Science 128:
1251 162, 16pp. https://doi.org/10.1007/s12040-019-1182-x

1252 Chen, J., Lee, H.S. 2013. Soft-sediment deformation structures in Cambrian siliciclastic and carbonate storm
1253 deposits (Shandong Province, China): Differential liquefaction and fluidization triggered by storm-wave
1254 loading. Sedimentary Geology 288, 81-94.

1255 Daxer, C., Sammartini, M., Molenaar, A., Piechl, T., Strasser, M., Moernaut, J. 2020. Morphology and
1256 spatio-temporal distribution of lacustrine mass-transport deposits in Wörthersee, Eastern Alps, Austria.
1257 In: Georgiopoulou, A., Amy, L.A., Benetti, S., Chaytor, J.D., Clare, M.A., Gamboa, D., Haughton, P.D.W.,
1258 Moernaut, J., Mountjoy, J.J. (Editors). Subaqueous mass movements and their consequences: Advances in
1259 process, understanding, monitoring and hazard assessments. Geological Society, London, Special
1260 Publications, 500, 235–254.

1261 Dechen, S., Aiping, S. 2012. Typical earthquake-induced soft-sediment deformation structures in the
1262 Mesoproterozoic Wumishan Formation, Yongding River Valley, Beijing, China and interpreted earthquake
1263 frequency. Journal of Palaeogeography, 1, 71-89. DOI: 10.3724/SP.J.1261.2012.00007

1264 de Vera, J., Granado, P., McClay, K. 2010. Structural evolution of the Orange Basin gravity-driven system,
1265 offshore Namibia. Marine and Petroleum Geology 27, 223-237

1266 Ben-Dor, Y., Neugebauer, I., Enzel, Y., Schwab, M.J., Tjallingii, R., Erel, Y., Brauer, A. 2019. Varves of
1267 the Dead Sea sedimentary record. Quaternary Science Reviews 215, 173-184.

1268 Elliot, C.G., Williams, P.F. 1988. Sediment slump structures: a review of diagnostic criteria and application
1269 to an example from Newfoundland. Journal of Structural Geology 10, 171-182.

1270 El-Isa, Z.H., Mustafa, H. 1986. Earthquake deformations in the Lisan deposits and seismotectonic
1271 implications. Geophysical Journal of the Royal Astronomical Society 86, 413-424.

1272 Ellis, M.A., Dunlap, W.J. 1988. Displacement variation along thrust faults: implications for the
1273 development of large faults. Journal of Structural Geology 10, 183-192.

1274 Ettensohn, F.R., Zhang, C., Gao, L., Lierman, R.T. 2011. Soft-sediment deformation in epicontinental
1275 carbonates as evidence of paleoseismicity with evidence for a possible new seismogenic indicator: Accordion
1276 fold. Sedimentary Geology 235, 222-233.

1277 Farrell, S.G. 1984. A dislocation model applied to slump structures, Ainsa Basin, South Central Pyrenees,
1278 Journal of Structural Geology 6, 727-736.

1279 Ferrill, D.A., Morris, A.P., Wigginton, S.S., Smart, K.J., McGinnis, R.N., Lehrmann, D. 2016. Deciphering
1280 thrust fault nucleation and propagation and the importance of footwall synclines. Journal of Structural
1281 Geology, 85, 1-11.

1282 Festa, A., Ogata, K., Pini, G.A., Dilek, Y., Alonso, J.L., 2016. Origin and significance of olistostromes in
1283 the evolution of orogenic belts: a global synthesis. Gondwana Research 29, 180–203.

1284 Fossen, H. 2016. Structural Geology. 2nd Edition. Cambridge University Press, Cambridge, UK, p.510.

1285 Frey Martinez, J., Cartwright, J., Hall, B. 2005. 3D seismic interpretation of slump complexes: examples
1286 from the continental margin of Israel. Basin Research 17, 83-108.

1287 Frey-Martinez, J., Cartwright, J., James, D. 2006. Frontally confined versus frontally emergent submarine
1288 landslides: A 3D seismic characterisation. Marine and Petroleum Geology23, 585-604.

1289 Frydman, S., Charrach, J., Goretsky, I. 2008. Geotechnical properties of evaporite soils of the Dead Sea area.
1290 Engineering Geology101, 236-244.

1291 Gao, Y., Jiang, Z., Best, J.L., Zhang, J. 2020. Soft-sediment deformation structures as indicators of tectono-
1292 volcanic activity during evolution of a lacustrine basin: A case study from the Upper Triassic Ordos Basin,
1293 China. Marine and Petroleum Geology 115, 104250.

1294 Garcia-Tortosa, F.J., Alfaro, P., Gibert, L., Scott, G. 2011. Seismically induced slump on an extremely
1295 gentle slope (<1°) of the Pleistocene Tecopa paleolake (California). Geology 39, 1055-1058.

1296 Garfunkel, Z., 1981, Internal structure of the Dead Sea leaky transform (rift) in relation to plate kinematics:
1297 Tectonophysics, 80, 81-108.

1298 Georgiopoulou, A., Amy, L.A., Benetti, S., Chaytor, J.D., Clare, M.A., Gamboa, D., Haughton, P.D.W.,
1299 Moernaut, J., J. J. Mountjoy, J.J. 2020. Subaqueous Mass Movements and their Consequences: Advances in Process
1300 Understanding, Monitoring and Hazard Assessments. Geological Society, London, Special Publications, 500,
1301 pp.634. https://doi.org/10.1144/SP500

1302 Gibert, L., Alfaro, P., Garcıa-Tortosa, F.J., Scott, G. 2011. Superposed deformed beds produced by single
1303 earthquakes (Tecopa Basin, California): Insights into paleoseismology. Sedimentary Geology, 235, 148–159.

1304 Gibert, L., Sanz de Galdeano, C., Alfaro, P., Scott, G., Lopez Garrido, A.C. 2005. Seismic-induced slump
1305 in Early Pleistocene deltaic deposits of the Baza Basin (SE Spain). Sedimentary Geology 179, 279-294.

1306 Grimm, K.A., Orange, D.L. 1997. Synsedimentary fracturing, fluid migration, and subaqueous mass
1307 wasting: Intrastratal microfractured zones in laminated diatomaceous sediments, Miocene Monterrey
1308 Formation, California, USA. Journal of Sedimentary Research 67, 601-613.

1309 Haliva-Cohen, A., Stein, M., Goldstein, S.L., Sandler, A., Starinsky, A. 2012. Sources and transport routes
1310 of fine detritus material to the Late Quaternary Dead Sea Basin. Quaternary Science Reviews 50, 55-70.

1311 Haase-Schramm, A., Goldstein, S.L., Stein, M. 2004. U-Th dating of Lake Lisan aragonite (late Pleistocene
1312 Dead Sea) and implications for glacial East Mediterranean climate change. Geochimica et Cosmochimica Acta
1313 68, 985-1005.

1314 Heifetz, E., Agnon, A., Marco, S. 2005. Soft sediment deformation by Kelvin Helmholtz Instability: A case
1315 from Dead Sea earthquakes. Earth Planet. Sci. Lett., 236, 497–504. Doi: 10.1016/j.epsl.2005.04.019

1316 Hou, Z., Chen, S., Zhang, S., Yang, H. 2020. Sedimentary deformation features as evidence for paleoseismic
1317 events in the middle Eocene in the Dongying Depression of the southern Bohai Bay Basin, eastern China.
1318 Canadian Journal of Earth Sciences, **57**: 954–970. doi.org/10.1139/cjes-2019-0160

1319 Hughes, A.N., Shaw, J.H. 2014. Fault displacement-distance relationships as indicators of contractional
1320 fault-related folding style. American Association of Petroleum Geologists Bulletin 98, 227-251.

1321 Huhn, K., Arroyo, M., Cattaneo, A., Clare, M.A., Gràcia, E., Harbitz, C.B., Krastel, S., Kopf, A., Løvholt, F.,
1322 Rovere, M., Strasser, M., Talling, P.J., Urgeles, R. 2020. Modern Submarine Landslide Complexes: A Short
1323 Review. In: Ogata, K., Festa, A., Pini, G.A. (Editors). Submarine landslides: subaqueous mass transport
1324 deposits from outcrops to seismic profiles. American Geophysical Union Monograph Series. 246, p.183-200.
1325 John Wiley & Sons Inc. 384pp. ISBN: 978-1-119-50058-2.

1326 Ichinose, G.A., Begin, Z.B., 2004. Simulation of tsunamis and lake seiches for the Late Pleistocene Lake
1327 Lisan and the Dead Sea. Geological Survey of Israel Report GSI/ 7/04. 50 pages

Ireland, M.T., Davies, R.J., Goulty, N.R., Moy, D.J. 2011. Thick slides dominated by regular-wavelength folds and thrusts in biosiliceous sediments on the Vema Dome offshore of Norway. Marine Geology, 289, 34-45.

Jablonska, D., Di Celma, C., Korneva, I., Tondi, E., Alsop, I. 2016. Mass-transport deposits within basinal carbonates from southern Italy. *Italian Journal of Geosciences*, 135, 30-40.

Jablonska, D., Di Celma, C., Tondi, E., Alsop, G.I. 2018. Internal architecture of mass-transport deposits in basinal carbonates: A case study from southern Italy. *Sedimentology 65, 1246-1276. doi:* 10.1111/sed.12420

Jolly, B.A., Lonergan, L., Whittaker, A.C., 2016. Growth history of fault-related folds and interaction with seabed channels in the toe-thrust region of the deep-water Niger delta. Marine and Petroleum Geology 70, 58-76.

Kagan, E.J., Stein, M., Marco, S. 2018. Integrated palaeoseismic chronology of the last glacial Lake Lisan: From lake margin seismites to deep-lake mass transport deposits. Journal of Geophysical Research: Solid Earth 123, (4) 2806-2824.

Kempf, P., Moernaut, J. 2021. Age uncertainty in recurrence analysis of paleoseismic records. Journal of Geophysical research, Solid Earth doi: 10.1029/2021JB021996.

Ken-Tor, R., Agnon, A., Enzel, Y., Marco, S., Negendank, J.F.W., and Stein, M., 2001. High-resolution geological record of historic earthquakes in the Dead Sea basin: J. Geophys. Res., v. 106, p.2221-2234.

Knipe, R.J. 1986. Deformation mechanism path diagrams for sediments undergoing lithification. Memoir of the Geological Society of America 166, 151-160.

Korneva, I., Tondi, E., Jablonska, D., Di Celma, C., Alsop, I., Agosta, F. 2016. Distinguishing tectonically- and gravity-driven synsedimentary deformation structures along the Apulian platform margin (Gargano Promontory, southern Italy). Marine and Petroleum Geology 73, 479-491.

Krastel, S., Behrmann, J-H., V¨olker, D., Stipp, M., Berndt, C., Urgeles, R., Chaytor, J., Huhn, K., Strasser, M., Harbitz, C.B. 2014. Submarine Mass Movements and Their Consequences, Advances in Natural and Technological Hazards Research 37, 683pp. DOI 10.1007/978-3-319-00972-8, © Springer International Publishing Switzerland.

Kuhlmann, J., Huhn, K., Ikari, M.J. 2016. Do embedded volcanoclastic layers serve as potential glide planes?: An integrated analysis from the Gela Basin offshore southern Sicily. Lamarche, G., Mountjoy, J., Bull, S., Hubble, T., Krastel, S., Lane, E., Micallef, A., Moscardelli, L., Mueller, C., Pecher, I., Woelz, S. (eds.), Submarine Mass Movements and their Consequences, Advances in Natural and Technological Hazards Research 41, p.273-280. DOI 10.1007/978-3-319-20979-1_27.

Kumar, P.C., Omosanya, K.O., Eruteya, O.E., Sain, K. 2021. Geomorphological characterization of basal flow markers during recurrent mass movement: A case study from the Taranaki Basin, offshore New Zealand. Basin Research 33, 2358–2382. DOI: 10.1111/bre.12560

Lamarche, G., Mountjoy, J., Bull, S., Hubble, T., Krastel, S., Lane, E., Micallef, A., Moscardelli, L., Mueller, C., Pecher, I., Woelz, S. 2016. Submarine mass movements and their consequences: Progress and challenges. Lamarche, G., Mountjoy, J., Bull, S., Hubble, T., Krastel, S., Lane, E., Micallef, A., Moscardelli, L., Mueller, C., Pecher, I., Woelz, S. (eds.), Submarine Mass Movements and their Consequences, Advances in Natural and Technological Hazards Research 41, p.1-14. DOI 10.1007/978-3-319-20979-1_1

Lenz, B.L., Sawyer, D.E. 2021. Mass Transport Deposits in Reflection Seismic Data Offshore Oregon, USA. Basin Research, doi: 10.1111/BRE.12611

Levi, T., Weinberger, R., Aïfa, T., Eyal, Y., S. Marco, S. 2006a. Injection mechanism of clay-rich sediments into dikes during earthquakes, Geochemistry, Geophysics, and Geosystems 7, no. 12, Q12009.

Levi, T., Weinberger, R., Aïfa, T., Eyal, Y., S. Marco, S. 2006b. Earthquake-induced clastic dikes detected by anisotropy of magnetic susceptibility, Geology, 34(2), 69–72.

Levi, T., Weinberger, R., Alsop, G.I., Marco, S. 2018. Characterizing seismites with anisotropy of magnetic susceptibility. *Geology* 46 (9), 827-830.

1375 Liang, L., Qiao, X., Dai, F., Zhong, N., Jiang, H. 2021. Seismically triggered soft-sediment deformation
1376 structures in Tashkorgan lacustrine sediments, northeastern Pamir, China. Quaternary International.
1377 https://doi.org/10.1016/j.quaint.2021.06.021

1378 Locat, J., Leroueil, S., Locat, A., Lee, H. 2014. Weak Layers: Their Definition and Classification from a
1379 Geotechnical Perspective. In: Krastel, S., Behrmann, J-H., V¨olker, D., Stipp, M., Berndt, C., Urgeles, R.,
1380 Chaytor, J., Huhn, K., Strasser, M., Harbitz, C.B. (eds.), Submarine Mass Movements and Their
1381 Consequences, Advances in Natural and Technological Hazards Research 37, 3-12. DOI 10.1007/978-3-319-
1382 00972-8 1, © Springer International Publishing Switzerland.

1383 Lu, Y., Waldmann, N., Alsop, G.I., Marco, S. 2017. Interpreting soft sediment deformation and mass transport
1384 deposits as seismites in the Dead Sea depocenter. Journal of Geophysical Research: Solid Earth. 122, 8305-
1385 8325.

1386 Lu, Y., Marco, S., Wetzler, N., Fang, X., Alsop, G. I., Hubert-Ferrari, A. 2021a. A paleoseismic record
1387 spanning 2-Myr reveals episodic late Pliocene deformation in the western Qaidam Basin, NE Tibet.
1388 Geophysical Research Letters, 48, e2020GL090530. https://doi.org/10.1029/2020GL090530

1389 Lu, Y., Moernaut, J., Waldmann, N., Bookman, R., Alsop, G.I., Hubert-Ferrari, A. Strasser, M., Wetzler, N.,
1390 Agnon, A., Marco, S., 2021b. Orbital- and millennial-scale changes in lake levels facilitate earthquake-
1391 triggered mass failures in the Dead Sea Basin. Geophysical Research Letters,48 (14) e2021GL093391.
1392 https://doi.org/10.1029/2021GL093391

1393 Lu, Y., Moernaut, J., Bookman, R., Waldmann, N., Wetzler, N., Agnon, A., Marco, S., Alsop, G.I., Strasser,
1394 M., Hubert-Ferrari, A. 2021c. A new approach to constrain the seismic origin for prehistoric turbidites as
1395 applied to the Dead Sea Basin. Geophysical Research Letters, 48, e2020GL090947.
1396 *http://doi.org*/10.1029/2020GL090947

1397 Maltman, A. 1984. On the term soft-sediment deformation. Journal of Structural Geology 6, 589-592.

1398 Maltman, A. 1994a. Introduction and Overview. In: Maltman, A. (Editor) The Geological Deformation of
1399 Sediments. Chapman & Hall, London. p.1-35.

1400 Maltman, A. 1994b. Deformation structures preserved in rocks. In: Maltman, A. (Editor) The Geological
1401 Deformation of Sediments. Chapman & Hall, London. p.261-307.

1402 Marco, S., Stein, M., Agnon, A., and Ron, H., 1996. Long term earthquake clustering: a 50,000 year
1403 paleoseismic record in the Dead Sea Graben: J. Geophys. Res., 101, 6179-6192.

1404 Marco, S., Hartal, M., Hazan, N., Lev, L., Stein, M. 2003. Archaeology, history, and geology of the A.D.
1405 749 earthquake, Dead Sea transform. Geology 31, 665-668.

1406 Migowski, C., Agnon, A., Bookman, R., Negendank, J.F.W., and Stein, M., 2004. Recurrence pattern of
1407 Holocene earthquakes along the Dead Sea transform revealed by varve-counting and radiocarbon dating of
1408 lacustrine sediments: Earth and Planetary Science Letters, 222, 301-314.

1409 Miller, W.J. 1922. Intraformational corrugated rocks. Journal of Geology 30,587-610.

1410 Moernaut, J., Van Daele, M., Heirman, K., Wiemer, G., Molenaar, A., Vandorpe, T., Melnick, D., Hajdas, I.,
1411 Pino, M., Urrutia, M.P., De Batist, M. 2019. The subaqueous landslide cycle in south-central Chilean lakes:
1412 The role of tephra, slope gradient and repeated seismic shaking. Sedimentary Geology, 381, 84-105.

1413 Moernaut, J. 2020. Time-dependent recurrence of strong earthquake shaking near plate boundaries: A lake
1414 sediment perspective. Earth Science Reviews 210, 103344.

1415 Molenaar, A., Moernaut, J., Wiemer, G., Dubois, N., Strasser, M. 2019. Earthquake impact on active margins:
1416 Tracing surficial remobilization and seismic strengthening in a slope sedimentary sequence. Geophysical
1417 Research Letters, 46, 6015-6023. 10.1029/2019GL082350

1418 Molenaar, A., Van Daele, M., Vandorpe, T., Degenhart, G., De Batist, M., Urrutia, M.P., Pino, M., Strasser,
1419 M., Moernaut, J. 2021. What controls the remobilization and deformation of surficial sediment by seismic
1420 shaking? Linking lacustrine slope stratigraphy to great earthquakes in South–Central Chile. Sedimentology.
1421 https://doi.org/10.1111/sed.12856

1422 Moretti, M., Alfaro, P., Caselles, O., Canas, J.A., 1999. Modelling seismites with a digital shaking table.
1423 Tectonophysics 304, 369–383.

Moretti, M., Sabato, L. 2007. Recognition of trigger mechanisms for soft-sediment deformation in the Pleistocene lacustrine deposits of the Sant'Arcangelo Basin (Southern Italy): Seismic shock vs. overloading. Sedimentary Geology 196, 31-45.

Moretti,M., Van Loon, A.J.T., 2014. Restrictions to the application of 'diagnostic' criteria for recognizing ancient seismites. Journal of Palaeogeography 3, 162–173.

Morley, C.K., von Hagke, C., Hansberry, R.L., Collins, A.S., Kanitpanyacharoen, W., King, R. 2017. Review of major shale-dominated detachment and thrust characteristics in the diagenetic zone: Part 1, meso- and macro-scopic scale. Earth Science Reviews173, 168-228.

Morley, C.K., Naghadeh, D.H. 2018. Tectonic compaction shortening in toe region of isolated listric normal fault, North Taranaki Basin, New Zealand. Basin Research 30, 424-436.

Morsilli, M., Bucci, M.G., Gliozzi, E., Lisco, S., Moretti, M. 2020. Sedimentary features influencing the occurrence and spatial variability of seismites (late Messinian, Gargano Promontory, southern Italy). Sedimentary Geology 401, 105628.

Moscardelli L., Wood L. 2008. New classification system for mass transport complexes in offshore Trinidad. Basin Res 20:73–98.

Muraoka, H., Kamata, H., 1983. Displacement distribution along minor fault traces. Journal of Structural Geology 5, 483-495.

Nuriel,P., Weinberger, R., Kylander-Clark, A.R.C., Hacker, B.R., Cradock, J.P. 2017. The onset of the Dead Sea transform based on calcite age-strain analyses. Geology 45, 587-590.

Obermeier, S.F. 2009. Using liquefaction-induced and other soft-sediment features for paleoseismic analysis. International Geophysics, 95, 497-564. DOI: 10.1016/S0074-6142(09)95007-0

Ogata, K., Mutti, E., Pini, G.A., Tinterri, R., 2012. Mass transport-related stratal disruption within sedimentary mélanges: Examples from the northern Apennines (Italy) and south-central Pyrenees (Spain). Tectonophysics 568–569, 185–199.

Ogata, K., Pogacnik, Z., Pini, G.A., Tunis, G., Festa, A., Camerlenghi, A., Rebesco, M., 2014. The carbonate mass transport deposits of the Paleogene Friuli Basin (Italy/ Slovenia): Internal anatomy and inferred genetic processes. Marine Geology 356, 88–110. https://doi.org/10.1016/j.margeo.2014.06.014.

Ogata, K., Festa, A., Pini, G.A. 2020. Submarine Landslides: Subaqueous Mass Transport Deposits from Outcrops to Seismic Profiles, Geophysical Monograph 246, First Edition. Edited by Kei Ogata, Andrea Festa, and Gian Andrea Pini. 2020 American Geophysical Union. Published by John Wiley & Sons, Inc. ISBN: 978-1-119-50058-2.

Ogawa, Y., Mori, S., 2021, Gravitational sliding or tectonic thrusting?: Examples and field recognition in the Miura-Boso subduction zone prism, in Wakabayashi, J., and Dilek, Y., Editors., Plate Tectonics, Ophiolites, and Societal Significance of Geology: A Celebration of the Career of Eldridge Moores: Geological Society of America Special Paper 552, 197–232, https://doi.org/10.1130/2021.2552(10).

O'Leary, D.W., Laine, E. 1996. Proposed criteria for recognizing intrastratal deformation features in marine high resolution seismic reflection profiles. Geo-Marine Letters, 16, 305-312.

Ortner, H., 2007. Styles of soft-sediment deformation on top of a growing fold system in the Gosau Group at Muttekopf, Northern Calcareous Alps, Austria: Slumping versus tectonic deformation, Sedimentary Geology, 196, 99-118.

Ortner, H., Kilian, S. 2016. Sediment creep on slopes in pelagic limestones: Upper Jurassic of Northern Calcareous Alps, Austria. Sedimentary Geology 344, 350-363.

Owen, G., Moretti, M. 2011. Identifying triggers for liquefaction-induced soft-sediment deformation in sands. Sedimentary Geology 235, 141-147.

Palladino, G., Grippa, A., Bureau, D., Alsop, G.I., Hurst, A. 2016. Emplacement of sandstone intrusions during contractional tectonics. Journal of Structural Geology 89, 239-249.

Palladino, G., Alsop, G.I., Grippa, A., Zvirtes, G., Phillip, R.P., Hurst, A. 2018. Sandstone-filled normal faults: A case study from Central California. *Journal of Structural Geology* 110, 86-101.

1472 Palladino, G., Alsop, G.I., Grippa, A., Seers, T., Hurst, A. 2021. Sandstone intrusions along different types
1473 of faults and their effect on fluid flow in siliclastic reservoirs. Geological Society Special Publication,
1474 Silcock, S., Huuse, M. Bowman, M., Hurst, A., Cobain, S. (Editors) Subsurface Sand Remobilization and
1475 Injection. 493, 273-286. https://doi.org/10.1144/SP493-2018-45

1476 Porat, N., Levi, T., Weinberger, R. 2007. Possible resetting of quartz OSL signals during
1477 earthquakes – evidence from late Pleistocene injection dikes, Dead Sea basin, Israel. Quaternary
1478 Geochronology2, 272-277.

1479 Posamentier, H.W., Martinsen, O.J. 2011. The character and genesis of submarine mass-transport deposits:
1480 Insights from outcrop and 3D seismic data. Mass transport deposits in Deepwater settings: Society for
1481 Sedimentary Geology (SEPM) Special Publication 96, 7-38.

1482 Prasad, S., Negendank, J.F.W., Stein, M. 2009. Varve counting reveals high resolution radiocarbon
1483 reservoir age variations in palaeolake Lisan. Journal of Quaternary Science 24, 690-696.

1484 Pratt, B.R., Rule, R.G. 2021. A Mesoproterozoic carbonate platform (lower Belt Supergroup of western North
1485 America): Sediments, facies, tides, tsunamis and earthquakes in a tectonically active intracratonic basin. Earth
1486 Science Reviews 217, 103626. https://doi.org/10.1016/j.earscirev.2021.103626

1487 Ramsay, J.G. 1967. Folding and Fracturing of Rocks. McGraw-Hill, New York. 568pp.

1488 Reis, A.T., Araújo, E., Silva, C.G., Cruz, A.M., Gorini, C., Droz, L., Migeon, S., Perovano, R., King, I.,
1489 Bache, F. 2016. Effects of a regional décollement level for gravity tectonics on late Neogene to recent
1490 large-scale slope instabilities in the Foz do Amazonas Basin, Brazil. Marine and Petroleum Geology 75,
1491 29-52.

1492 Rich, J.L., 1950. Flow markings, groovings, and intrastratal crumplings as criteria for recognition of slope
1493 deposits, with illustrations from Silurian rocks of Wales. Bulletin of the American Association of Petroleum
1494 Geologists 34, 717-741.

1495 Rossetti, D.F., Goes, A.M. 2000. Deciphering the sedimentological imprint of paleoseismic events: an
1496 example from the Aptian Codo Formation, northern Brazil. Sedimentary Geology, 135, 137–156.

1497 Sammartini, M., Moernaut, J., Anselmetti, F.S., Hilbe, M., Lindhorst, K., Praet, N., Strasser, M. 2020. An
1498 Atlas of Mass-Transport Deposits in Lakes. In: Ogata, K., Festa, A., Pini, G.A. (Editors). Submarine
1499 landslides: subaqueous mass transport deposits from outcrops to seismic profiles. American Geophysical
1500 Union Monograph Series. 246, p.201-226. John Wiley & Sons Inc. 384pp. ISBN: 978-1-119-50058-2.

1501 Sammartini, M., Moernaut, J., Kopf, A., Stegmann, S., Fabbri, S.C., Anselmetti, F.S., Strasser, M.. 2021.
1502 Propagation of frontally confined subaqueous landslides: Insights from combining geophysical,
1503 sedimentological, and geotechnical analysis. Sedimentary Geology 416, 105877.

1504 Scarselli, N., McClay, K., Elders, C. 2016. Seismic geomorphology of Cretaceous megaslides offshore
1505 Namibia (Orange Basin): Insights into segmentation and degradation of gravity-driven linked systems.
1506 Marine and Petroleum Geology 75, 151-180.

1507 Shanmugam, G. 2017. Global case studies of soft-sediment deformation structures (SSDS): Definitions,
1508 classifications, advances, origins, and problems. Journal of Palaeogeography 6, 251-320.

1509 Sharman, G.R., Graham, S.A., Masalimova, L.U., Shumaker, L.E., King, P.R. 2015. Spatial patterns of
1510 deformation and palaeoslope estimation within the marginal and central portions of a basin-floor mass-
1511 transport deposit, Taranaki Basin, New Zealand. Geosphere, 11, 266-306.

1512 Smith, J.V. 2000. Flow pattern within a Permian submarine slump recorded by oblique folds and deformed
1513 fossils, Ulladulla, south-eastern Australia. *Sedimentology*, 47, 357-366.

1514 Sneh, A., Weinberger, R. 2014. Major structures of Israel and Environs, Scale 1:50,000. Israel
1515 Geological Survey, Jerusalem.

1516 Sobiesiak, M., Kneller, B.C., Alsop, G.I., Milana, J.P. 2017. Sub-seismic scale folding and thrusting within
1517 an exposed mass transport deposit: A case study from NW Argentina. *Journal of Structural Geology* 96,
1518 176-191.

1519 Sobiesiak, M., Kneller, B.C., Alsop, G.I., Milana, J.P. 2018. Styles of basal interaction beneath mass
1520 transport deposits. Marine and Petroleum Geology 98, 629-639.

Sobiesiak, M., Kneller, B.C., Alsop, G.I., Milana, J.P. 2020. Block generation, deformation and interaction of mass-transport deposits with the seafloor: An outcrop-based study of the Carboniferous Paganzo Basin (Cerro Bola, NW Argentina). In: Ogata, Kei; Festa, Andrea; Pini, Gian Andrea (Editors) *Submarine landslides: subaqueous mass transport deposits from outcrops to seismic profiles*. American Geophysical Union Monograph Series, 246, p.91-104. John Wiley & Sons Inc. 384pp. ISBN: 978-1-119-50058-2.

Steventon, M.J., Jackson, C,A-L, Hodgson, D.M., Johnson, H.D. 2019. Strain analysis of a seismically imaged mass-transport complex, offshore Uruguay. Basin Research 31, 600-620.

Steventon, M.J., Jackson, C.A-L., Johnson, H.D., Hodgson, D.M., Kelly, S., Omma, J., Gopon, C., Stevenson, C., Fitch, P. 2021. Evolution of a sand-rich submarine channel–lobe system, and the impact of mass-transport and transitional-flow deposits on reservoir heterogeneity: Magnus Field, Northern North Sea. Petroleum Geoscience, 27, petgeo2020-095. https://doi.org/10.1144/petgeo2020-095

Tang, W., Zhang, Y., Pe-Piper, G., Piper, D.J.W., Guo, Z., Li, W. 2020. Soft-sediment deformation structures in alkaline lake deposits of Lower Permian Fengcheng Formation, Junggar Basin, NW China: Implications for syn-sedimentary tectonic activity. Sedimentary Geology 406, 105719.

Torfstein, A., Haase-Schramm, A., Waldmann, N., Kolodny, Y., Stein, M. 2007. U-Th, delta O-18 and paleomagnetic dating of a mid-Pleistocene lacustrine sequence: The Amora Formation, Mount Sedom, Israel. Geochimica Et Cosmochimica Acta, 71(15), A1031–A1031.

Törő, B., Pratt, B.R., 2015. Eocene paleoseismic record in the Green River Formation, Fossil Basin, Wyoming — implications of synsedimentary deformation structures in lacustrine carbonate mudstones. Journal of Sedimentary Research 85, 855–884.

Törő, B., Pratt, B.R., 2015b. Characteristics and implications of sedimentary deformation features in the Green River Formation (Eocene) in Utah and Colorado. In: Vanden Berg, M.D., Ressetar, R., Birgenheier, L.P. (Eds.), Geology of Utah's Uinta Basin and Uinta Mountains. Utah Geological Association Publication 45, 371–422.

Törő, B., Pratt, B.R., 2016. Sedimentary record of seismic events in the Eocene Green River Formation and its implications for regional tectonics on lake evolution (Bridger Basin, Wyoming). Sedimentary Geology 344, 175-204

Törő, B., Pratt, B.R., Renaut, R.W. 2015. Tectonically induced change in lake evolution recorded by seismites in the Eocene Green River Formation, Wyoming. Terra Nova, 27, 218–224.

Van Daele, M., Moernaut, J., Doom, L., Boes, E., Fontijn, K. Heirman, K., Vandoorne, W., Hebbeln, D., Pino, M., Urrutia, R., Brummer, R., De Batist, M. 2015. A comparison of the sedimentary records of the 1960 and 2010 great Chilean earthquakes in 17 lakes: Implications for quantitative lacustrine palaeoseismology. Sedimentology, 62, 1466-1496.

Van Loon, A.J., Pisarska-Jamrozy, M., Nartiss, M., Krievans, M., Soms, J. 2016. Seismites resulting from high frequency, high-magnitude earthquakes in Latvia caused by Late Glacial glacio-isostatic uplift. Journal of Palaeogeography 5, 363–380.

an Loon, A.J., Han, Z., Han, Y. 2013. Origin of the vertically orientated clasts in brecciated shallow-marine limestones of the Chaomidian Formation (Furongian, Shandong Province, China). Sedimentology 60, 1059-1070.)

Van Loon, A.J,. 2014. Seismites and their soft-sediment deformation structures. Geologos 20/2, p. 166.

Waldron, J.W.F., Gagnon, J-F. 2011. Recognizing soft-sediment structures in deformed rocks of orogens. Journal of Structural Geology 33, 271-279.

Walker, W., Jobe, Z.R., Sarf, J.F., Wood, L. 2021. Progradational slope architecture and sediment distribution in outcrops of the mixed carbonate-siliciclastic Bone Spring Formation, Permian Basin, west Texas. Geosphere 17, 1268–1293, https://doi.org/10.1130/GES02355.1.

Wattrus, N.J., Rausch, D.E., Cartwright, J. 2003. Soft-sediment deformation in Lake Superior: evidence for an immature polygonal fault system. In: Van Rensbergen, P., Hillis, R.R., Maltman, A.J., Morley, C.K. (Edirors) Subsurface sediment mobilization. Geological Society, London, Special Publications, 216, 323-334.

Weinberger, R., Levi, T., Alsop, G.I., Eyal, Y. 2016. Coseismic horizontal slip revealed by sheared clastic dikes in the Dead Sea basin. Geological Society of America Bulletin 128, 1193-1206.

Weinberger, R., Levi, T., Alsop. G.I., Marco, S. 2017. Kinematics of Mass Transport |Deposits revealed by magnetic fabrics. Geophysical Research Letters 44, 7743-7749. doi: 10.1002/2017GL074471.

Wetzler, N., Marco, S., Heifetz, E. 2010. Quantitative analysis of seismogenic shear-induced turbulence in lake sediments. Geology 38, 303-306.

Williams, E. 1960. Intra-stratal flow and convolute folding. Geological Magazine 97 (3), 208-214.

Wils, K., Deprez, M., Kissel, C., Vervoort, M., Van Daele, M., Daryono, M.R., Cnudde, V., Natawidjaja, D.H., De Batist, M. 2021. Earthquake doublet revealed by multiple pulses in lacustrine seismo-turbidites. Geology, 49, https://doi. org/10.1130/G48940.1

Woźniak, P.P., Belzyt, S., Pisarska-Jamroży, M., Woronko B., Lamsters, K., Nartišs, M., Bitinas, A. 2021. Liquefaction and re-liquefaction of sediments induced by uneven loadingand glacigenic earthquakes: Implications of results from the LatvianBaltic Sea coast. Sedimentary Geology 421, 105944.

Figure Captions

Figure 1 Cartoons of a) sequential failure model, b) synchronous failure model, and c) secondary failure model with older events (Time 1) at the base of the diagram and younger events (Time 8) towards the top of each column. During sequential failure (a), the contemporary sediment surface fails repeatedly as new sediment is deposited leading to multiple mass transport deposits (MTDs) that in each case form at the time of sediment deposition. The surficial MTDs are cut by an overlying erosive surface and sedimentary cap (in orange) deposited from suspension after each event. During synchronous failure (b), surficial MTDs and sub-surface fold and thrust systems (FATS) form concurrently during a single failure event. Sub-surface FATS are covered by overburden and are therefore not cut by erosive surfaces and sedimentary caps. FATS are bound by upper and lower intrastratal detachments, which deform sediments in the sub-surface that are significantly older than the failure event (e.g. stratigraphy from Time 1 is deformed during Time 6). In the secondary failure model (c), MTDs created during surficial failure become buried and focus later secondary intrastratal deformation and sub-surface detachments along their margins resulting in overprinting structures.

Figure 2 a) General map showing tectonic plates in the Middle East and location of the Dead Sea Fault (DSF) which transfers opening in the Red Sea to the Taurus-Zagros collision zone. Study area marked by the red box in the Dead Sea Basin. b) Map of the Dead Sea (based on Sneh and Weinberger, 2014) showing the position of the Miflat, Masada, Peratzim and Wadi Zin localities referred to in the text. The map also highlights the limits of the Lisan Formation, together with the general movement direction of the fold and thrust systems and MTD's around the basin.

Figure 3 a) Photograph and close-up (b) of infilled desiccation cracks that form neptunian dykes that are cut by an erosive unconformity marked by cobbles in the Lisan Formation (Wadi Zin). c) Neptunian dyke with the infill displaying a crude horizontal stratification of rounded pebbles (Peratzim). d) Photograph and line drawing (e) of erosive unconformity cutting crudely stratified neptunian dykes. These are then offset by a normal fault, which is subsequently truncated by a bed-parallel detachment. Inset in d) shows details of the irregular erosive unconformity. Photographs f) and g) show close-ups of the normal fault offsetting the neptunian dykes and the normal fault being cut by the detachment, respectively. h) Photograph and i) close-up of an irregular erosive surface truncating the hinge and both limbs of an underlying slump fold. The erosive surface is overlain by a sedimentary cap that infills the underlying topography and has a flat horizontal top surface (Peratzim).

Figure 4 Photographs of SSD folds formed during density-driven surficial deformation in MTDs. a) Periodically spaced aragonite-cored anticlines that form 'fingers' penetrating upwards into overlying detrital-rich sediment (Masada). b) Aragonite-cored anticlines penetrating upwards into detrital-rich sediment that 'sinks' downwards into synclines. c) Photograph and d) close-up of billow folds from Miflat, and e) billow folds at Peratzim, where aragonite-cored anticlines rise up into detrital-rich beds that sink downwards into intervening synclines. In each case the surficial folds are cut by an overlying erosive surface and sedimentary cap. f) Upright billow folds that are progressively sheared over during downslope-directed movement of the MTD (Peratzim). g, h, i) Photographs of upright aragonite-cored anticlines that are carried on later thrust ramps (Peratzim). The upright folds are back-rotated on later thrust ramps that cut across them (i).

Figure 5 Graded sedimentary caps containing a) cm-scale folded fragments (Peratzim) and b) graded aragonite fragments (Miflat). The sedimentary caps are parallel to underlying and overlying aragonite-detrital laminae representing background sedimentation. c) Photograph and d) line drawing showing depositional thickening of an MTD in the hangingwall of a growth fault (Masada). e) Close-up photograph of a normal fault and its subsequent truncation by overlying detachment. f) Photograph and g) line drawing of depositional thickening of an MTD in the hangingwall of a growth fault (Peratzim). h) Close-up photograph showing a normal fault cut by several later intrastratal detachments to create a 'sawtooth' profile. The normal fault is draped by overlying stratigraphy indicating that it later became inactive.

Figure 6 a) Aragonite laminae are interfolded with a sedimentary cap that displays dramatic changes in thickness with a horizontal top indicating syn-depositional folding at the surface of a MTD (Peratzim). Later vertical fractures and sedimentary dykes cross-cut the MTD. b) Folded aragonite laminae that are draped by an overlying sedimentary cap above the MTD (Peratzim). c) Photograph and d, e) line drawings of a fold and thrust culmination formed above a detachment marked by small sediment injections (Miflat). The culmination is overlain by an erosive surface and infilling sedimentary cap indicating it formed at the surface. The overlying detrital-rich beds onlap onto the structural high created by the underlying folds, indicating that the culmination continued to grow after deposition of the cap. f) Photograph and g) line drawing of a detachment-bound fold and thrust system (FATS) that arches an overlying sequence of sediment which acted as a roof to the duplex. The sediment package overlying the roof displays thickening off the crest of the culmination, indicating that deformation occurred in the shallow sub-surface. h, j) Photographs and i) line drawing of a detachment-bound FATS that arches the overlying sequence. The overlying detrital bed displays a marked thickening off the crest of the culmination indicating that the FATS developed in the shallow sub-surface.

Figure 7 a, b) Photographs and c) line drawing of a fold and thrust culmination formed above a detachment (Miflat). The culmination is overlain by a stratigraphic package that maintains its thickness over the crest, and which is then cut across by an erosive surface and infilling detrital sequence indicating it formed in the shallow sub-surface. Arching of the erosive surface, coupled with thickening of the overlying detrital beds off the crest of the culmination, indicates that the culmination continued to grow after deposition of the overlying sediments. d, f, h) Photographs and e, g) line drawings of a detachment-bound fold and thrust duplex that locally depresses the lower detachment and arches the upper detachment (Miflat). Immediately overlying stratigraphic packages maintain thickness over the culmination, while upper parts of the overburden are thinned over the crest of the culmination indicating that the FATS developed in the shallow sub-surface. i) Photograph and j) line drawing of FATS that creates an arching of two overlying erosive unconformity surfaces. (Miflat). Arching of stacked unconformities indicates that the culmination continued to grow in the shallow sub-surface over a period of time.

Figure 8 a) Overview photograph and b, e, h) detailed photographs with line drawing (c, f, i) of detachment-bound conjugate normal faults (Masada). Close-up photographs (d, g, j) show details of gouge and cut-offs developed across the upper detachment surface. Truncation of overlying faults (c, d) indicates that deformation occurred in the sub-surface.

Figure 9 a, c) Photographs and b, d) line drawings of conjugate normal faults that are cut by an upper detachment leading to repetition of stratigraphy across the underlying graben (Miflat). An early detachment (1) is downfaulted in the graben and is at the same stratigraphic level as the later detachment (3). e) Schematic summary with circled numbers referring to the relative timing of faulting and detachments based on cross-cutting relationships. Repetition of overburden stratigraphy can only be achieved through sub-surface intrastratal detachments rather than erosive truncation. f, h) Photographs and g) line drawings of conjugate normal faults that are cut by an upper detachment leading to repetition of stratigraphy across the underlying graben (Peratzim). Details of repeated stratigraphy are shown in h) with circled numbers referring to the relative timing of faulting and detachments.

Figure 10 a) Overview photograph, b) interpreted photograph and, c) line drawing of detachment-bound conjugate normal faults (Masada). Close-up photographs (d-j) show details of cut-offs and highlight stratigraphic repetition or 'missing' stratigraphy across the upper detachment surface. k, l) Normal faults becoming listric and rotating into the lower detachment, which is marked by pockets of gouge. Circled numbers refer to the relative timing of faulting and detachments. Repetition of overburden stratigraphy can only be achieved through sub-surface intrastratal detachments rather than erosive truncation.

Figure 11 a) Overview photograph, b) detailed photograph, and c) line drawing of detachment zone cutting a normal fault that is traced through 1.5 m of overburden (Miflat). The normal fault is cut by an upper detachment beneath an overlying gypsum horizon. In the photographs (a-c), matching coloured pink and orange squares (footwall) and circles (hangingwall) mark offset horizons across the normal fault, with displacement generally decreasing towards the upper reference point ('R' in yellow circle). d) Displacement-distance (D-D) graph plotted for the normal fault with hangingwall cut-off markers (coloured circles) defining a displacement profile drawn from the yellow reference point (R) at the right-hand origin. e, f) Photographs showing details of the detachment-bounded fold and thrust system (FATS) that displaces and segments the overlying normal fault. The intrastratal detachment zone is therefore younger than the most recent sediment offset by the normal fault and formed in the sub-surface beneath >1.5 m of overburden.

Figure 12 a, c) Photographs and b, d) line drawings of a intrastratal detachment zone cutting a normal fault that is traced through 1.5 m of overburden (Miflat). The detachment zone comprises extensional and contractional folds and thrusts that form downslope of where detachments ramp through the stratigraphy. Repetition of stratigraphy, coupled with truncation of the overlying normal fault, indicates that the detachment FATS formed in the sub-surface. e) Photograph, f) overview photograph and, g) line drawing of a intrastratal detachment zone and associated FATS formed beneath ~2 m of overburden and a gypsum horizon. h) Close-up photograph and, i) line drawing of downslope verging FATS formed directly beneath upslope-dipping normal faults.

Figure 13 a) Overview photograph, b) photograph, and c) line drawing of detachment zone and associated FATS that forms beneath ~4 m of overburden and overlying gypsum horizon (Miflat). Detailed photographs are provided of the western (d, e) and eastern (f, g) parts of the section. Normal faults in the overburden are cut by detachments beneath the gypsum horizon, and become listric and root downwards into the underlying intrastratal detachment zone. The FATS is developed downslope of where normal faults in the overburden sole into the detachment zone and formed in the sub-surface.

Figure 14 a) Photograph and b) line drawing of thrusts causing folding in an overlying gypsum horizon. The thrusts are then cut by a intrastratal detachment zone that later forms beneath the gypsum (Miflat). c) Photograph and d) line drawing of normal faults causing folding in an overlying gypsum horizon. The normal faults are then cut by a later intrastratal detachment zone (Sedom). e) Detachment folds that form in a competent gypsum horizon that is carried on an underlying detachment. f) Photograph, g) line drawing and, h) close-up photograph of multiple MTD horizons that are offset by later normal faults (Miflat). Normal faults are truncated by intrastratal detachments that are traced for 2 m into the overburden, indicating that detachments formed in the sub-surface. i) Photograph, j) line drawing and, k) close-up photograph of sediment injections that intrude overburden above an intrastratal FATS. Sediment injections taper upwards and cut the upper detachment indicating that they formed shortly after movement on the FATS had ceased.

Figure 15 a) Photograph, b) overview photograph, and c) line drawing of sediment injections that form above a detachment-bound FATS (Miflat). d) Detailed photograph and e) line drawing of a duplex in the FATS and the braided upper detachment system from which sediment injections are sourced.

Figure 16 a) Overview photograph, b) photograph, and c) line drawing of sedimentary dykes and injections intruding overburden above an intrastratal FATS (Miflat). Sedimentary dykes are cut by thrusts in the FATS, as well as overlying detachments. d, e) Detailed photographs of sedimentary dykes being cut and displaced by detachments. f) Overview photograph, g) photograph, and h) line drawing of sedimentary injections forming along an upper detachment above an intrastratal FATS (Miflat). i, j) Details of sedimentary injections which locally 'pond' on the upslope margin of a normal fault that cuts the detachments and injections.

Figure 17 a) Overview photograph, b) photograph, c) detailed photograph, and d) line drawing of an older MTD 1 and its sedimentary cap being repeated around a later recumbent fold that is part of a younger MTD 2 (Miflat). MTD 1 is locally separated into two sub-units by an undeformed package of aragonite laminae. e) Overview photograph, f) photograph, g) detailed colour-coded photograph, and h) line drawing of an older MTD 1 and its sedimentary cap being cut by thrusts associated with MTD 2 (Peratzim). The sedimentary cap to MTD 2 remains undeformed and is overlain by FATS that creates a duplex. i, j) Details of duplex that arches up an overlying panel of sediment indicating that the intrastratal FATS formed in the sub-surface.

Figure 18 a) Photograph, and b) line drawing of a FATS that forms above an MTD (Miflat). Early normal faults that offset the MTD are locally reactivated as thrusts. c) Overview photograph, d) photograph, and e) line drawing of an intrastratal detachment zone with conjugate normal faults forming above an older MTD (Miflat). Details of billow folds within the MTD that are cut by an overlying erosive surface and sedimentary cap are shown in f).

Figure 19 a) Overview photograph, b) photograph, and c) line drawing of a detachment that forms beneath an MTD (Miflat). d) Photograph and e) line drawing of early normal faults being cut by the detachment that is separated from the overlying MTD by a thin panel of undeformed sediment. The normal faults are truncated by the intrastratal detachment rather than the erosive base of the MTD. f) Overview photograph, g) photograph and h) line drawing of MTDs being cut by normal faults that are truncated by a detachment. i, j) Photographs of MTD 1 and MTD 2 being cut by the normal fault, while MTD 3 overlies the intrastratal detachment. k) Photograph of a detachment formed beneath an MTD that is locally separated into two sub-units by an undeformed package of laminae. Only one sedimentary cap is developed above the upper sub-unit.

Figure 20 a) Cartoon summarising structures used to distinguish deformation created at the surface (MTD) versus sub-surface (FATS) and also during secondary reworking of MTDs. Criteria are based on observations from the present study (denoted by figure numbers) and are separated into b) surficial deformation of MTDs (circled blue letters A-N), c) intrastratal secondary reworking of buried MTDs (boxed green roman numerals i-vii), and d) sub-surface intrastratal deformations in FATS (circled red numbers 1-21). Sub-surface reworking and FATS develop concurrently with deformation of surficial sediments during single events.

Figure 1

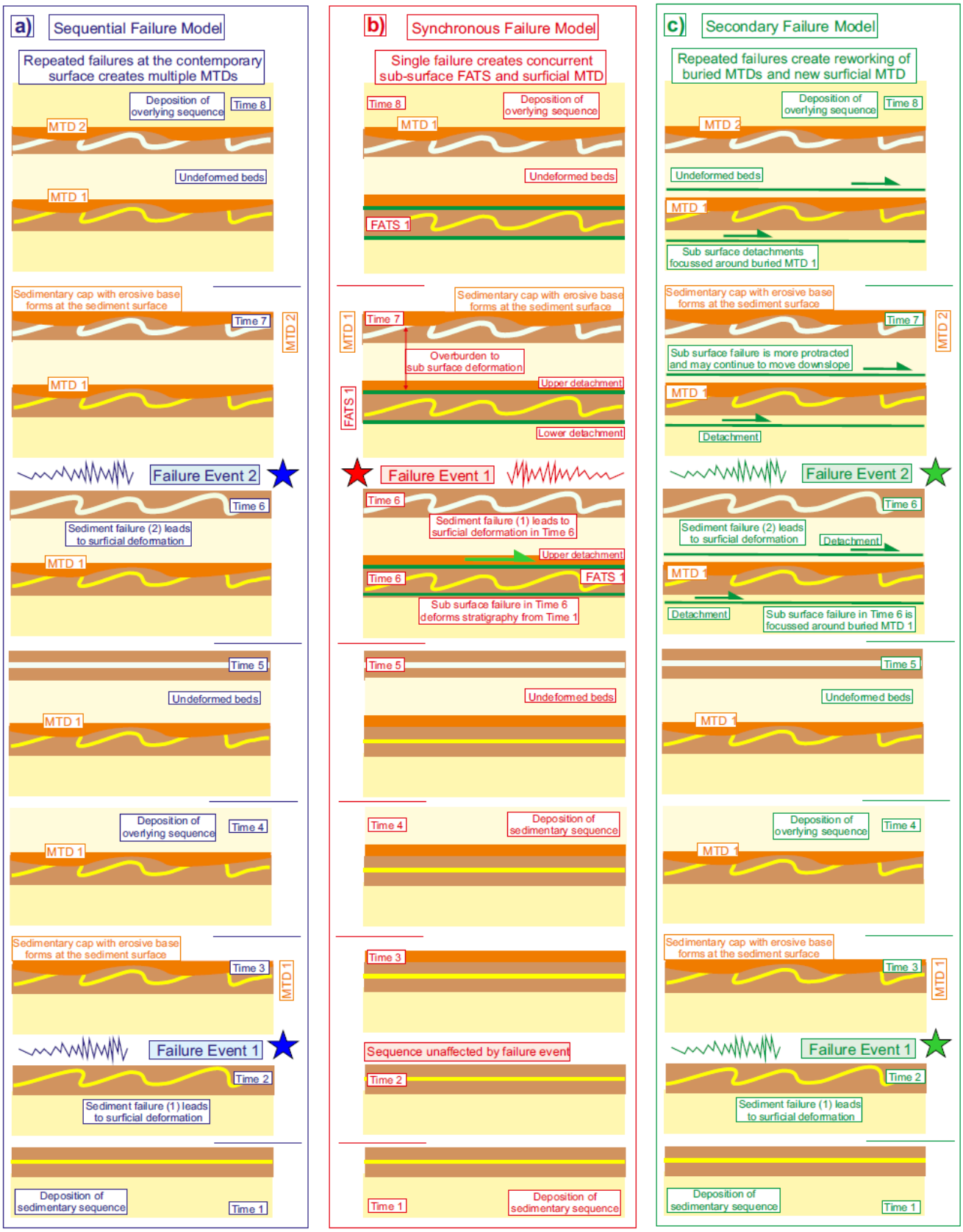
a)
Sequential Failure Model
Repeated failures at the contemporary surface creates multiple MTDs
Deposition of overlying sequence
Time 8
MTD 2
Undeformed beds
MTD 1
Sedimentary cap with erosive base forms at the sediment surface
Time 7
MTD 2
MTD 1
Failure Event 2
Time 6
Sediment failure (2) leads to surficial deformation
MTD 1
Time 5
Undeformed beds
MTD 1
Deposition of overlying sequence
Time 4
MTD 1
Sedimentary cap with erosive base forms at the sediment surface
Time 3
MTD 1
Failure Event 1
Time 2
Sediment failure (1) leads to surficial deformation
Deposition of sedimentary sequence
Time 1
b)
Synchronous Failure Model
Single failure creates concurrent sub-surface FATS and surficial MTD
Time 8
Deposition of overlying sequence
MTD 1
Undeformed beds
FATS 1
Sedimentary cap with erosive base forms at the sediment surface
MTD 1
Time 7
Overburden to sub surface deformation
FATS 1
Upper detachment
Lower detachment
Failure Event 1
Time 6
Sediment failure (1) leads to surficial deformation in Time 6
Upper detachment
Time 6
FATS 1
Sub surface failure in Time 6 deforms stratigraphy from Time 1
Time 5
Undeformed beds
Time 4
Deposition of sedimentary sequence
Time 3
Sequence unaffected by failure event
Time 2
Time 1
Deposition of sedimentary sequence
c)
Secondary Failure Model
Repeated failures create reworking of buried MTDs and new surficial MTD
Deposition of overlying sequence
Time 8
MTD 2
Undeformed beds
MTD 1
Sub surface detachments focussed around buried MTD 1
Sedimentary cap with erosive base forms at the sediment surface
Time 7
MTD 2
Sub surface failure is more protracted and may continue to move downslope
MTD 1
Detachment
Failure Event 2
Time 6
Sediment failure (2) leads to surficial deformation
Detachment
MTD 1
Detachment
Sub surface failure in Time 6 is focussed around buried MTD 1
Time 5
Undeformed beds
MTD 1
Deposition of overlying sequence
Time 4
MTD 1
Sedimentary cap with erosive base forms at the sediment surface
Time 3
MTD 1
Failure Event 1
Time 2
Sediment failure (1) leads to surficial deformation
Deposition of sedimentary sequence
Time 1

Figure 2

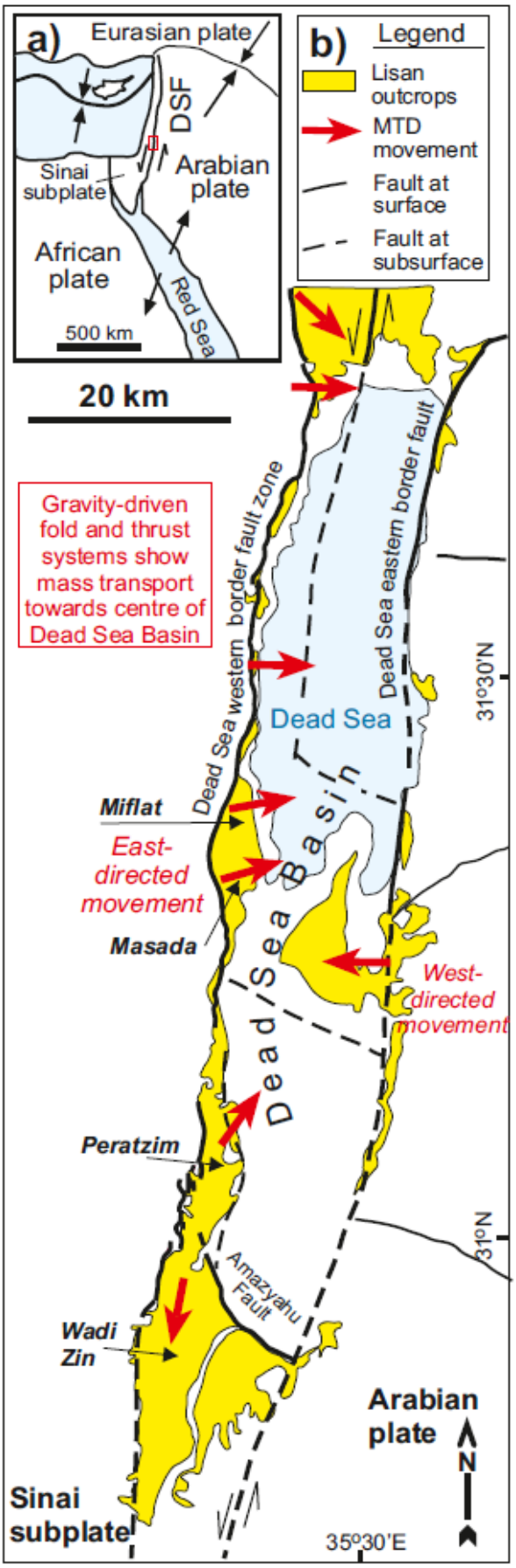
a)
Eurasian plate
DSF
Sinai subplate
Arabian plate
African plate
Red Sea
500 km
b)
Legend
Lisan outcrops
MTD movement
Fault at surface
Fault at subsurface
20 km
Gravity-driven fold and thrust systems show mass transport towards centre of Dead Sea Basin
Dead Sea western border fault zone
Dead Sea eastern border fault
Dead Sea
Dead Sea Basin
31°30'N
Miflat
East-directed movement
Masada
West-directed movement
Peratzim
31°N
Amazyahu Fault
Wadi Zin
Arabian plate
N
Sinai subplate
35°30'E

Figure 3

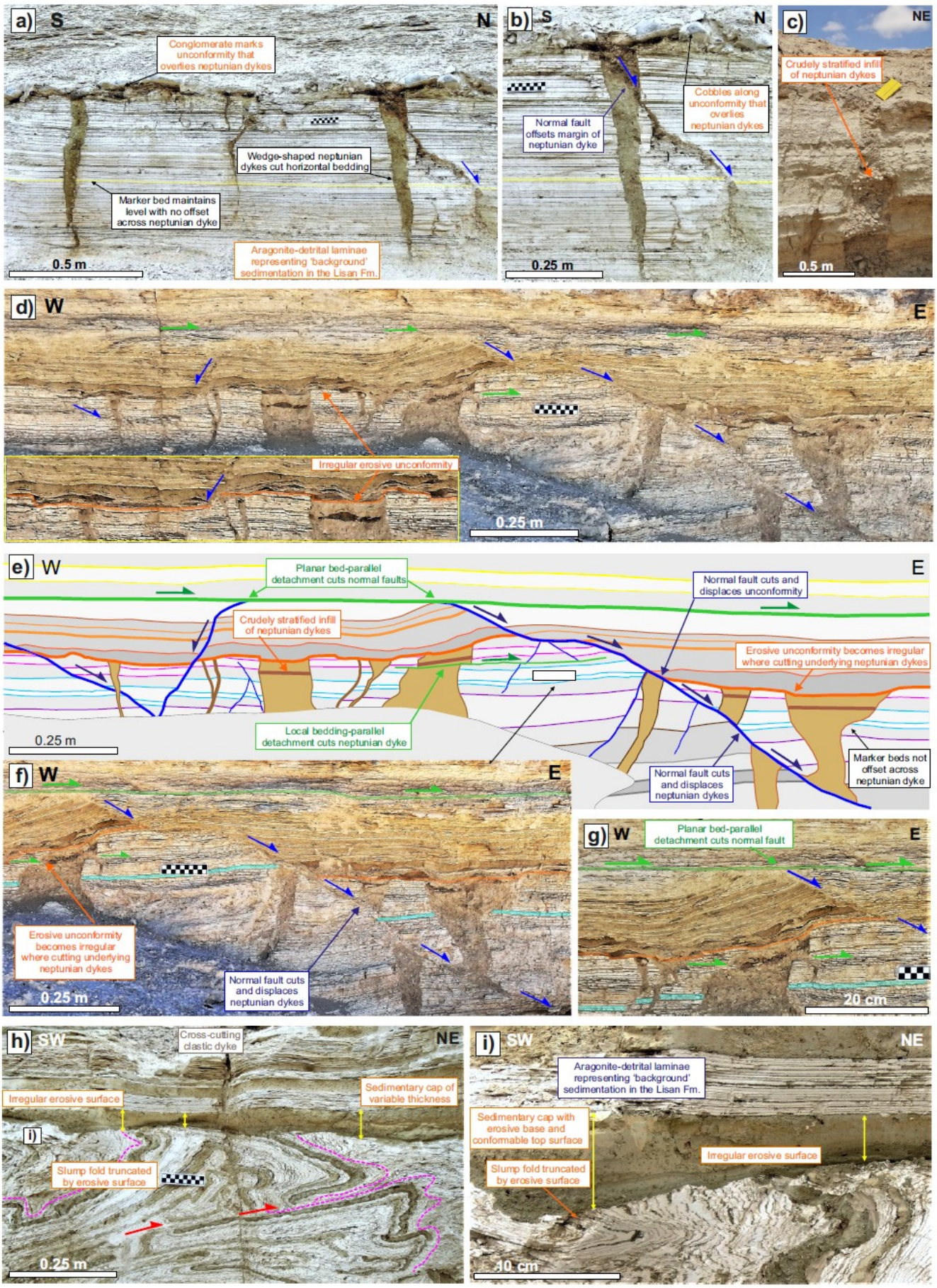
a) S
N
Conglomerate marks unconformity that overlies neptunian dykes
Wedge-shaped neptunian dykes cut horizontal bedding
Marker bed maintains level with no offset across neptunian dyke
Aragonite-detrital laminae representing 'background' sedimentation in the Lisan Fm.
0.5 m
b) S
N
Normal fault offsets margin of neptunian dyke
Cobbles along unconformity that overlies neptunian dykes
0.25 m
c) NE
Crudely stratified infill of neptunian dykes
0.5 m
d) W
E
Irregular erosive unconformity
0.25 m
e) W
E
Planar bed-parallel detachment cuts normal faults
Crudely stratified infill of neptunian dykes
Normal fault cuts and displaces unconformity
Erosive unconformity becomes irregular where cutting underlying neptunian dykes
Local bedding-parallel detachment cuts neptunian dyke
0.25 m
Normal fault cuts and displaces neptunian dykes
Marker beds not offset across neptunian dyke
f) W
E
Erosive unconformity becomes irregular where cutting underlying neptunian dykes
0.25 m
Normal fault cuts and displaces neptunian dykes
g) W
Planar bed-parallel detachment cuts normal fault
E
20 cm
h) SW
NE
Cross-cutting clastic dyke
Irregular erosive surface
Sedimentary cap of variable thickness
i)
Slump fold truncated by erosive surface
0.25 m
i) SW
NE
Aragonite-detrital laminae representing 'background' sedimentation in the Lisan Fm.
Sedimentary cap with erosive base and conformable top surface
Irregular erosive surface
Slump fold truncated by erosive surface
10 cm

Figure 4

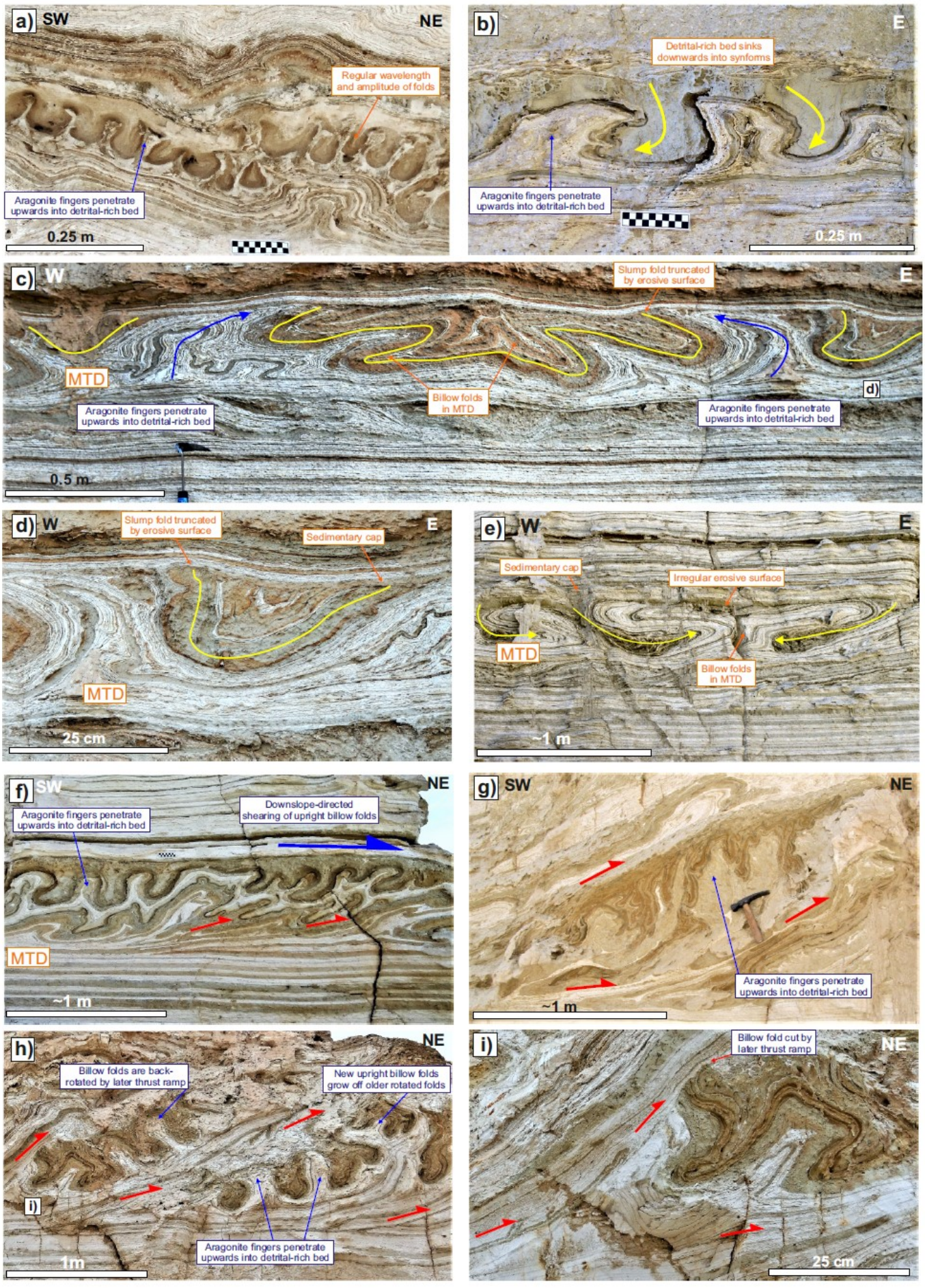
a) SW
NE
Regular wavelength and amplitude of folds
Aragonite fingers penetrate upwards into detrital-rich bed
0.25 m
b)
E
Detrital-rich bed sinks downwards into synforms
Aragonite fingers penetrate upwards into detrital-rich bed
0.25 m
c) W
E
Slump fold truncated by erosive surface
MTD
Billow folds in MTD
Aragonite fingers penetrate upwards into detrital-rich bed
d)
Aragonite fingers penetrate upwards into detrital-rich bed
0.5 m
d) W
E
Slump fold truncated by erosive surface
Sedimentary cap
MTD
25 cm
e) W
E
Sedimentary cap
Irregular erosive surface
MTD
Billow folds in MTD
~1 m
f) SW
NE
Aragonite fingers penetrate upwards into detrital-rich bed
Downslope-directed shearing of upright billow folds
MTD
~1 m
g) SW
NE
Aragonite fingers penetrate upwards into detrital-rich bed
~1 m
h)
NE
Billow folds are back-rotated by later thrust ramp
New upright billow folds grow off older rotated folds
i)
Aragonite fingers penetrate upwards into detrital-rich bed
1m
i)
Billow fold cut by later thrust ramp
NE
25 cm

Figure 5

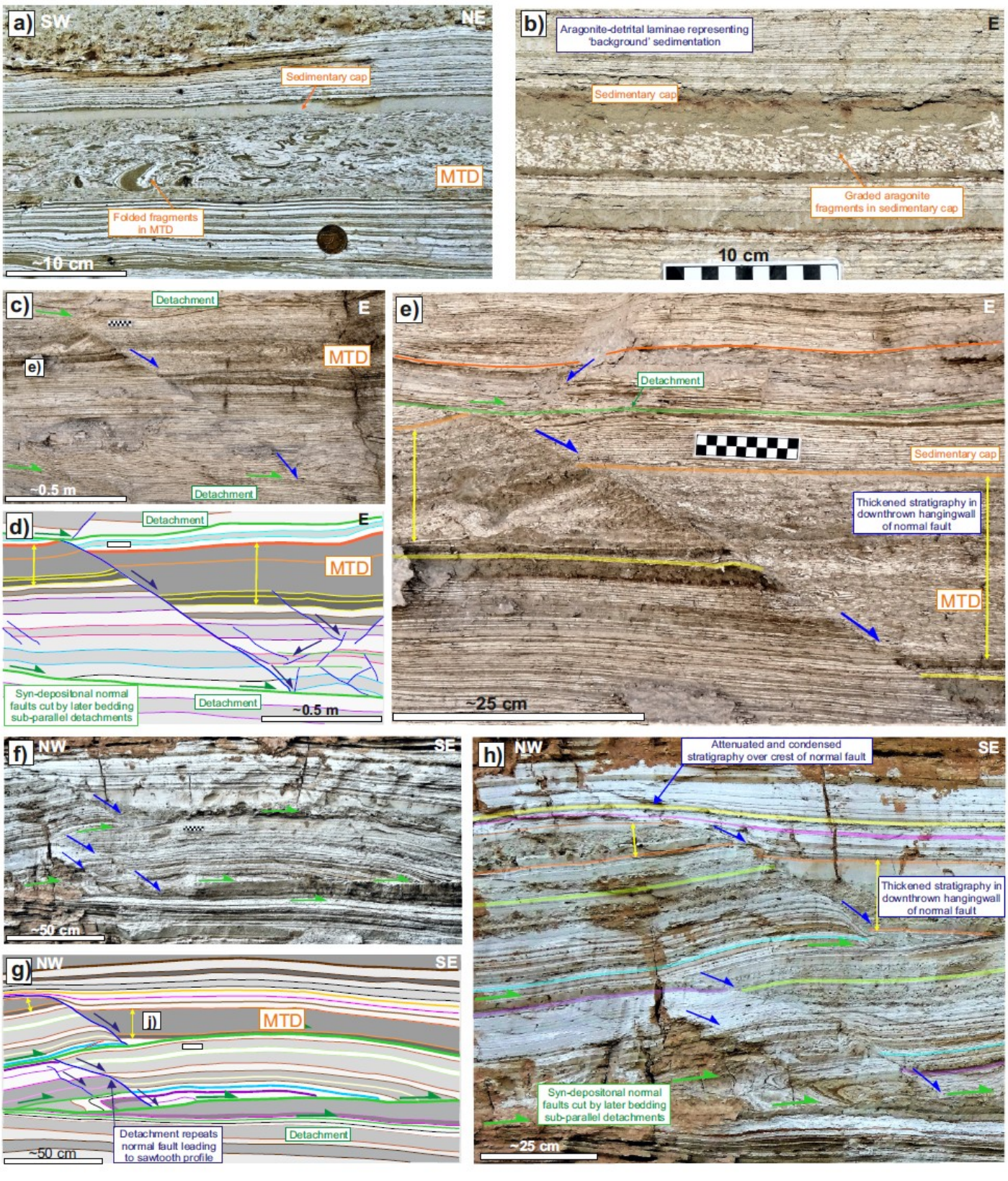
a)
SW
NE
Sedimentary cap
MTD
Folded fragments in MTD
~10 cm
b)
Aragonite-detrital laminae representing 'background' sedimentation
E
Sedimentary cap
Graded aragonite fragments in sedimentary cap
10 cm
c)
Detachment
E
e)
MTD
~0.5 m
Detachment
d)
Detachment
E
MTD
Syn-depositonal normal faults cut by later bedding sub-parallel detachments
Detachment
~0.5 m
e)
E
Detachment
Sedimentary cap
Thickened stratigraphy in downthrown hangingwall of normal fault
MTD
~25 cm
f)
NW
SE
~50 cm
g)
NW
SE
j)
MTD
Detachment repeats normal fault leading to sawtooth profile
Detachment
~50 cm
h)
NW
Attenuated and condensed stratigraphy over crest of normal fault
SE
Thickened stratigraphy in downthrown hangingwall of normal fault
Syn-depositonal normal faults cut by later bedding sub-parallel detachments
~25 cm

Figure 6

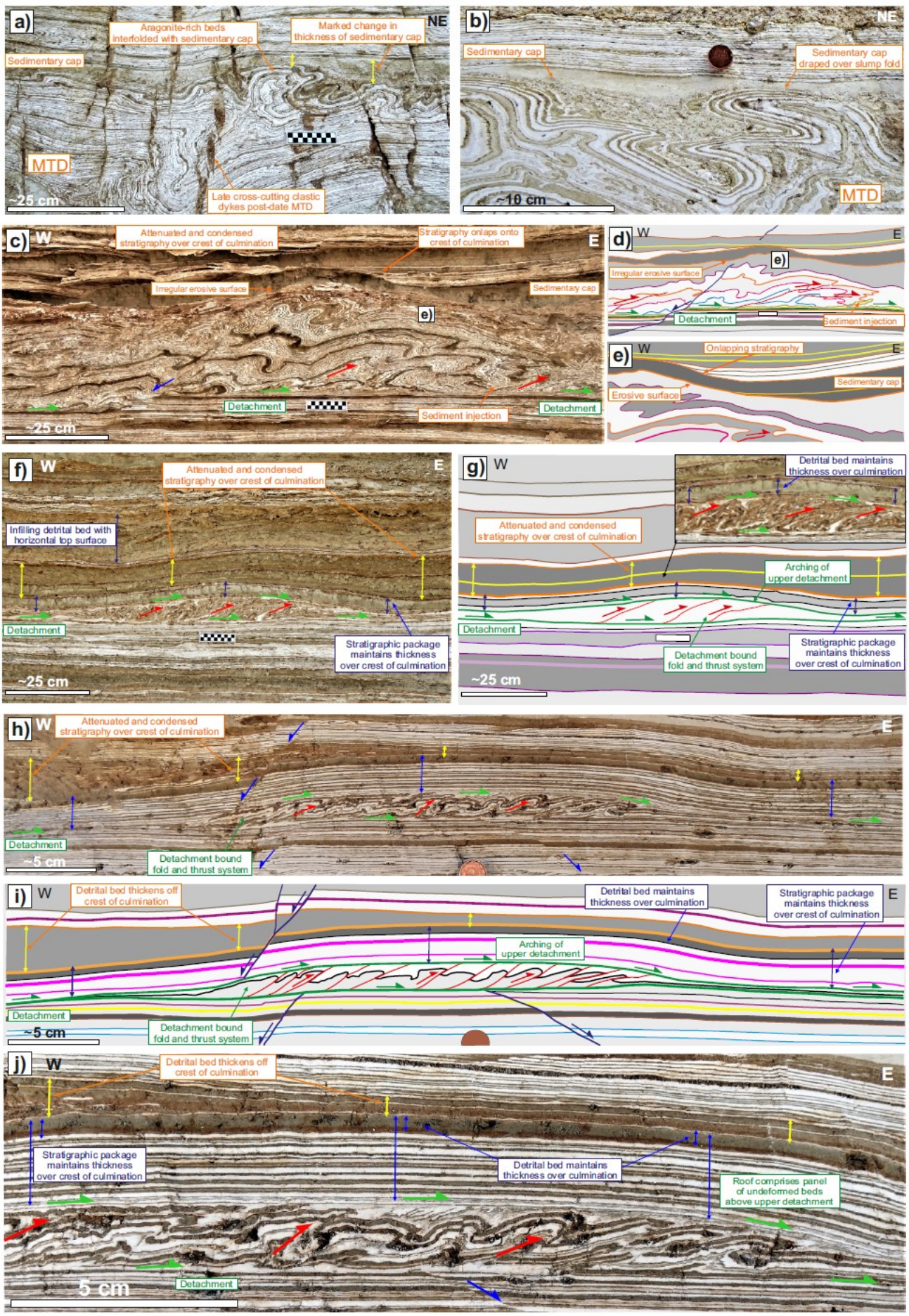
a)
Aragonite-rich beds interfolded with sedimentary cap
Marked change in thickness of sedimentary cap
NE
Sedimentary cap
MTD
Late cross-cutting clastic dykes post-date MTD
~25 cm
b)
NE
Sedimentary cap
Sedimentary cap draped over slump fold
~10 cm
MTD
c)
W
E
Attenuated and condensed stratigraphy over crest of culmination
Stratigraphy onlaps onto crest of culmination
Irregular erosive surface
Sedimentary cap
e)
Detachment
Sediment injection
Detachment
~25 cm
d)
W
E
e)
Irregular erosive surface
Detachment
Sediment injection
e)
W
E
Onlapping stratigraphy
Sedimentary cap
Erosive surface
f)
W
E
Attenuated and condensed stratigraphy over crest of culmination
Infilling detrital bed with horizontal top surface
Detachment
Stratigraphic package maintains thickness over crest of culmination
~25 cm
g)
W
Detrital bed maintains thickness over culmination
Attenuated and condensed stratigraphy over crest of culmination
Arching of upper detachment
Detachment
Detachment bound fold and thrust system
Stratigraphic package maintains thickness over crest of culmination
~25 cm
h)
W
E
Attenuated and condensed stratigraphy over crest of culmination
Detachment
~5 cm
Detachment bound fold and thrust system
i)
W
E
Detrital bed thickens off crest of culmination
Detrital bed maintains thickness over culmination
Stratigraphic package maintains thickness over crest of culmination
Arching of upper detachment
Detachment
~5 cm
Detachment bound fold and thrust system
j)
W
E
Detrital bed thickens off crest of culmination
Stratigraphic package maintains thickness over crest of culmination
Detrital bed maintains thickness over culmination
Roof comprises panel of undeformed beds above upper detachment
5 cm
Detachment

Figure 7

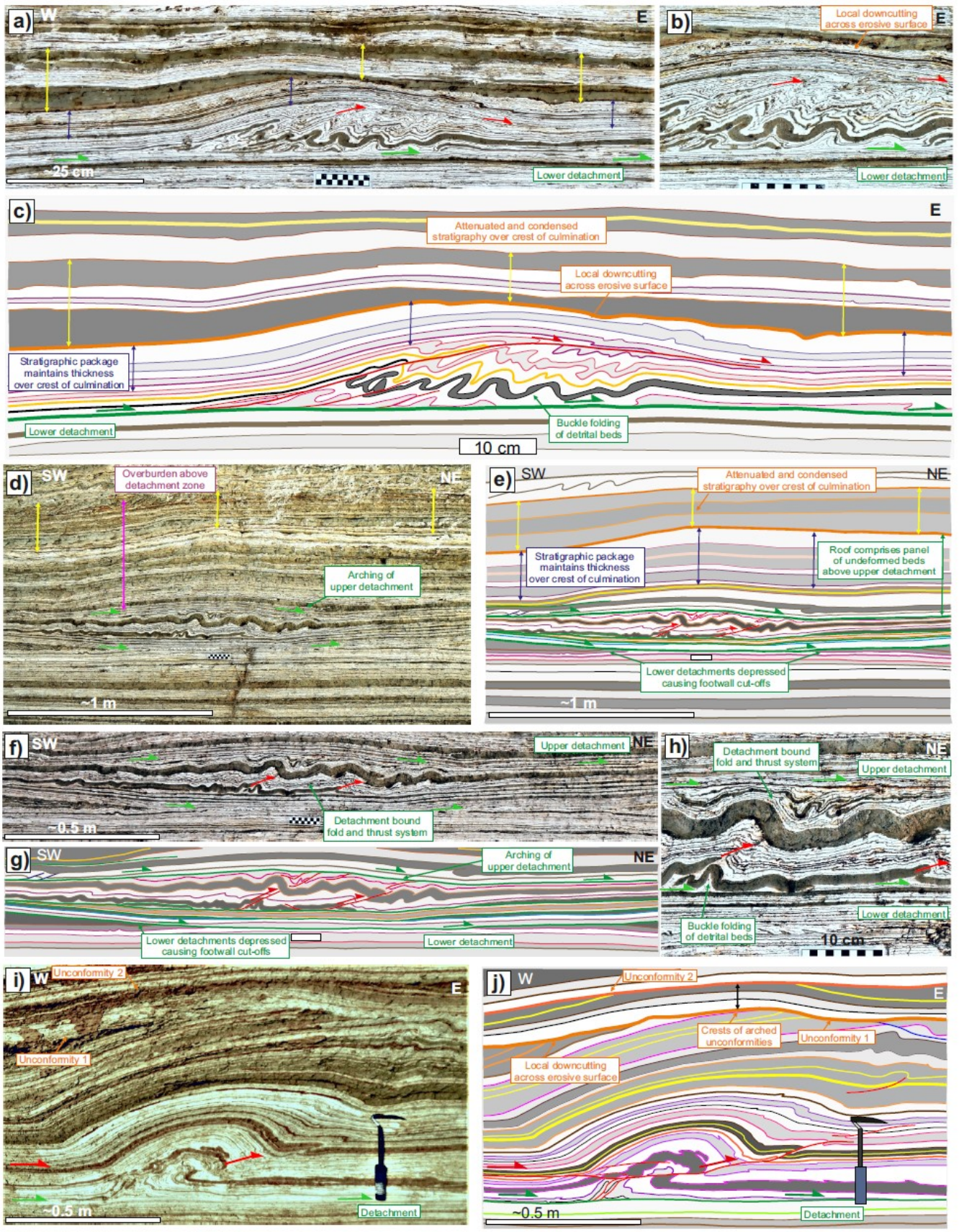
a)
W
E
~25 cm
Lower detachment
b)
Local downcutting across erosive surface
E
Lower detachment
c)
E
Attenuated and condensed stratigraphy over crest of culmination
Local downcutting across erosive surface
Stratigraphic package maintains thickness over crest of culmination
Lower detachment
Buckle folding of detrital beds
10 cm
d)
SW
Overburden above detachment zone
NE
Arching of upper detachment
~1 m
e)
SW
Attenuated and condensed stratigraphy over crest of culmination
NE
Stratigraphic package maintains thickness over crest of culmination
Roof comprises panel of undeformed beds above upper detachment
Lower detachments depressed causing footwall cut-offs
~1 m
f)
SW
Upper detachment
NE
~0.5 m
Detachment bound fold and thrust system
g)
SW
Arching of upper detachment
NE
Lower detachments depressed causing footwall cut-offs
Lower detachment
h)
Detachment bound fold and thrust system
NE
Upper detachment
Lower detachment
Buckle folding of detrital beds
10 cm
i)
W
Unconformity 2
E
Unconformity 1
~0.5 m
Detachment
j)
W
Unconformity 2
E
Crests of arched unconformities
Unconformity 1
Local downcutting across erosive surface
~0.5 m
Detachment

Figure 8

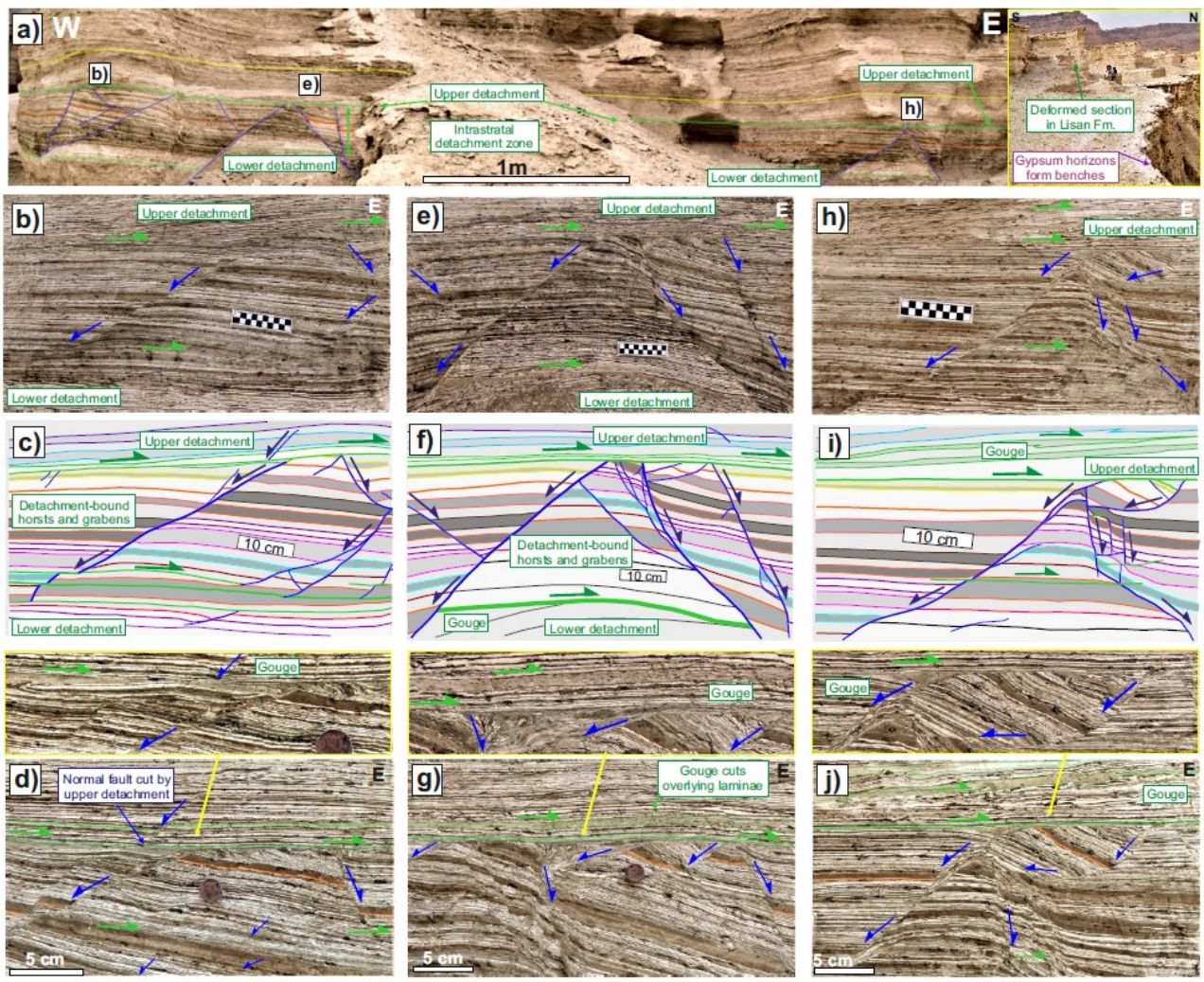
a) W
E
b)
e)
h)
Upper detachment
Intrastratal detachment zone
1m
Lower detachment
S
N
Deformed section in Lisan Fm.
Gypsum horizons form benches
Detachment-bound horsts and grabens
10 cm
Gouge
Normal fault cut by upper detachment
Gouge cuts overlying laminae
5 cm

Figure 9

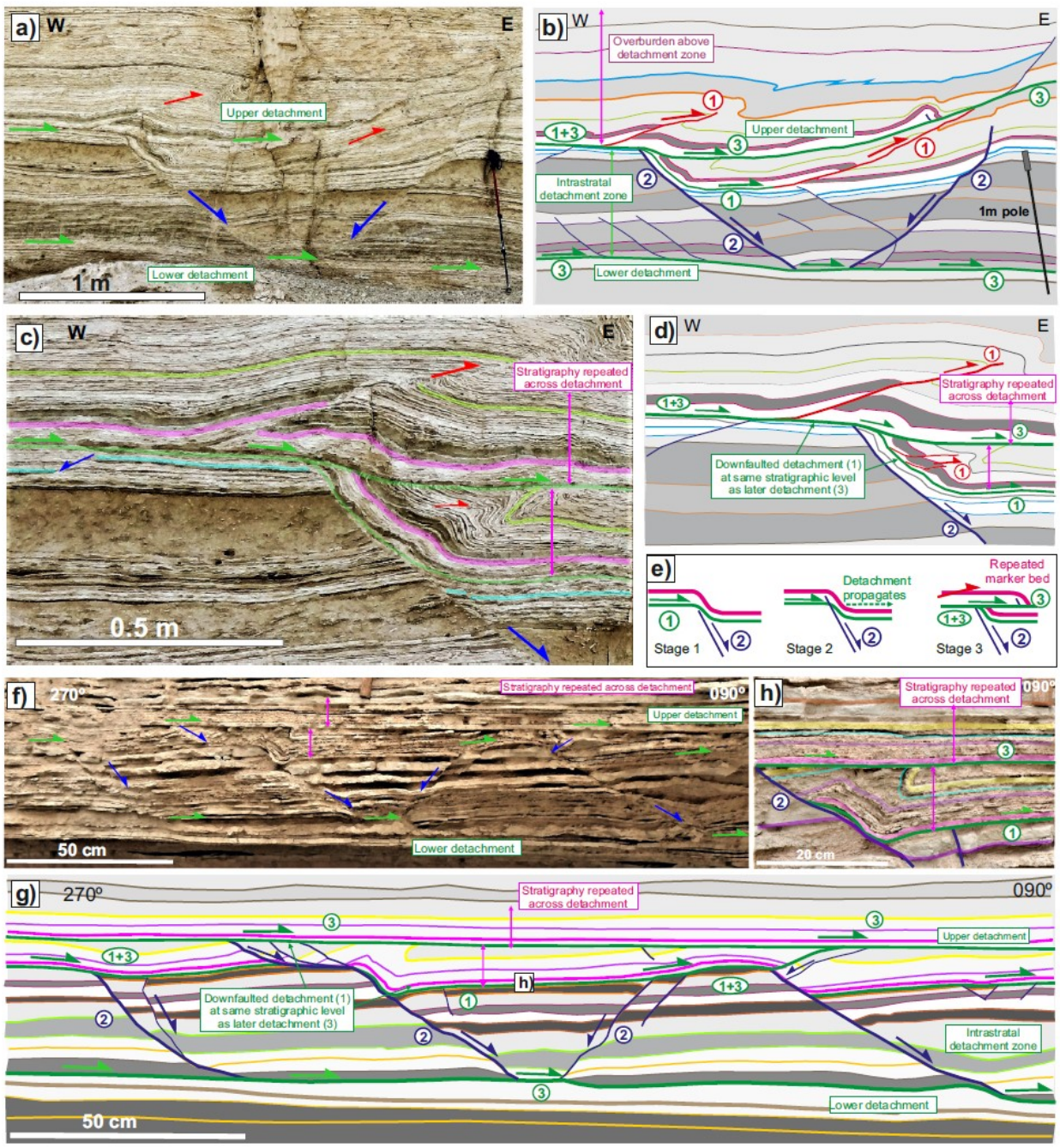
a)
W
E
Upper detachment
1 m
Lower detachment
b)
W
E
Overburden above detachment zone
1
1+3
3
Upper detachment
Intrastratal detachment zone
2
1m pole
Lower detachment
c)
W
E
Stratigraphy repeated across detachment
0.5 m
d)
W
E
Stratigraphy repeated across detachment
Downfaulted detachment (1) at same stratigraphic level as later detachment (3)
e)
Detachment propagates
Repeated marker bed
Stage 1
Stage 2
Stage 3
f)
270°
090°
Stratigraphy repeated across detachment
Upper detachment
50 cm
Lower detachment
h)
Stratigraphy repeated across detachment
090°
20 cm
g)
270°
090°
Stratigraphy repeated across detachment
Upper detachment
Downfaulted detachment (1) at same stratigraphic level as later detachment (3)
Intrastratal detachment zone
Lower detachment
50 cm

Figure 10

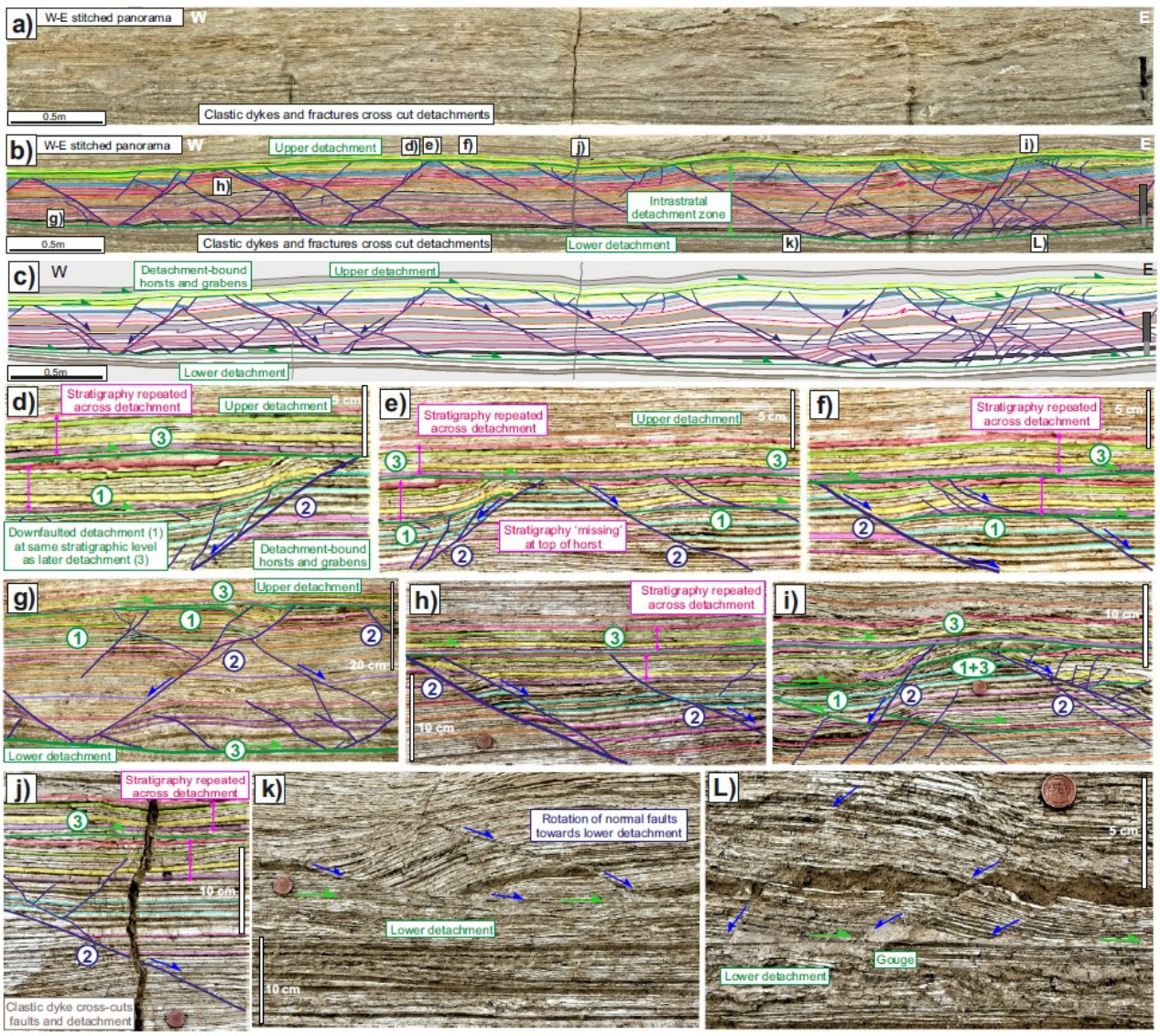
a)
W-E stitched panorama
W
E
0.5m
Clastic dykes and fractures cross cut detachments
b)
W-E stitched panorama
W
E
Upper detachment
d)
e)
f)
j)
i)
h)
g)
Intrastratal detachment zone
0.5m
Clastic dykes and fractures cross cut detachments
Lower detachment
k)
L)
c)
W
E
Detachment-bound horsts and grabens
Upper detachment
0.5m
Lower detachment
d)
Stratigraphy repeated across detachment
Upper detachment
5 cm
Downfaulted detachment (1) at same stratigraphic level as later detachment (3)
Detachment-bound horsts and grabens
e)
Stratigraphy repeated across detachment
Upper detachment
5 cm
Stratigraphy 'missing' at top of horst
f)
Stratigraphy repeated across detachment
5 cm
g)
Upper detachment
20 cm
Lower detachment
h)
Stratigraphy repeated across detachment
10 cm
i)
10 cm
1+3
j)
Stratigraphy repeated across detachment
10 cm
Clastic dyke cross-cuts faults and detachment
k)
Rotation of normal faults towards lower detachment
Lower detachment
10 cm
L)
5 cm
Gouge
Lower detachment

Figure 11

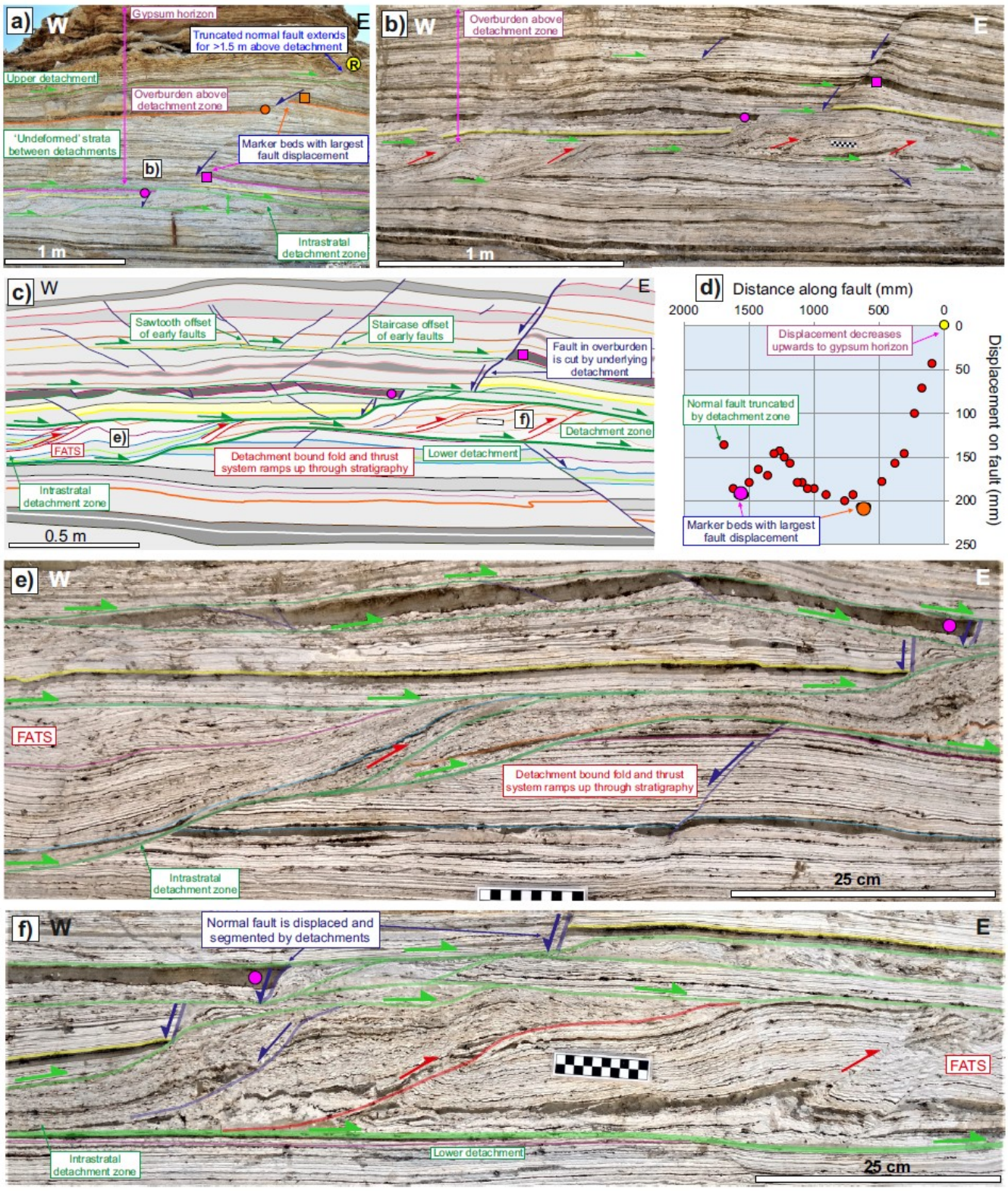
a)
W
E
Gypsum horizon
Truncated normal fault extends for >1.5 m above detachment
R
Upper detachment
Overburden above detachment zone
'Undeformed' strata between detachments
Marker beds with largest fault displacement
b)
Intrastratal detachment zone
1 m
b)
W
E
Overburden above detachment zone
1 m
c)
W
E
Sawtooth offset of early faults
Staircase offset of early faults
Fault in overburden is cut by underlying detachment
f)
e)
FATS
Detachment zone
Lower detachment
Detachment bound fold and thrust system ramps up through stratigraphy
Intrastratal detachment zone
0.5 m
d)
Distance along fault (mm)
2000
1500
1000
500
0
Displacement decreases upwards to gypsum horizon
Normal fault truncated by detachment zone
Marker beds with largest fault displacement
Displacement on fault (mm)
0
50
100
150
200
250
e)
W
E
FATS
Detachment bound fold and thrust system ramps up through stratigraphy
Intrastratal detachment zone
25 cm
f)
W
E
Normal fault is displaced and segmented by detachments
FATS
Intrastratal detachment zone
Lower detachment
25 cm

Figure 12

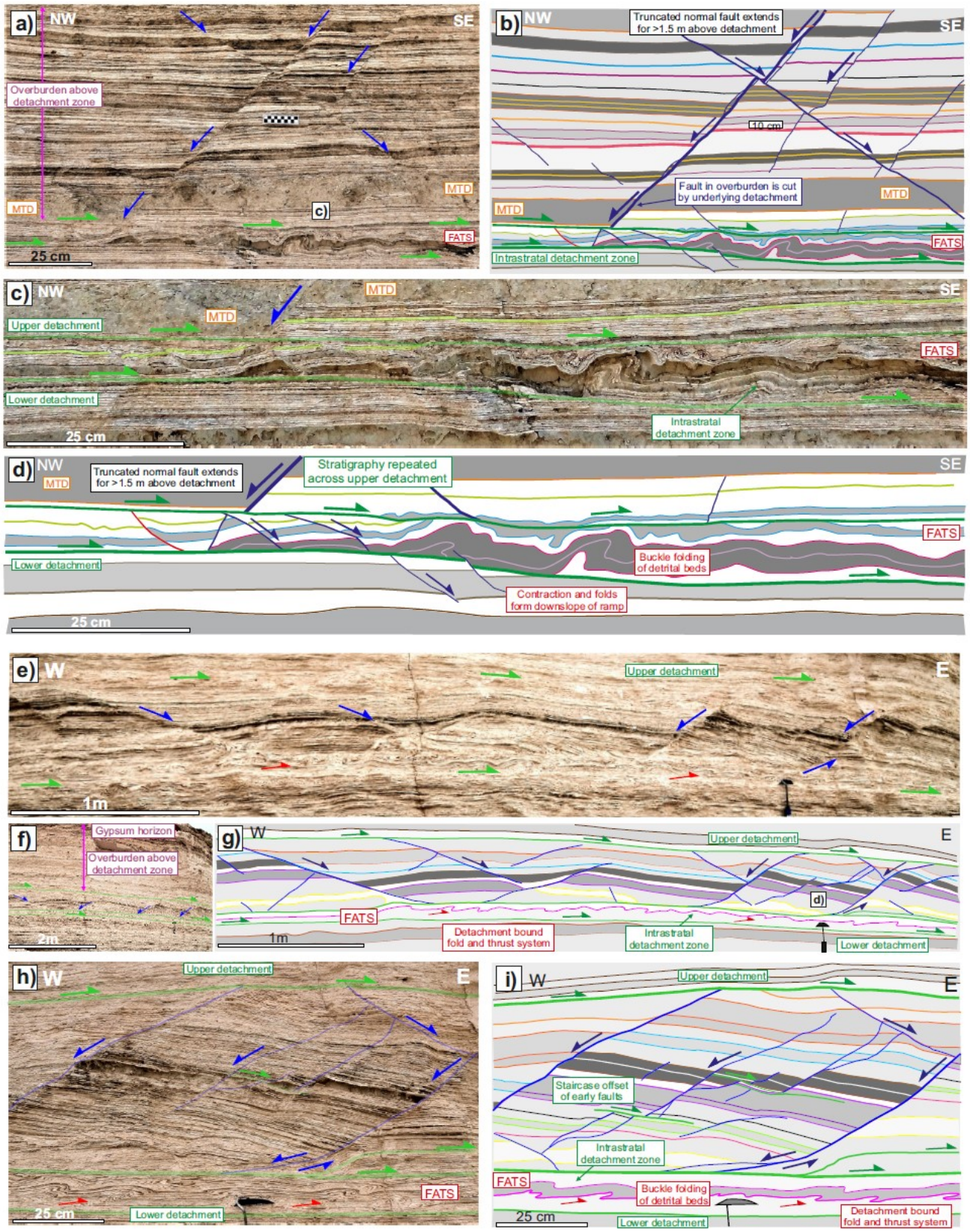
a)
NW
SE
Overburden above detachment zone
MTD
MTD
c)
MTD
FATS
25 cm
b)
NW
Truncated normal fault extends for >1.5 m above detachment
SE
10 cm
Fault in overburden is cut by underlying detachment
MTD
MTD
FATS
Intrastratal detachment zone
c)
NW
MTD
MTD
SE
Upper detachment
FATS
Lower detachment
Intrastratal detachment zone
25 cm
d)
NW
MTD
Truncated normal fault extends for >1.5 m above detachment
Stratigraphy repeated across upper detachment
SE
FATS
Lower detachment
Buckle folding of detrital beds
Contraction and folds form downslope of ramp
25 cm
e)
W
Upper detachment
E
1m
f)
Gypsum horizon
Overburden above detachment zone
2m
g)
W
Upper detachment
E
d)
FATS
1m
Detachment bound fold and thrust system
Intrastratal detachment zone
Lower detachment
h)
W
Upper detachment
E
FATS
25 cm
Lower detachment
i)
W
Upper detachment
E
Staircase offset of early faults
Intrastratal detachment zone
FATS
Buckle folding of detrital beds
25 cm
Lower detachment
Detachment bound fold and thrust system

Figure 13

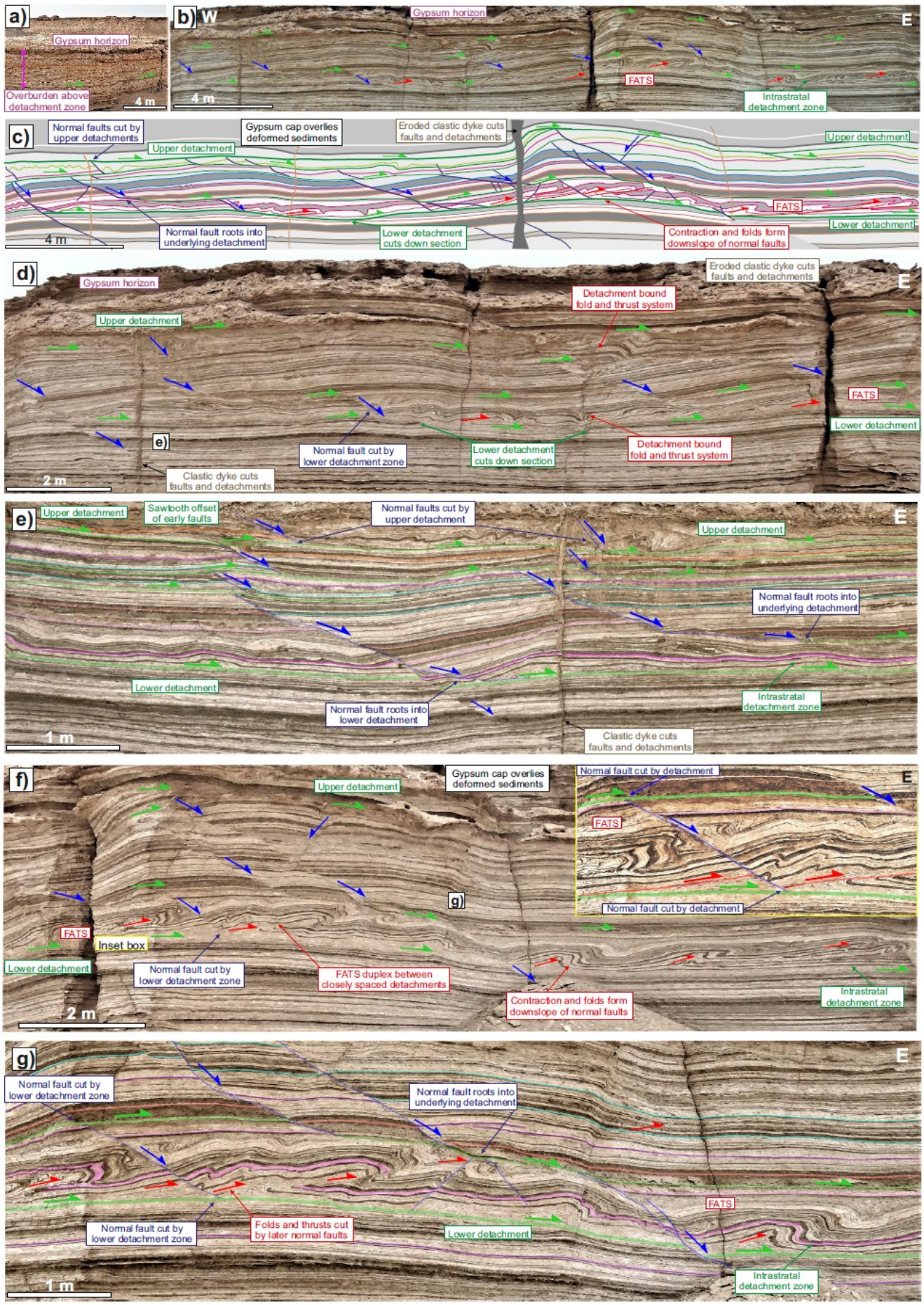
a)
Gypsum horizon
Overburden above detachment zone
4 m
b)
W
E
Gypsum horizon
FATS
Intrastratal detachment zone
4 m
c)
Normal faults cut by upper detachments
Upper detachment
Gypsum cap overlies deformed sediments
Eroded clastic dyke cuts faults and detachments
Upper detachment
FATS
Lower detachment
Normal fault roots into underlying detachment
Lower detachment cuts down section
Contraction and folds form downslope of normal faults
4 m
d)
Gypsum horizon
Upper detachment
Eroded clastic dyke cuts faults and detachments
E
Detachment bound fold and thrust system
FATS
Lower detachment
e)
Normal fault cut by lower detachment zone
Lower detachment cuts down section
Detachment bound fold and thrust system
Clastic dyke cuts faults and detachments
2 m
e)
Upper detachment
Sawtooth offset of early faults
Normal faults cut by upper detachment
E
Upper detachment
Normal fault roots into underlying detachment
Lower detachment
Normal fault roots into lower detachment
Intrastratal detachment zone
Clastic dyke cuts faults and detachments
1 m
f)
Upper detachment
Gypsum cap overlies deformed sediments
Normal fault cut by detachment
E
FATS
g)
Normal fault cut by detachment
FATS
Inset box
Lower detachment
Normal fault cut by lower detachment zone
FATS duplex between closely spaced detachments
Contraction and folds form downslope of normal faults
Intrastratal detachment zone
2 m
g)
E
Normal fault cut by lower detachment zone
Normal fault roots into underlying detachment
FATS
Normal fault cut by lower detachment zone
Folds and thrusts cut by later normal faults
Lower detachment
Intrastratal detachment zone
1 m

Figure 14

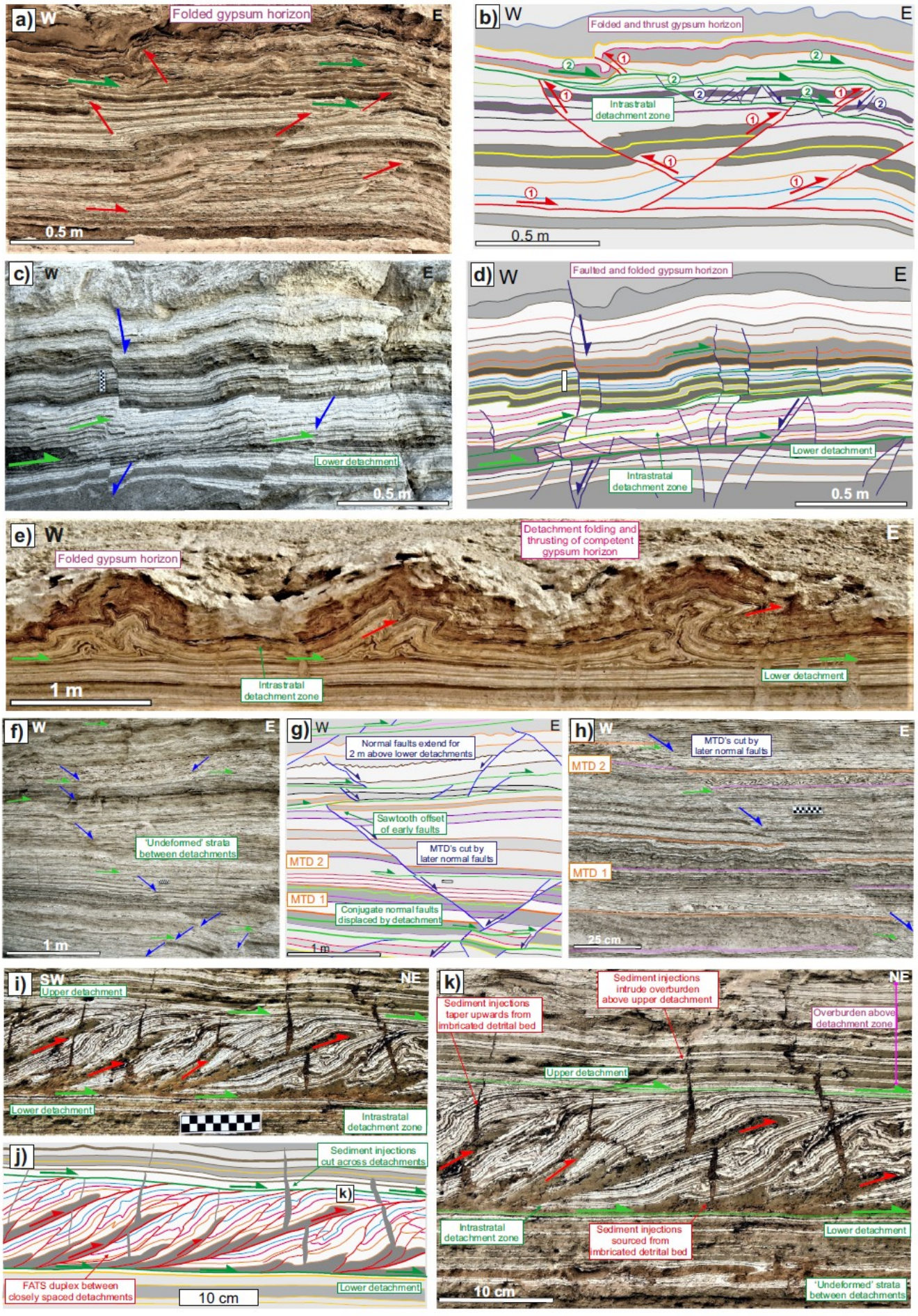
a) W
Folded gypsum horizon
E
0.5 m
b) W
Folded and thrust gypsum horizon
E
Intrastratal detachment zone
0.5 m
c) W
E
Lower detachment
0.5 m
d) W
Faulted and folded gypsum horizon
E
Lower detachment
Intrastratal detachment zone
0.5 m
e) W
Folded gypsum horizon
Detachment folding and thrusting of competent gypsum horizon
E
1 m
Intrastratal detachment zone
Lower detachment
f) W
E
'Undeformed' strata between detachments
1 m
g) W
E
Normal faults extend for 2 m above lower detachments
Sawtooth offset of early faults
MTD's cut by later normal faults
MTD 2
MTD 1
Conjugate normal faults displaced by detachment
1 m
h) W
E
MTD's cut by later normal faults
MTD 2
MTD 1
25 cm
i) SW
Upper detachment
NE
Lower detachment
Intrastratal detachment zone
j)
Sediment injections cut across detachments
k)
FATS duplex between closely spaced detachments
10 cm
Lower detachment
k)
Sediment injections taper upwards from imbricated detrital bed
Sediment injections intrude overburden above upper detachment
NE
Overburden above detachment zone
Upper detachment
Intrastratal detachment zone
Sediment injections sourced from imbricated detrital bed
Lower detachment
10 cm
'Undeformed' strata between detachments

Figure 15

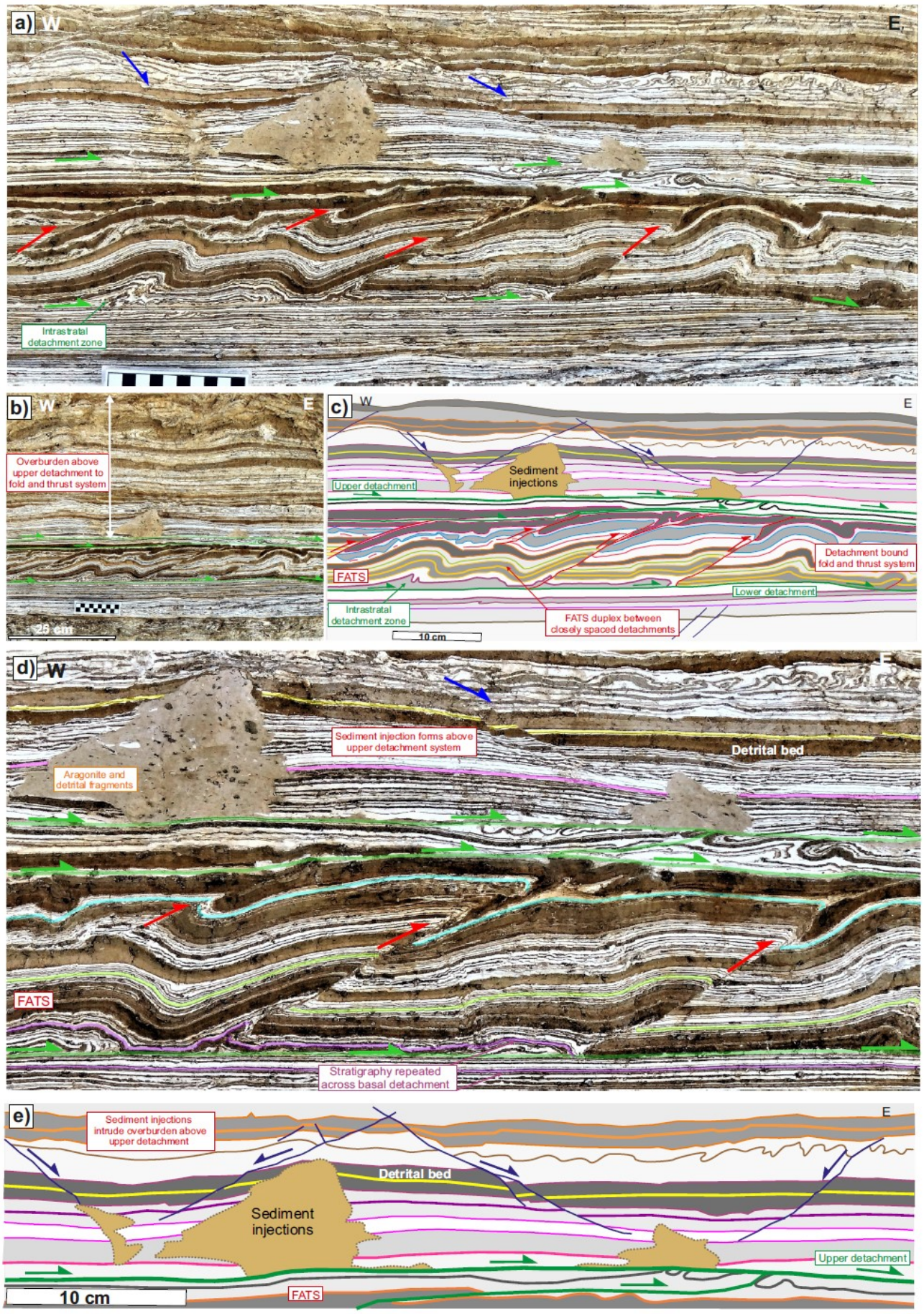
a)
W
E
Intrastratal detachment zone
b)
W
E
Overburden above upper detachment to fold and thrust system
25 cm
c)
W
E
Sediment injections
Upper detachment
FATS
Intrastratal detachment zone
10 cm
Detachment bound fold and thrust system
Lower detachment
FATS duplex between closely spaced detachments
d)
W
E
Sediment injection forms above upper detachment system
Detrital bed
Aragonite and detrital fragments
FATS
Stratigraphy repeated across basal detachment
e)
E
Sediment injections intrude overburden above upper detachment
Detrital bed
Sediment injections
Upper detachment
10 cm
FATS

Figure 16

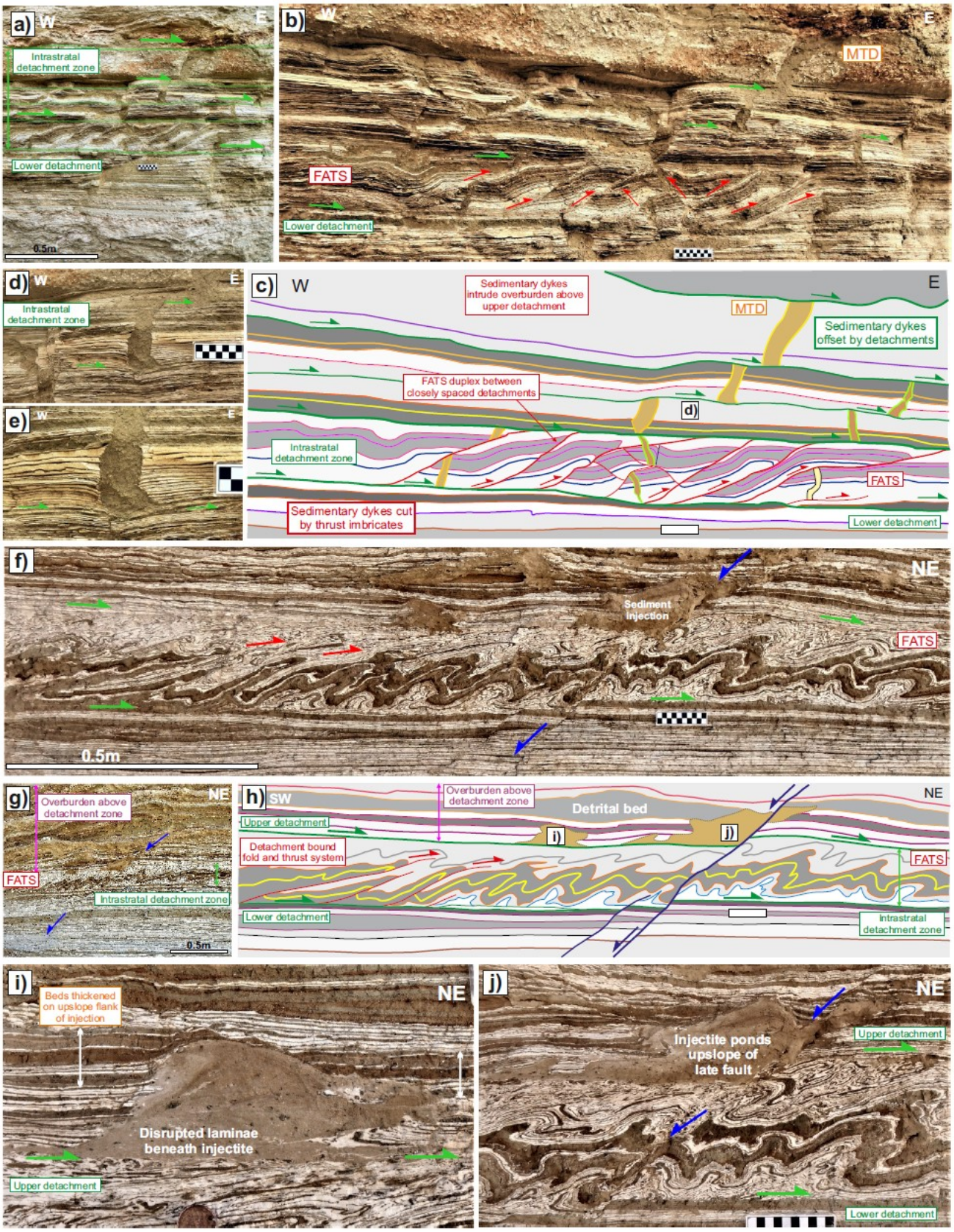
a)
W
E
Intrastratal detachment zone
Lower detachment
0.5m
b)
W
E
MTD
FATS
Lower detachment
d)
W
E
Intrastratal detachment zone
e)
W
E
c)
W
E
Sedimentary dykes intrude overburden above upper detachment
MTD
Sedimentary dykes offset by detachments
FATS duplex between closely spaced detachments
d)
Intrastratal detachment zone
FATS
Sedimentary dykes cut by thrust imbricates
Lower detachment
f)
NE
Sediment injection
FATS
0.5m
g)
NE
Overburden above detachment zone
FATS
Intrastratal detachment zone
0.5m
h)
SW
NE
Overburden above detachment zone
Detrital bed
Upper detachment
i)
j)
Detachment bound fold and thrust system
FATS
Lower detachment
Intrastratal detachment zone
i)
NE
Beds thickened on upslope flank of injection
Disrupted laminae beneath injectite
Upper detachment
j)
NE
Injectite ponds upslope of late fault
Upper detachment
Lower detachment

Figure 17

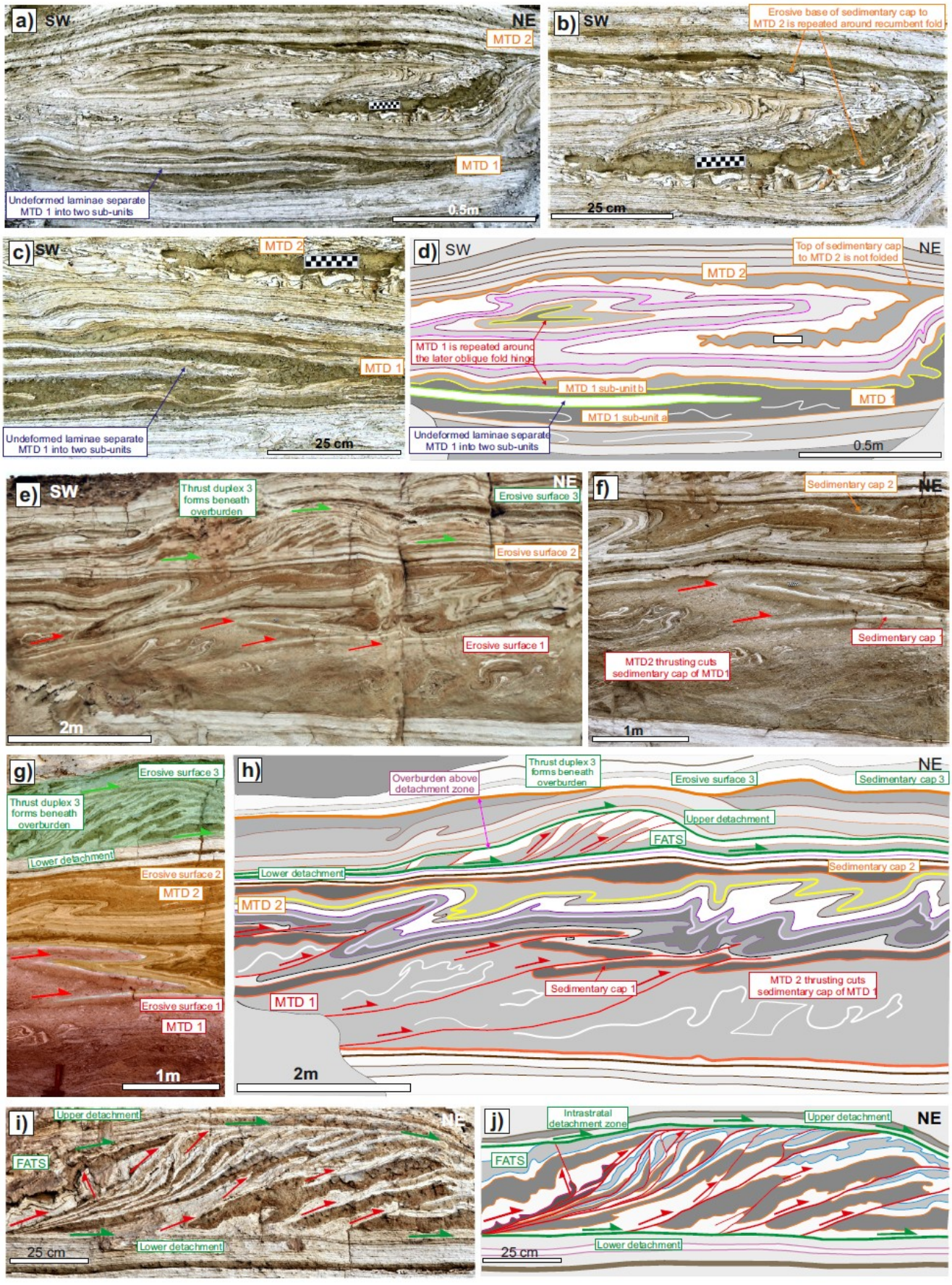
a) SW
NE
MTD 2
MTD 1
Undeformed laminae separate MTD 1 into two sub-units
0.5m
b) SW
Erosive base of sedimentary cap to MTD 2 is repeated around recumbent fold
25 cm
c) SW
MTD 2
MTD 1
Undeformed laminae separate MTD 1 into two sub-units
25 cm
d) SW
Top of sedimentary cap to MTD 2 is not folded
NE
MTD 2
MTD 1 is repeated around the later oblique fold hinge
MTD 1 sub-unit b
MTD 1
MTD 1 sub-unit a
Undeformed laminae separate MTD 1 into two sub-units
0.5m
e) SW
Thrust duplex 3 forms beneath overburden
NE
Erosive surface 3
Erosive surface 2
Erosive surface 1
2m
f)
Sedimentary cap 2
NE
Sedimentary cap 1
MTD2 thrusting cuts sedimentary cap of MTD1
1m
g)
Erosive surface 3
Thrust duplex 3 forms beneath overburden
Lower detachment
Erosive surface 2
MTD 2
Erosive surface 1
MTD 1
1m
h)
Overburden above detachment zone
Thrust duplex 3 forms beneath overburden
Erosive surface 3
NE
Sedimentary cap 3
Upper detachment
FATS
Lower detachment
Sedimentary cap 2
MTD 2
Sedimentary cap 1
MTD 2 thrusting cuts sedimentary cap of MTD 1
MTD 1
2m
i)
Upper detachment
NE
FATS
25 cm
Lower detachment
j)
Intrastratal detachment zone
Upper detachment
NE
FATS
25 cm
Lower detachment

Figure 18

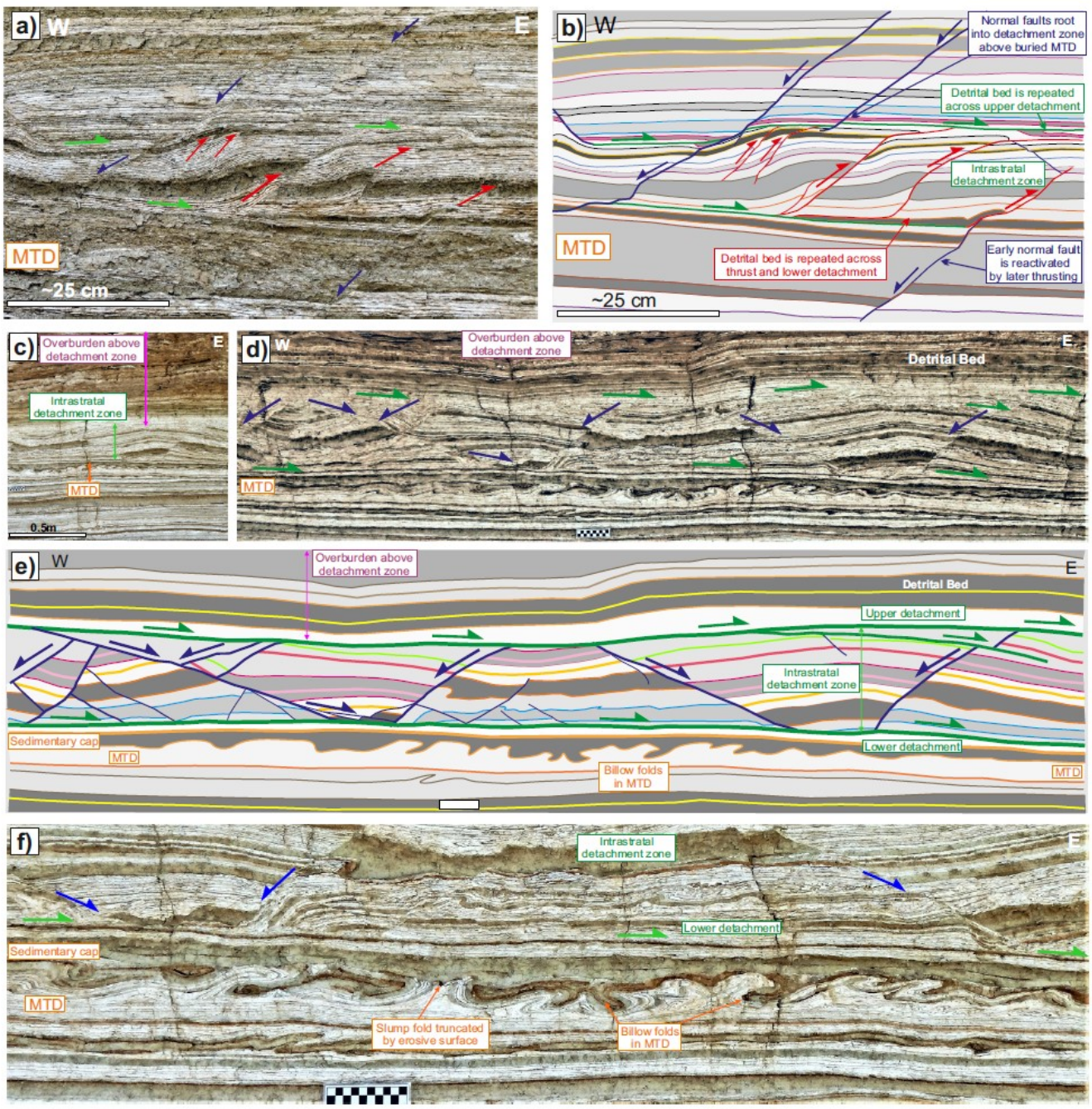
a) W
E
MTD
~25 cm
b) W
Normal faults root into detachment zone above buried MTD
Detrital bed is repeated across upper detachment
Intrastratal detachment zone
MTD
Detrital bed is repeated across thrust and lower detachment
Early normal fault is reactivated by later thrusting
~25 cm
c)
Overburden above detachment zone
E
Intrastratal detachment zone
MTD
0.5m
d) W
Overburden above detachment zone
Detrital Bed
E
MTD
e) W
Overburden above detachment zone
Detrital Bed
E
Upper detachment
Intrastratal detachment zone
Sedimentary cap
MTD
Lower detachment
Billow folds in MTD
MTD
f)
Intrastratal detachment zone
E
Lower detachment
Sedimentary cap
MTD
Slump fold truncated by erosive surface
Billow folds in MTD

Figure 19

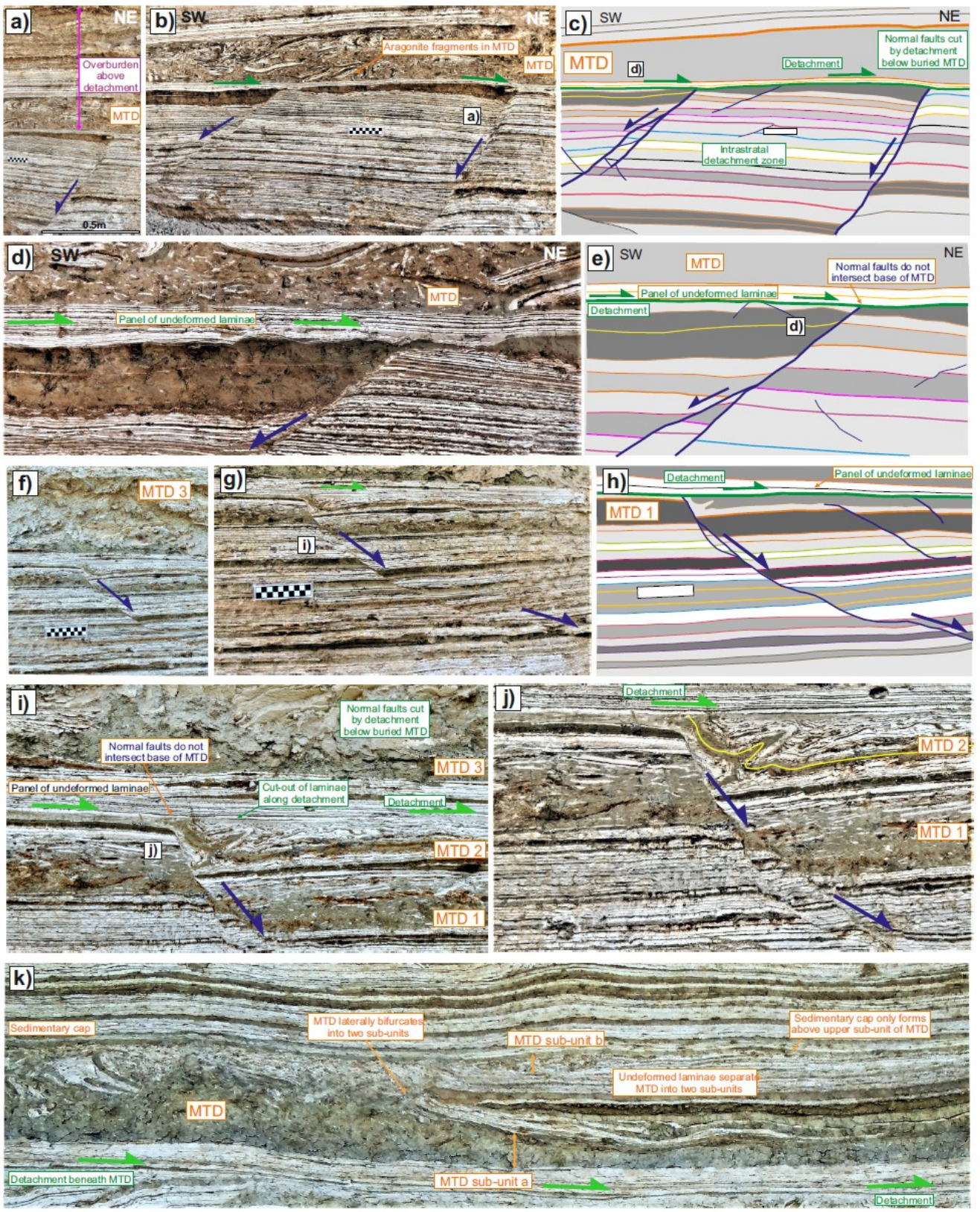
a)
NE
Overburden above detachment
MTD
0.5m
b)
SW
NE
Aragonite fragments in MTD
MTD
a)
c)
SW
NE
MTD
d)
Detachment
Normal faults cut by detachment below buried MTD
Intrastratal detachment zone
d)
SW
NE
MTD
Panel of undeformed laminae
e)
SW
MTD
NE
Normal faults do not intersect base of MTD
Panel of undeformed laminae
Detachment
d)
f)
MTD 3
g)
i)
h)
Detachment
Panel of undeformed laminae
MTD 1
i)
Normal faults cut by detachment below buried MTD
Normal faults do not intersect base of MTD
MTD 3
Panel of undeformed laminae
Cut-out of laminae along detachment
Detachment
j)
MTD 2
MTD 1
j)
Detachment
MTD 2
MTD 1
k)
Sedimentary cap
MTD laterally bifurcates into two sub-units
MTD sub-unit b
Sedimentary cap only forms above upper sub-unit of MTD
Undeformed laminae separate MTD into two sub-units
MTD
Detachment beneath MTD
MTD sub-unit a
Detachment

Figure 20

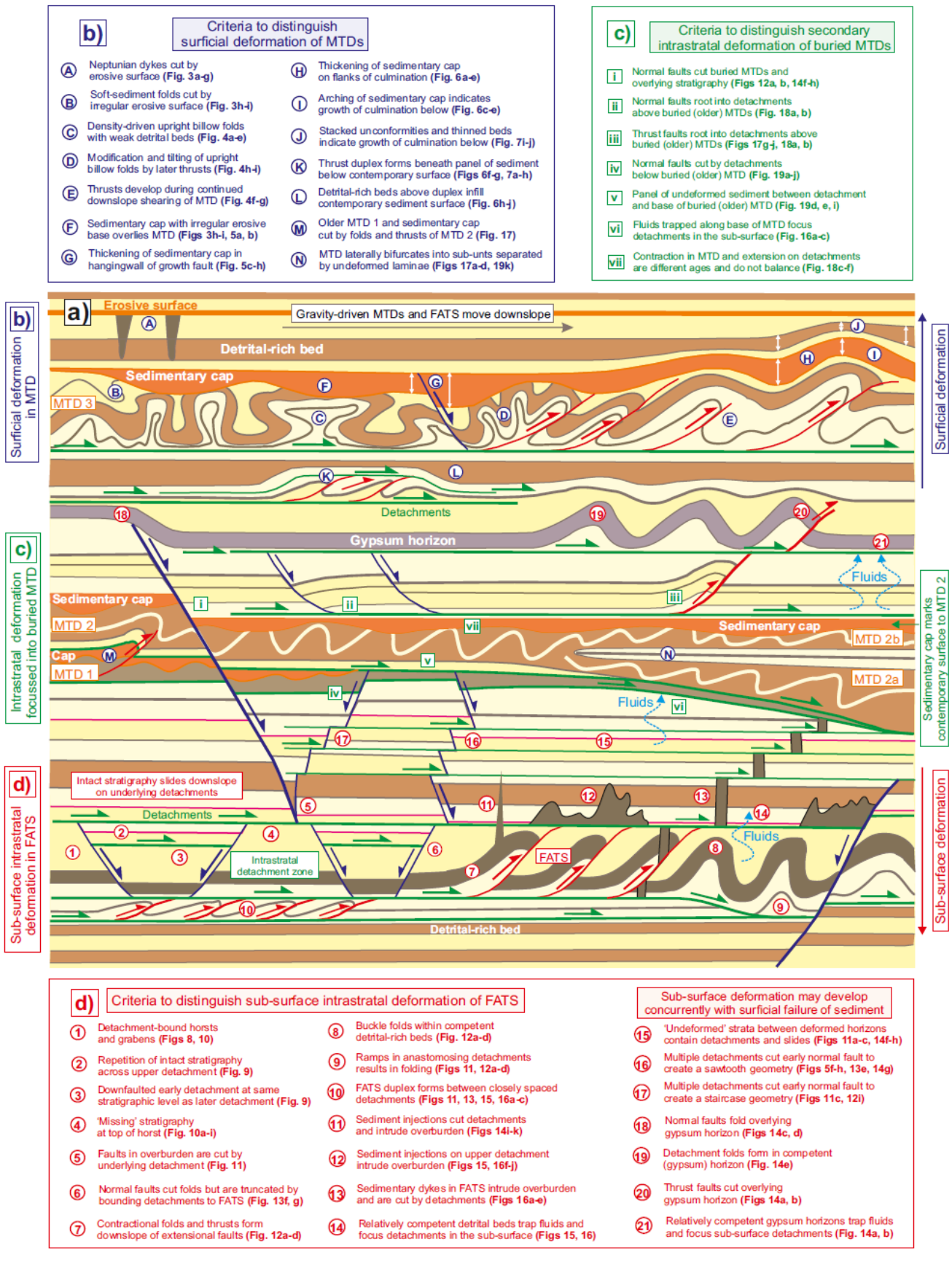
b)
Criteria to distinguish surficial deformation of MTDs
A Neptunian dykes cut by erosive surface (Fig. 3a-g)
B Soft-sediment folds cut by irregular erosive surface (Fig. 3h-l)
C Density-driven upright billow folds with weak detrital beds (Fig. 4a-e)
D Modification and tilting of upright billow folds by later thrusts (Fig. 4h-l)
E Thrusts develop during continued downslope shearing of MTD (Fig. 4f-g)
F Sedimentary cap with irregular erosive base overlies MTD (Figs 3h-i, 5a, b)
G Thickening of sedimentary cap in hangingwall of growth fault (Fig. 5c-h)
H Thickening of sedimentary cap on flanks of culmination (Fig. 6a-e)
I Arching of sedimentary cap indicates growth of culmination below (Fig. 6c-e)
J Stacked unconformities and thinned beds indicate growth of culmination below (Fig. 7i-j)
K Thrust duplex forms beneath panel of sediment below contemporary surface (Figs 6f-g, 7a-h)
L Detrital-rich beds above duplex infill contemporary sediment surface (Fig. 6h-j)
M Older MTD 1 and sedimentary cap cut by folds and thrusts of MTD 2 (Fig. 17)
N MTD laterally bifurcates into sub-units separated by undeformed laminae (Figs 17a-d, 19k)
c)
Criteria to distinguish secondary intrastratal deformation of buried MTDs
i Normal faults cut buried MTDs and overlying stratigraphy (Figs 12a, b, 14f-h)
ii Normal faults root into detachments above buried (older) MTDs (Fig. 18a, b)
iii Thrust faults root into detachments above buried (older) MTDs (Figs 17g-j, 18a, b)
iv Normal faults cut by detachments below buried (older) MTD (Fig. 19a-j)
v Panel of undeformed sediment between detachment and base of buried (older) MTD (Fig. 19d, e, i)
vi Fluids trapped along base of MTD focus detachments in the sub-surface (Fig. 16a-c)
vii Contraction in MTD and extension on detachments are different ages and do not balance (Fig. 18c-f)
b) Surficial deformation in MTD
a)
Erosive surface
Gravity-driven MTDs and FATS move downslope
Detrital-rich bed
Sedimentary cap
MTD 3
Surficial deformation
Detachments
Gypsum horizon
Fluids
c) Intrastratal deformation focussed into buried MTD
Sedimentary cap
MTD 2
Cap
MTD 1
Sedimentary cap
MTD 2b
MTD 2a
Fluids
Sedimentary cap marks contemporary surface to MTD 2
d) Sub-surface intrastratal deformation in FATS
Intact stratigraphy slides downslope on underlying detachments
Detachments
Intrastratal detachment zone
FATS
Fluids
Detrital-rich bed
Sub-surface deformation
d)
Criteria to distinguish sub-surface intrastratal deformation of FATS
1 Detachment-bound horsts and grabens (Figs 8, 10)
2 Repetition of intact stratigraphy across upper detachment (Fig. 9)
3 Downfaulted early detachment at same stratigraphic level as later detachment (Fig. 9)
4 'Missing' stratigraphy at top of horst (Fig. 10a-i)
5 Faults in overburden are cut by underlying detachment (Fig. 11)
6 Normal faults cut folds but are truncated by bounding detachments to FATS (Fig. 13f, g)
7 Contractional folds and thrusts form downslope of extensional faults (Fig. 12a-d)
8 Buckle folds within competent detrital-rich beds (Fig. 12a-d)
9 Ramps in anastomosing detachments results in folding (Figs 11, 12a-d)
10 FATS duplex forms between closely spaced detachments (Figs 11, 13, 15, 16a-c)
11 Sediment injections cut detachments and intrude overburden (Figs 14i-k)
12 Sediment injections on upper detachment intrude overburden (Figs 15, 16f-j)
13 Sedimentary dykes in FATS intrude overburden and are cut by detachments (Figs 16a-e)
14 Relatively competent detrital beds trap fluids and focus detachments in the sub-surface (Figs 15, 16)
Sub-surface deformation may develop concurrently with surficial failure of sediment
15 'Undeformed' strata between deformed horizons contain detachments and slides (Figs 11a-c, 14f-h)
16 Multiple detachments cut early normal fault to create a sawtooth geometry (Figs 5f-h, 13e, 14g)
17 Multiple detachments cut early normal fault to create a staircase geometry (Figs 11c, 12i)
18 Normal faults fold overlying gypsum horizon (Figs 14c, d)
19 Detachment folds form in competent (gypsum) horizon (Fig. 14e)
20 Thrust faults cut overlying gypsum horizon (Figs 14a, b)
21 Relatively competent gypsum horizons trap fluids and focus sub-surface detachments (Fig. 14a, b)